



HAL
open science

Computer simulations of model materials inspired by energy applications

Stefano Mossa

► **To cite this version:**

Stefano Mossa. Computer simulations of model materials inspired by energy applications. Materials Science [cond-mat.mtrl-sci]. Université Joseph Fourier Grenoble, 2015. tel-02945204

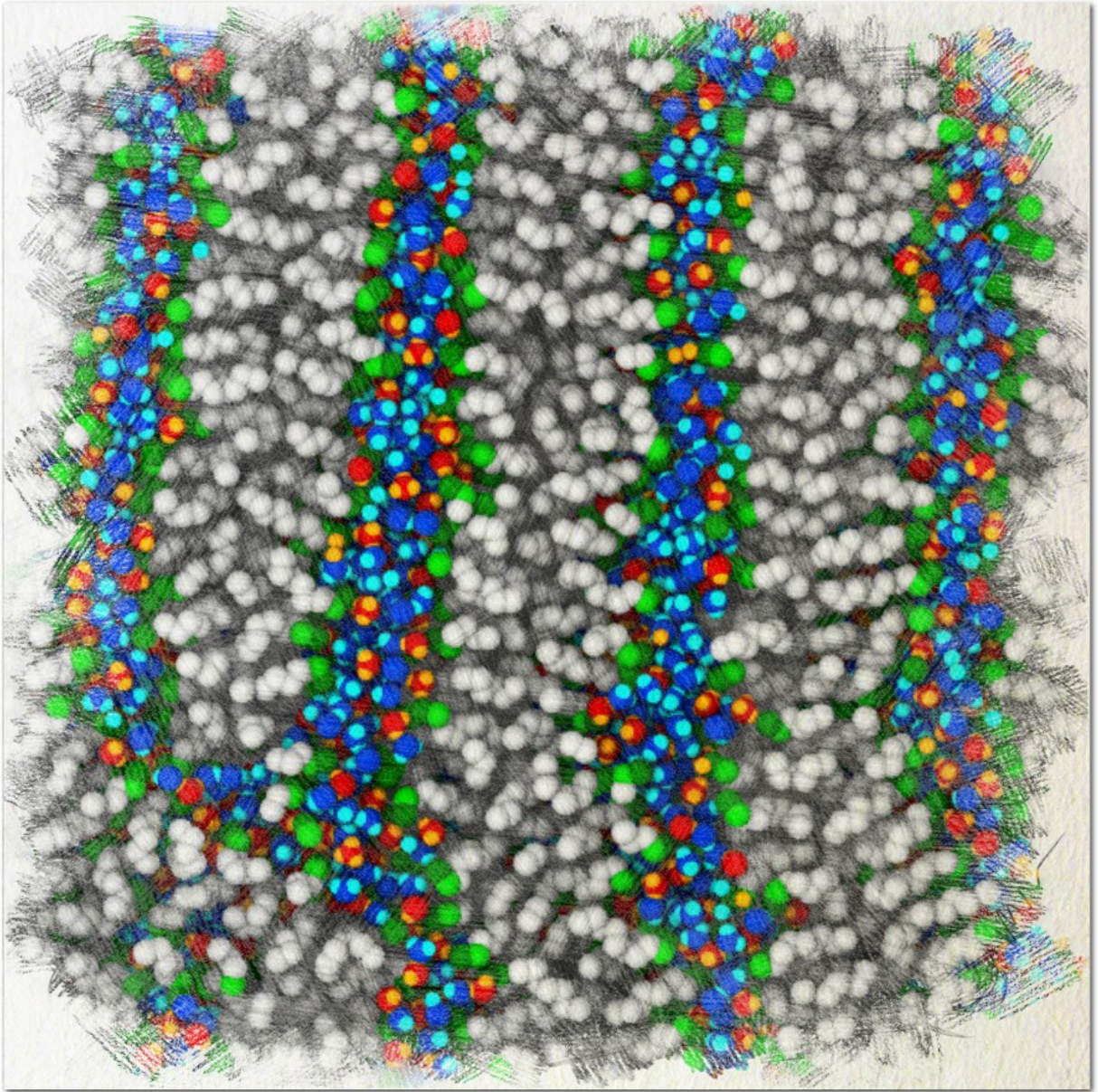
HAL Id: tel-02945204

<https://hal.science/tel-02945204>

Submitted on 25 Sep 2020

HAL is a multi-disciplinary open access archive for the deposit and dissemination of scientific research documents, whether they are published or not. The documents may come from teaching and research institutions in France or abroad, or from public or private research centers.

L'archive ouverte pluridisciplinaire **HAL**, est destinée au dépôt et à la diffusion de documents scientifiques de niveau recherche, publiés ou non, émanant des établissements d'enseignement et de recherche français ou étrangers, des laboratoires publics ou privés.



**Université "Joseph Fourier" de Grenoble
École Doctorale de Physique**

Habilitation à Diriger des Recherches

**Computer simulations of model materials
inspired by energy applications**

Stefano Mossa

July 16th 2015



**Université "Joseph Fourier" – Grenoble
École Doctorale de Physique**

Habilitation à Diriger des Recherches

**Computer simulations of model materials
inspired by energy applications**

présenté par

Stefano MOSSA

Commissariat à l'Énergie Atomique et aux Énergies Alternatives, CEA Grenoble
Institut Nanoscience et Cryogénie (INAC)
Structures et Propriétés d'Architectures Moléculaires (SPrAM)
Unité Mixte de Recherche 5819 (CEA, CNRS, UJF)

Grenoble, July 16th 2015

Membres du Jury

Jean-Louis BARRAT – LIPHY, Université "Joseph Fourier" Grenoble

Marie-Liesse DOUBLET – ICG, Université Montpellier 2

Giuseppe FOFFI – LPS, Université Paris-Sud (**rapporteur**)

Pierre LEVITZ – PHENIX, UPMC Paris (**rapporteur**)

Natalio MINGO – LITEN, CEA Grenoble

Giancarlo RUOCCO – Università di Roma "La Sapienza" (**rapporteur**)



a

Rosalinda & Primo

Contents

1 My trajectory to Grenoble	7
1.1 As an introduction	7
1.2 My background & scientific profile	8
1.3 Scientific cases before joining the CEA (in just a few pages)	9
1.3.1 Supercooled liquids and the glass transition	9
1.3.2 Water: the liquid-liquid phase transition	12
1.3.3 Passive & active soft matter	13
1.3.4 Beyond materials: statistical mechanics of random networks	15
1.4 Settled at the CEA Grenoble: present & future	17
1.4.1 Topic A: Interplay of structure & transport in complex electrolytes	18
1.4.2 Topic B: Heat & sound at the nanoscale	20
2 A. Inhomogeneous structure and transport in electrolytes	21
2.1 Fuel cells & batteries	21
2.2 Heterogeneous water transport in Nafion thin-films	25
2.3 Water confined in ionic surfactants nano-structures	33
2.4 Electrolytes for Li ⁺ transport	43
3 B. Heat and sound in glasses and nanostructured materials	49
3.1 Thermal properties at the nanoscale	49
3.2 Glasses and elastic heterogeneities	50
3.3 Nanostructuring: superlattices	60

Chapter 1

My trajectory to Grenoble

1.1 As an introduction

I still remember the day when, for the first time, I thought it would have been possible for me to study physics at the University. We were sitting in the theatre at my High School, the mythical “*Convitto Nazionale Domenico Cirillo*” in Bari, attending a few presentations given by University Professors. The usual advertisement day for future fresh-men in the different disciplines, just to try to convince people that “if you choose my field, you will be intellectually satisfied and your life will be settled for ever”. An elderly man was talking, a full professor in canon law, not really an exciting speech. An other man was wandering around, casual clothes, trying to find an electric plug to connect his overhead projector (!). I remember I have thought: here it is, the usual Italian academic rubbish, the boss has already started to speak while his servant tries to solve his problems.

I was mistaken. The servant actually was the emissary from the physics department, an expert in high magnetic fields, working to the development of part of the LEP at CERN. He started by stating: “*I am happy to be the last one talking. I will not make the mistakes my colleagues made before me*”. Next he continued, saying that if we had the desire to work a lot (he actually used very peculiar words to express the concept), learn to correctly speak and write English and travel around the world, physics was the good choice. He was quite scary, the speech was not that successful, a future of law or marketing was already decided for most of us. But it actually worked for me.

This is how someone who had already spent five years translating from ancient Latin and Greek, studying history and philosophy, enjoying history of arts, with no background in mathematics and physics at all, found himself attending classes on mathematical methods for physics, theoretical physics, electromagnetism, statistical mechanics. And everything the man was talking about, finally happened. At the beginning it was hard, my self-estimation was really challenged in a few final exams, and cannot count the nights spent to try to advance in this new intellectual world. The following was simpler: I obtained my Master, my Ph.D., I learnt to speak and write English and French, travelled around quite a lot, both in the Old and New world. I was in contact with bright people, started to interact with younger students, enjoyed very different styles in societies and ways of life. I finally landed in France, where I settled and opened a new period of my existence.

Now: how to better celebrate my trajectory to Grenoble and this new start by finally discussing my HDR thesis! Dear Reader, please find in this memoir, after an agile résumé of my juvenile work, an overview of my most recent research activities and future plans. This would not have been possible without the hard work provided by: Daiane Damasceno Borges, Samuel Hanot, Hideyuki Mizuno, Veerapandian Ponnuchamy and, last but not least, Ioannis Skarmoutsos.

Bonne lecture!

1.2 My background & scientific profile

First a few details about my professional profile. I am a physicist, trained in theoretical physics, with a strong background in statistical mechanics of disordered systems. My main research tools are computer simulations, both classical molecular dynamics and Monte Carlo, and advanced numerical analysis methods, including optimization techniques and data analysis. During my carrier I have mainly focused on the general broad subjects of physics of liquids and soft matter, covering a vast range of scientific cases. Since 2007, when I have joined CEA, I have started to increasingly shift my interests to materials science, developing a new activity in atomistic and mesoscopic computer simulations of numerical models inspired to novel energies applications. In this new general framework, I can efficiently exploit my previous experience and knowledge of the behaviour of complex condensed matter in its different forms.

My top-ten most cited papers cover large part of my heterogeneous research interests, which witnesses the impact of my work in quite different scientific domains. Large part of my career corresponds to long-term periods spent in research institutions of worldwide reputation, including "La Sapienza" University in Roma, Boston University, "Pierre et Marie Curie" University in Paris, the European Synchrotron Radiation Facility (ESRF) and, at present, the "Commissariat à l'Énergie Atomique et aux Énergies Alternatives (CEA) in Grenoble. In each one of these inspiring research centres, I have contributed substantial work, in collaborations with more senior scientists and young students, including both theoreticians and experimentalists.

Most part of the articles I have co-authored contain results of computer simulations and data analysis performed by myself. 44 publications in refereed journals are referenced on the Web of Science (WoS) databases, including 3 published on PNAS, 4 on PRL, 1 in ACS Nano, 2 on EPL. My h-index is currently 19 according to the WoS (21 according to the Google Scholar indexes), with a total of about 1900 citations and an average of 44 citations per article. 4 papers have been cited more than 100 times, 6 more than 50. My attitude in being involved in advanced and sometimes risky research projects is evident from the inhomogeneous time-distribution of scientific publications, which also has been impacted by mobility and carrier issues.

My intense theoretical activity has been complemented by systematic collaborations with experimentalists. In particular, during my stay at the ESRF, I have substantially strengthened my knowledge in scattering techniques, including elastic and inelastic X-Rays and Neutrons scattering. This is quite unusual in the community of theoretical physicists, who are normally used to work with static and dynamic structure factors, or intermediate scattering functions, but very seldom are familiar with the experimental facilities where these quantities are actually measured. I also have experience in interacting with scientists with different backgrounds (chemists for example) and younger people (graduate and undergraduate students). Indeed, although my teaching experience is limited, my interactions with students have always been systematic. In particular, although not entitled to formally assume thesis directions, I already have supervised on a daily basis a certain number of graduate and undergraduate students.

In what follows I will try to give a very concise overview of my scientific activity prior to my arrival at the CEA. Next I will introduce my main present research lines, which are the topic of this work and will be expanded in the following two Chapters. I have chosen to include the references cited in the text in the footnotes, rather than gathering them at the end of the manuscript. Articles which I have co-authored are indicated by a ★.

1.3 Scientific cases before joining the CEA (in just a few pages)

One could broadly define this initial part of my activity as physics of disordered systems, based on computer simulation of simple models. Emphasis is not on the details of the interactions among the different systems units but, rather, on universal processes controlled by the generic nature of involved forces. This is a quite effective attitude that I have always kept, also in more recent times. The nature of the scientific cases below has been dictated by both my personal interests and, obviously, the scopes of my different Post Doc projects. The discussion is organized as very short disciplinary highlights more than just providing a chronological list of scientific issues. This also helps to demonstrate the existence of underlying common threads connecting different subjects.

Some of the topics discussed below are of direct relevance for my present work on model materials inspired by energy applications. Keywords include physics of the liquid state, water, locally preferred structures in bulk phases, vibrational excitations in disordered systems. Others have an implicit interest, focusing on general features like dynamical properties on long times scales, the relation between dynamics and thermodynamics, or systems in out-of-equilibrium conditions.

1.3.1 Supercooled liquids and the glass transition

The supercooled liquid state, with its spectacular slowing down of dynamics, eventually leading to glass formation, is one of the main puzzles of condensed matter theory¹. The most intriguing issue is the observation, on lowering temperature for instance, of enormous changes in structural relaxation times when typical structural correlation functions only show very minor modifications. Questions originating from these observations include the existence/absence of a true thermodynamic glass phase transition, the nature of the order parameter to probe, the link between dynamics and properties of the underlying energy landscapes.

Spin glasses. – I have got acquainted with these ideas since the very early stage of my career, when I contributed to the development of a Potts spin-glass model². The smart Hamiltonian proposed enjoyed a gauge symmetry that forbade spontaneous magnetization. As a consequence, the associated phase diagram had the very nice feature of showing a vanishing region of non-zero spontaneous magnetization, with a glassy phase extending down to zero temperature. In that paper, we characterized the spin glass phase and gave a few hints about the slow relaxation dynamics of the model. Although I did not go back to this work since, the model has been revisited many times in different contexts, as witnessed by the quite high number of citations of the original paper. It also has constituted one of the case studies for quantifying the performances of the *Janus* super-computer³, expressly developed for the numerical simulation of spin glass models.

The potential energy landscape. – Very soon after the above work, I moved to more realistic off-lattice models for molecular supercooled liquids, focusing on the slowing down of the dynamics eventually leading to the glass transition. In those years, huge amount of work was being devoted

¹L. Berthier and G. Biroli. *Theoretical perspective on the glass transition and amorphous materials*. *Reviews of Modern Physics* **83**, 587, 2011.

²E. Marinari, S. Mossa, and G. Parisi. *Glassy Potts model: A disordered Potts model without a ferromagnetic phase*. *Phys. Rev. B* **59**, 8401–8404, 1999*

³F. Belletti, M. Cotallo, A Cruz, L. A. Fernandez, A. Gordillo, A. Maiorano, F. Mantovani, E. Marinari, V. Martin-Mayor, A Muñoz-Sudupe, et al. *Simulating spin systems on IANUS, an FPGA-based computer*. *Comput. Phys. Commun.* **178**, 208–216, 2008.

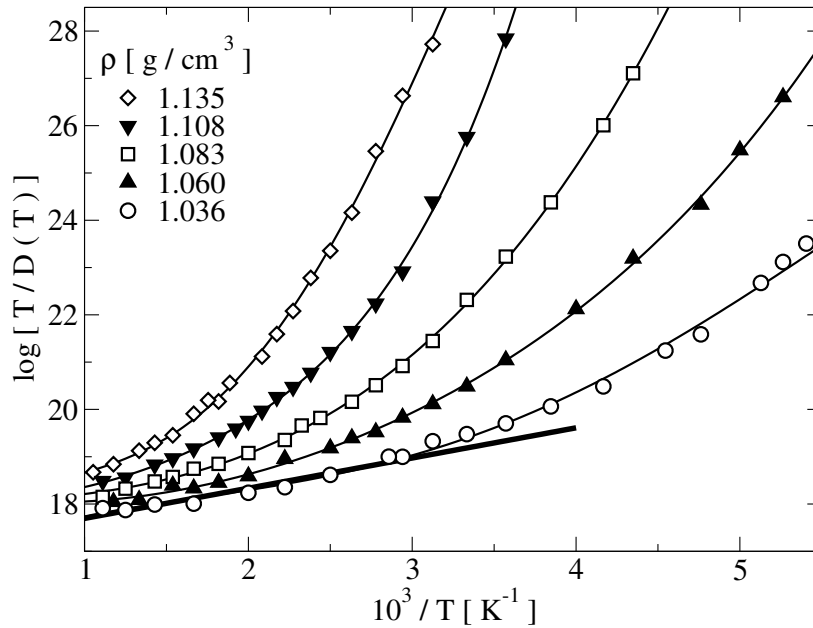


Figure 1.1: Simulation data for a model orthoterphenyl molecular liquid. $\log[T/D(T)]$ with $D(T)$ the translational diffusion constant is plotted as a function of $1/T$, at the indicated values of system density, ρ . The bold solid line is the Arrhenius fit to the high-temperature portion of the data $T > T^*(\rho)$ for $\rho = 1.036 \text{ g/cm}^3$. The Figure is taken from Ref.⁹.

to the concept of potential energy landscapes (PEL)⁴: a particular thermodynamic state of a liquid system is described by one point on a multi-dimensional potential energy surface, which can be characterized in terms of local energy minima with the associated basins of attraction. The multiplicity of these minima, the configurational entropy, is directly related to the long-time dynamics and controls the slowing down on lowering temperature. The results shown in Fig. 1.1 are an example of our very extended body of computational data, related to a rigid three-sites model for the molecular glass former orthoterphenyl. We investigated in details the relation between dynamics and configurational entropy⁵ and showed that a complete characterization of the PEL provides all the information needed for describing the thermodynamics of the system, allowing to develop a complete PEL equation of state^{6–8}.

Additional data were also included in Refs.^{9,10}. These papers are a nice example of how, sometimes, crucial issues are simply overlooked and not completely clarified before addressing much

⁴A. Heuer. *Exploring the potential energy landscape of glass-forming systems: from inherent structures via metabasins to macroscopic transport*. J. Phys.: Condens. Matter **20**, 373101, 2008.

⁵S. Mossa, E. La Nave, H. Stanley, C. Donati, F. Sciortino, and P. Tartaglia. *Dynamics and configurational entropy in the Lewis-Wahnström model for supercooled orthoterphenyl*. Phys. Rev. E **65**, 041205, 2002^{*}.

⁶E. La Nave, S. Mossa, and F. Sciortino. *Potential Energy Landscape Equation of State*. Phys. Rev. Lett. **88**, 2002^{*}.

⁷E. La Nave, F. Sciortino, P. Tartaglia, C. D. Michele, and S. Mossa. *Numerical evaluation of the statistical properties of a potential energy landscape*. J. Phys.: Condens. Matter **15**, S1085–S1094, 2003^{*}.

⁸E. La Nave, S. Mossa, F. Sciortino, and P. Tartaglia. *Liquid stability in a model for ortho-terphenyl*. J. Chem. Phys. **120**, 6128–34, 2004^{*}.

⁹G. Tarjus, D. Kivelson, S. Mossa, and C. Alba-Simionesco. *Disentangling density and temperature effects in the viscous slowing down of glassforming liquids*. J. Chem. Phys. **120**, 6135–41, 2004^{*}.

¹⁰G. Tarjus, S. Mossa, and C. Alba-Simionesco. *Response to: "Comment on 'Disentangling density and temperature effects in the viscous slowing down of glassforming liquids'"*(J. Chem. Phys. **121**, 11503 (2004)). J. Chem. Phys. **121**, 11505–11506, 2004^{*}.

more complicated questions. In this case the question answered was the relative importance in the supercooling process associated to temperature or density. Note that this is in general an important question if one observes that most part of experiments are performed at constant pressure, implying that both quantities vary at each investigated state point.

Interestingly, we also demonstrated that the concept of PEL turns out to be useful in out-of-equilibrium conditions also, when ageing is present or complex patterns for the thermal history of the system are considered, as in the case of the so-called Kovacs effect¹¹⁻¹⁴. The correlated notion of *effective* temperature in out-of-equilibrium systems is also interesting, as we will see below in the paragraph devoted to active matter.

Geometrical frustration & locally preferred structures. – More recently, the focus of the research on the glass transition has shifted to non-topographic¹⁵ descriptions, leaving aside the PEL representation and focusing on more complex concepts, like the notion of dynamical heterogeneity¹. Substantial work is also devoted to the design of increasingly complex observables, with the goal to demonstrate the existence (or absence) of diverging length scales associated to diverging time scales at the glass transition. Point-to-set correlations or overlap functions with quenched reference states are specialized keywords in these cases¹.

We also provided some contribution to a non-topographic view of the glass transition with our work on the concept of local topological order. The idea is that both supercooling and glass formation are connected to the interplay between extension of a locally stable *icosahedral* liquid order, different than that of the crystal, and global constraints associated with tiling of the entire space. These cannot be satisfied by a five-fold symmetry, and the resulting competition is the geometric (or topological) frustration, whose increasing extent on lowering temperature controls the slowing down of the dynamics. In a series of papers^{16,17} we solved a shortcoming of this argument related to the stability of the local structure in the bulk. Indeed, we demonstrated that, as in the case of an isolated cluster formed by 13 particles, the ground state of a cluster embedded in a liquid-like environment is still icosahedral. The crucial idea was to implement a mean-field-like liquid background, avoiding to impose any crystalline-like symmetry (as it is the case with periodic boundary conditions in MD), which hinders full expression of the icosahedral order.

Short-times dynamics in supercooled liquids. – The phenomena described above naturally refer to dynamics on very extended time scales, associated to the exploration of different minima on the energy landscape. The short times dynamics, associated to the exploration of the internal structure of the basins of attraction of the minima, also present important issues. These concern the main features of vibrational dynamics, which originally motivated my interest in scattering

¹¹S. Mossa, G. Ruocco, F. Sciortino, and P. Tartaglia. *Quenches and crunches: Does the system explore in ageing the same part of the configuration space explored in equilibrium?* *Philos. Mag. Part B* **82**, 695–705, 2002★.

¹²S. Mossa, E. La Nave, F. Sciortino, and P. Tartaglia. *Aging and energy landscapes: application to liquids and glasses.* *Eur. Phys. J. B - Condens. Matter* **30**, 351–355, 2002★.

¹³S. Mossa, E. L. Nave, P. Tartaglia, and F. Sciortino. *Equilibrium and out-of-equilibrium thermodynamics in supercooled liquids and glasses.* *J. Phys.: Condens. Matter* **15**, S351–S357, 2003★.

¹⁴S. Mossa and F. Sciortino. *Crossover (or Kovacs) Effect in an Aging Molecular Liquid.* *Phys. Rev. Lett.* **92**, 045504, 2004★.

¹⁵L. Berthier and J. P. Garrahan. *Nontopographic description of inherent structure dynamics in glassformers.* *J. Chem. Phys.* **119**, 4367–4371, 2003.

¹⁶S. Mossa and G. Tarjus. *Locally preferred structure in simple atomic liquids.* *J. Chem. Phys.* **119**, 8069, 2003★.

¹⁷S. Mossa and G. Tarjus. *An operational scheme to determine the locally preferred structure of model liquids.* *J. Non-Cryst. Solids* **352**, 4847–4850, 2006★.

processes and spectroscopy techniques. Indeed, moving to more realistic molecular systems, the main goal of my Ph.D. thesis project was the development of a *flexible* model for orthoterphenyl¹⁸. Incoherent¹⁸ and coherent¹⁹ dynamics of density fluctuations were explored with unprecedented details, and we also managed to quantify the relative strengths of orientational and induced contributions to depolarized light scattering (DLS) spectra²⁰. Most important, we investigated in depth the nature of high frequency excitations in the liquid state, as those measured in inelastic X-rays scattering (IXS) experiments²¹. Finally, in Ref.²² we demonstrated the vibrational nature of the fast relaxation observed in Brillouin Light Scattering (BLS) experiments in orthoterphenyl.

The experience I developed at that time in directly calculating scattering spectra from system snapshots generated by simulation, has demonstrated to be crucial more recently, when I have gone back to the investigation of collective vibrational excitations in glasses and nanostructured materials, as we will see in Chapter 3.

1.3.2 Water: the liquid-liquid phase transition

Water is ubiquitous and plays a vital role in a panoply of systems and mechanisms, ranging from biological organisms to synthetic materials. Although some features of water are still not completely clarified, understanding and controlling its behaviour, also in extreme conditions or in particular configurations, including confinement, is crucial in many contexts.

My interest in water was triggered by a debated, elusive, and exotic issue: the existence of a liquid-liquid critical point in the very-low temperature and very-high pressure region of the phase diagram (see Ref.²³ for a recent review). Debated, because if its existence in numerical models is well established, the relevance for real water is still controversial. Elusive, insofar as very difficult to detect, due to the extreme conditions to produce in experiments. Exotic, in the sense that the impact of this feature on water behaviour at close-to-ambient conditions can be expected to be negligible.

More in details, during my PostDoc in Boston, we performed extensive computer simulations of the TIP5P water molecule²⁴, which at that time was considered to be closer to real water than any previously proposed models. In that work we attempted to unify the phenomena connected with the existence of a liquid-liquid phase transition and homogeneous nucleation in a single molecular dynamics simulation study. The phase behaviour was explored for a large range of deeply supercooled states, and we found evidences of the existence of a nonmonotonic "nose-shaped" temperature of maximum density line and a non-reentrant spinodal (see Fig. 1.2), and of the presence of a low-temperature phase transition. Also we observed the free evolution of bulk water to ice, and determined the time-temperature-transformation curves at different densities.

¹⁸S. Mossa, R. Di Leonardo, G. Ruocco, and M. Sampoli. *Molecular dynamics simulation of the fragile glass-former orthoterphenyl: A flexible molecule model*. Phys. Rev. E **62**, 612–630, 2000^{*}.

¹⁹S Mossa, G Ruocco, and M Sampoli. *Molecular dynamics simulation of the fragile glass former orthoterphenyl: A flexible molecule model. II. Collective dynamics*. Phys. Rev. E **64**, 021511, 2001^{*}.

²⁰S. Mossa, G. Ruocco, and M. Sampoli. *Orientational and induced contributions to the depolarized Rayleigh spectra of liquid and supercooled ortho-terphenyl*. J. Chem. Phys. **117**, 3289, 2002^{*}.

²¹S. Mossa, G. Monaco, G. Ruocco, M. Sampoli, and F. Sette. *Molecular dynamics simulation study of the high frequency sound waves in the fragile glass former orthoterphenyl*. J. Chem. Phys. **116**, 1077, 2002^{*}.

²²S Mossa, G Monaco, and G Ruocco. *Vibrational origin of the fast relaxation processes in molecular glass formers*. Europhys. Lett. **60**, 92–98, 2002^{*}.

²³N. Giovambattista. *The Liquid–Liquid Phase Transition, Anomalous Properties, and Glass Behavior of Polymorphic Liquids*. Liquid Polymorphism, 113–138, 2013.

²⁴M. Yamada, S. Mossa, H. E. Stanley, and F. Sciortino. *Interplay between time-temperature transformation and the liquid-liquid phase transition in water*. Phys. Rev. Lett. **88**, 195701, 2002^{*}.

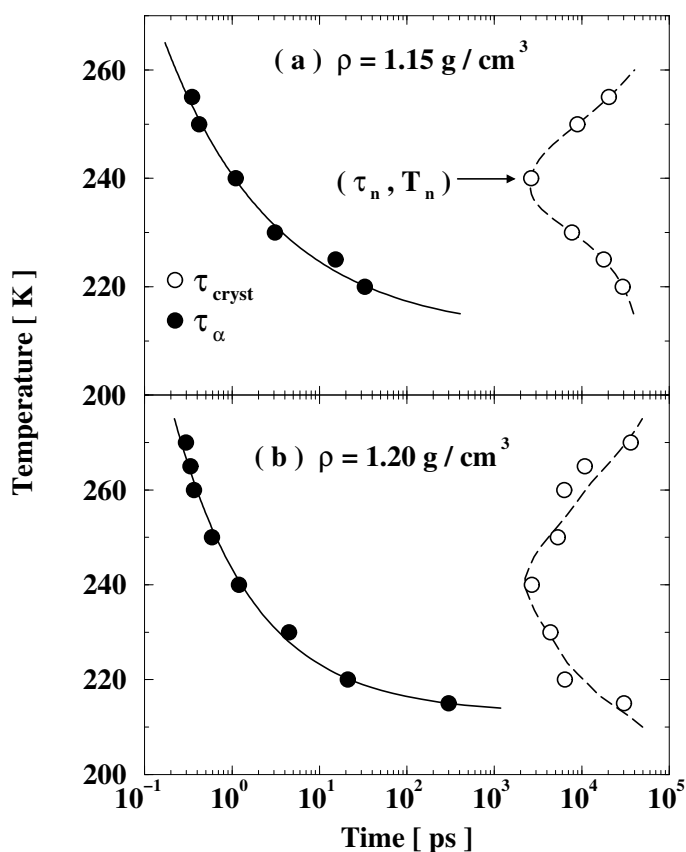


Figure 1.2: Average crystallization time (open circles) for the TIP5P water model, as a function of temperature at the two indicated densities ρ . A well-defined "nose" shape is visible, as measured for water solutions. We also show the structural relaxation times τ_α , as calculated from the self-intermediate scattering function $F_s(Q, t)$ (closed circles). Figure is taken from Ref.²⁴.

Our results were discussed in an extended series of papers^{24–27}. Recently, my interest in the physics of water has rekindled, as we will see in Chapter 2, but ambient conditions and nano-scale soft confinement are now the appropriate keywords.

1.3.3 Passive & active soft matter

Soft matter includes an incredibly extended range of materials, with many interesting features. These sometimes resemble at larger length scales those of atoms, but in many cases they do not. Indeed, as D. Frenkel writes in Ref.²⁸ referring to colloids: *"In many ways, colloids behave like giant atoms, and quite a bit of the colloid physics can be understood in this way. However, much of the*

²⁵H. E. Stanley, M. C. Barbosa, S. Mossa, P. A. Netz, F. Sciortino, F. W. Starr, and M. Yamada. *Statistical physics and liquid water at negative pressures*. *Physica A: Statistical Mechanics and its Applications* **315**, 281–289, 2002^{*}.

²⁶H. Stanley, M. Barbosa, S. Mossa, P. Netz, F. Sciortino, F. Starr, and M. Yamada. "Water at positive and negative pressures" in: *Liquids Under Negative Pressure*. Springer, 2002^{*}. 59–67

²⁷H. E. Stanley, S. V. Buldyrev, N. Giovambattista, E. La Nave, S. Mossa, A. Scala, F. Sciortino, F. W. Starr, and M. Yamada. *Application of statistical physics to understand static and dynamic anomalies in liquid water*. *J. Stat. Phys.* **110**, 1039–1054, 2003^{*}.

²⁸D. Frenkel. *Soft condensed matter*. *Physica A: Statistical Mechanics and its Applications* **313**, 1–31, 2002.

interesting behavior of colloids is related to the fact that they are, in many respects, not like atoms".

Colloidal suspensions & gels. – A nice example of very peculiar behaviour of colloidal suspensions is described in Refs.^{29,30}. There, we investigated a numerical model where colloids interact with short-ranged attractive and long-ranged repulsive interactions. The goal was to model the equilibrium cluster phase discovered in sterically stabilized colloidal systems in the presence of depletion interactions. We discovered that, at low packing fractions, the colloids form stable equilibrium clusters which act as building blocks of a cluster fluid, and scrutinized the possibility that this latter generates a low-density disordered arrested phase (a *gel*) via a glass transition, driven by the repulsive interaction. As an intriguing consequence, in this model the gel formation could be accurately described with the same physics of the glass formation in atomic and molecular liquids^{29–31}.

Aging in Laponite. – Other interesting physics in colloidal suspensions comes from a strongly anisotropic shape of the interacting units, rather than from the subtle interplay of heterogeneous interactions on different length scales. In Ref.³² we reported a Brownian dynamics simulation of the out-of-equilibrium (aging) dynamics in a colloidal suspension composed of rigid charged disks, one possible model for Laponite, a synthetic clay featuring quite complex equilibrium and out-of-equilibrium phase behaviour³³. We focused on this last feature, exploring the aging dynamics of the system in terms of single-particle and collective density fluctuations, mean-squared displacements, and rotational dynamics. Our data confirmed the complexity of the out-of-equilibrium dynamical behavior of this class of colloidal suspensions and, most important, suggested that an arrested disordered state driven by a repulsive Yukawa potential (a *Wigner glass*), was generated in the model. The relevance of our findings for the real system is under investigation.

Active matter. – In the above work, the system was driven in out-of-equilibrium conditions by an abrupt variation (quench) of the external temperature. Very often, however, soft matter is found in auto-generated non-equilibrium conditions. An obvious example is *active matter*, where the constituents absorb energy from their environment or from internal fuel tanks and dissipate it by carrying out internal movements, that lead to translational or rotational motion. This situation is ubiquitous in biology, e.g., in bacterial colonies or in the cell.

In a series of articles^{34–36} we studied by computer simulations two simple models for bio-inspired materials, where spherical particles and semi-flexible polymers were attached to motors, mimicking the non-conservative character of chemical reactions. Interestingly, we showed that the

²⁹F. Sciortino, S. Mossa, E. Zaccarelli, and P. Tartaglia. *Equilibrium Cluster Phases and Low-Density Arrested Disordered States: The Role of Short-Range Attraction and Long-Range Repulsion*. Phys. Rev. Lett. **93**, 055701, 2004★.

³⁰S. Mossa, F. Sciortino, P. Tartaglia, and E. Zaccarelli. *Ground-state clusters for short-range attractive and long-range repulsive potentials*. Langmuir **20**, 10756–63, 2004★.

³¹F. Sciortino, S. V. Buldyrev, C. De Michele, G. Foffi, N. Ghofraniha, E. La Nave, A. Moreno, S. Mossa, I. Saika-Voivod, P. Tartaglia, and E. Zaccarelli. *Routes to colloidal gel formation*. Comput. Phys. Commun. **169**, 166–171, 2005★.

³²S. Mossa, C. De Michele, and F. Sciortino. *Aging in a Laponite colloidal suspension: a Brownian dynamics simulation study*. J. Chem. Phys. **126**, 014905, 2007★.

³³B. Ruzicka and E. Zaccarelli. *A fresh look at the Laponite phase diagram*. Soft Matter **7**, 1268–1286, 2011.

³⁴D. Loi, S. Mossa, and L. F. Cugliandolo. *Effective temperature of active matter*. Phys. Rev. E **77**, 051111, 2008★.

³⁵D. Loi, S. Mossa, and L. F. Cugliandolo. *Effective temperature of active complex matter*. Soft Matter **7**, 3726, 2011★.

³⁶D. Loi, S. Mossa, and L. F. Cugliandolo. *Non-conservative forces and effective temperatures in active polymers*. Soft Matter **7**, 10193, 2011★.

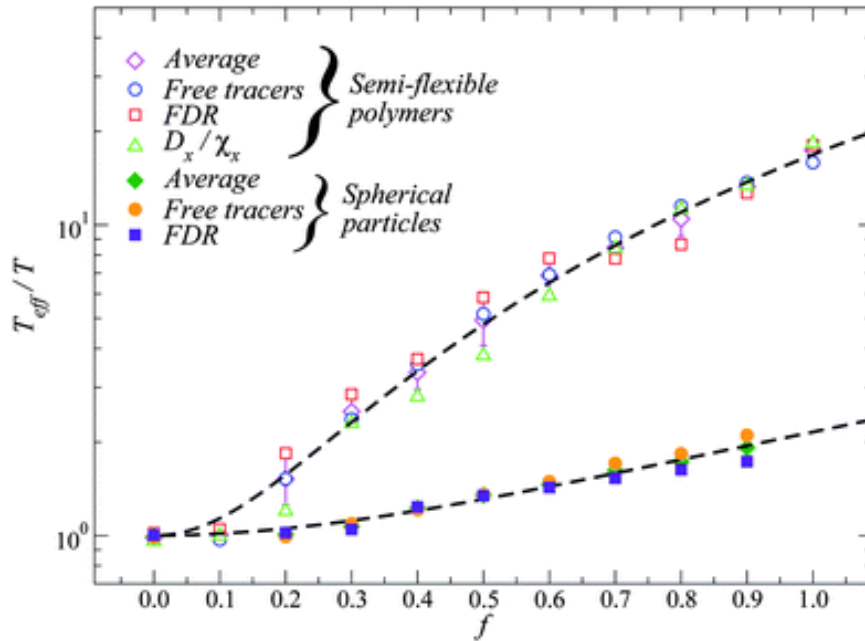


Figure 1.3: Effective temperature, T_{eff} as a function of the activity, f . This Figure summarizes the entire set of data that we generated, both for spherical self-propelled particles and motorized semi-flexible polymers, on a linear-logarithmic scale. The different sub-sets of data are indicated in the legend. Dashed lines are (empirical) power-law fits to the data, in the form $T_{eff}/T = 1 + \gamma f^2$. Figure is taken from Ref.³⁶.

out-of-equilibrium behaviour in the presence of chemical activity (controlled by the parameter f), where fluctuations are of origin different from just thermal fluctuations, can be rationalized in terms of a well-defined *effective* temperature, T_{eff} , fulfilling a generalized version of the fluctuation-dissipation theorem³⁴⁻³⁶. This was in analogy with the case of passive matter, driven in out-of-equilibrium conditions by external perturbations. The entire set of generated T_{eff} data is shown as a function of the level of activity in Fig. 1.3. Our studies are a nice example of application of out-of-equilibrium statistical mechanics concepts to biologically inspired systems. Since then, the interest in active matter from a statistical mechanics point of view, also in connection with the glass transition, has enormously increased (see, among many others, Ref.³⁷).

We conclude by noting that, surprisingly, systems including active matter seem to be promising for energy applications also. In Ref.³⁸, for instance, the use of self-propelled *Janus* particles, with one side made of catalytically active platinum powder while the other is coated with titanium, and immersed in a solution of sodium borohydride, results in a rate of hydrogen generation roughly nine times as fast as a fuel cell with conventional static catalytic nanoparticles.

1.3.4 Beyond materials: statistical mechanics of random networks

It is humorous to observe that two among my top-five cited papers focus on random networks, an interdisciplinary subject that I addressed just in those two occasions. In Ref.³⁹ we reported a

³⁷L. Berthier and J. Kurchan. *Non-equilibrium glass transitions in driven and active matter*. Nature Physics **9**, 310–314, 2013.

³⁸V. V. Singh, F. Soto, K. Kaufmann, and J. Wang. *Micromotor-Based Energy Generation*. Angewandte Chemie, 2015.

³⁹R Guimerà, S. Mossa, A. Turttschi, and L. A. N. Amaral. *The worldwide air transportation network: Anomalous centrality, community structure, and cities' global roles*. Proc. Natl. Acad. Sci. U. S. A. **102**, 7794–9, 2005★.

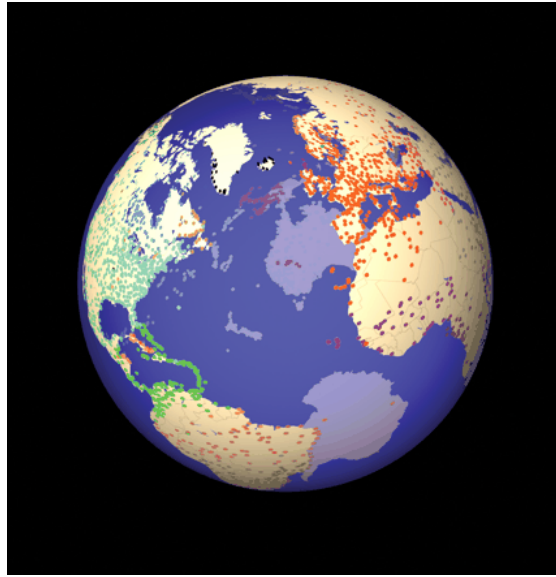


Figure 1.4: Communities in the giant component of the worldwide air transportation network. Each spot represents a city, and each color corresponds to a community of easily connected cities. Analysis reveals that the most important hubs, which serve as connectors between communities, are not necessarily the busiest ones or the most centrally located. The Figure is the cover image of the journal issue containing Ref.³⁹.

very detailed statistical study of the global airports network, based on real data. We found that the worldwide air transportation network is a *scale-free small-world* network but, contrary to the prediction of scale-free network models, the most connected cities are not necessarily the most central, resulting in anomalous values of the centrality. This paper is highly cited, and earned the cover page of the journal issue (see Fig. 1.4).

Also, in Ref.⁴⁰, we introduced a general model for the growth of scale-free networks under filtering information conditions, i. e. , when the nodes can process information about only a subset of the existing nodes in the network. We found that the distribution of the number of incoming links to a node decays as a power law with an exponential truncation. This is controlled not only by the system size but also by the subset of the network accessible to the node, a feature never considered previously. We also tested our model with empirical data for the World Wide Web and found agreement.

Interestingly, this paper was cited in Ref.⁴¹, in whose abstract one can read: "...*heresy within the medieval Catholic Church had many of the characteristics of a scale-free network*". This truly is an interdisciplinary impact! More seriously, the concept of random network has also been demonstrated to be relevant, for instance, for the topology of the potential energy landscapes of supercooled liquids⁴², which closes the circle (see above). Note that a renewed interest in this field is a possible perspective for my future work on energy-related matters. An obvious example is the investigation of issues related to energy-distribution networks⁴³.

⁴⁰S. Mossa, M. Barthélemy, H. Eugene Stanley, and L. Nunes Amaral. *Truncation of Power Law Behavior in "Scale-Free" Network Models due to Information Filtering*. Phys. Rev. Lett. **88**, 4, 2002^{*}.

⁴¹P. Ormerod and A. P. Roach. *The medieval inquisition: scale-free networks and the suppression of heresy*. Physica A: Statistical Mechanics and its Applications **339**, 645–652, 2004.

⁴²J. P. K. Doye. *Network Topology of a Potential Energy Landscape: A Static Scale-Free Network*. Phys. Rev. Lett. **88**, 238701, 2002.

⁴³M. Barthélemy. *Spatial networks*. Physics Reports **499**, 1–101, 2011.

1.4 Settled at the CEA Grenoble: present & future

As Umberto Eco wrote in the Preface of his *The Name of the Rose*⁴⁴: "...there was a widespread conviction that one should write only out of a commitment to the present, in order to change the world." Although Eco was referring to the political commitment of the intellectuals, similar concepts (the *enjeux sociétaux*) are increasingly permeating the present management of science in Europe in general, and at CEA in particular. Of course, this clearly is a global trend. For instance, scientists trained in condensed matter physics are increasingly moving to materials science, getting their hands dirty⁴⁵ while "following the rabbit" of research funding. Even if blindly generalizing this scheme to any form of research, including curiosity-driven one, looks to me questionable, I must admit that this general attitude still presents some interesting aspects. In particular, it can be quite efficient at providing clear guide-lines to orient the research activity in particular directions, or choosing among a virtually infinite range of interesting materials and physical mechanisms.

The background. – Conforming to the above situation, I have recently framed my scientific activity in terms of two technological applications:

- electric current **generation**, with emphasis on *fuel cells* applications and, more indirectly related, *thermoelectricity* devices
- energy **storage** applications, mostly *Lithium-ion batteries*.

Of course, this must be considered as a general framework, providing an *ex-post* applied perspective to my work. In what follows I will rather focus on specific physical processes active in complex materials used in novel energy devices, and on our investigation by computer simulation of static and dynamic properties of numerical models mimicking real systems.

In particular, we are interested in the interplay between nano-structure and mass or charge transport in soft materials. Our interest in hard matter is also lively, with emphasis on sound and heat transport at the nanoscale. These are increasingly important issues in most modern nano-structured materials, as we will see below. The final goal is therefore to clarify universal features generated by mixing of heterogeneous materials, with the formation of complex interfaces, providing a general consistent picture of the relation nano-structure/transport. This should supply additional guide for choosing most effective materials for energy applications and, even more ambitious goal, inspire the design of advanced materials with tailored properties.

Methodologically, we encode in our models general physical attributes, with limited attention to particular chemical compositions. This is a very effective strategy, which has led to impressive advances in other scientific contexts. Moreover, resting on elementary physical processes only allows a significant level of conceptual cross-fertilisation with other research fields. Most of our computational work is performed by using the massively parallel high-performance computing simulation tool LAMMPS⁴⁶, data analysis with self-developed codes. An additional goal of our work, in some circumstances, is to integrate the numerical data with experimental scattering results, obtained by using Neutrons and X-Rays as probes.

⁴⁴U. Eco. *The Name of the Rose*, trans. William Weaver (San Diego, 1983), 1983.

⁴⁵M. Shulman and M. Warner. *Physics gets its hands dirty*. *Nature Mater.* **14**, 361–361, 2015.

⁴⁶S. Plimpton. *Fast Parallel Algorithms for Short-Range Molecular Dynamics*. *J. Comp. Phys.* **117**, 1–19, 1995.

Confinement. – In what follows we will consider a large range of materials, in different configurations. One can, however, identify one common feature: *confinement*, even at the *nanoscale*. As a consequence, interfaces have no longer negligible extent compared to the bulk, generating different behaviours compared to the latter. We will consider the two situations where confinement is constituted by an *external* environment, like a hydrated ionomer thin film deposited on a substrate, or is *self-generated*. This is the case, for instance, of the auto-organization of the hydrophobic matrix in Nafion upon hydration, with the resulting formation of the ionic domains responsible for transport of water and protons. An other interesting case is the formation of a compact, symmetric and long-lived coordination shell around a Lithium ion when immersed in mixtures of organic solvents. In this case, the local confining environment dresses the ion and is mobile, following the charge in its dynamics and definitely controlling the ionic transport properties. Finally, interactions with an environment characterized by local heterogeneities of quite subtle (mechanical) nature, randomly distributed in the volume or concentrated at interfaces, also control transport of heat and sound in disordered solids and wisely nano-structured materials, as we will see below.

This work. – On this basis, I will detail below my recent scientific activity, which I organize here in two research topics. These are, again, linked by a common thread: non-trivial effects due to some form of confinement, both external and immobile, or dynamical and induced by the evolution of the system itself. The totality of the work discussed below is very recent, and all ideas I will discuss are parts of on-going projects. I have therefore refrained to partition the document in short-term and long-term activities. I am convinced that this would be an unnatural way of presenting my point of view on these issues, and would make less clear the perspectives of my present work.

Also, the discussion of the results will be quite qualitative, I have made a point of honour, for instance, to avoid any numbered equations. In a few cases, however, I will go more in depth with the discussion of some issues, which to my opinion better illustrate what kind of insightful information can be extracted from simulation data. For all details, however, the Reader should refer to the original published articles.

1.4.1 Topic A: Interplay of structure & transport in complex electrolytes

Chapter 2 is devoted to my investigation of complex electrolytes. Focus is on different aspects of confinement, and how this feature impacts transport properties. Together with electrodes, optimized electrolytes are crucial in polymer electrolytes fuel cells and Lithium-ion batteries technologies.

Performances of polymer electrolytes for applications in polymer-electrolyte membranes fuel cells (PEMFC) are determined by the interplay between transport properties of polar fluids (water) and charges, and the nanostructure of a charged confining polymer matrix (see, for instance, Ref.⁴⁷ and references therein). Two system configurations are of interest: the bulk, far from any boundaries, and at the interface with solid phases, as the formation of Nafion thin films in the catalytic layer (see Refs.^{48–50}). Main issues include: understanding the impact of the nanostructure

⁴⁷S. Lyonard, S. Mossa, and F. Lefebvre-Joud. *SSPC-16 Conference Proceedings SSI Special Issue*. Solid State Ionics **252**, SSPC-16 Conference Proceedings SSI Special Issue, 1 –, 2013.

⁴⁸D. Damasceno Borges, K. Malek, S. Mossa, G. Gebel, and A. A. Franco. *Effect of Surface Hydrophilicity on the Formation of Nafion Thin Films Inside PEMFC Catalyst Layers: A Computational Study*. ECS Trans. **45**, 101–108, 2013^{*}.

⁴⁹D. Damasceno Borges, A. A. Franco, K. Malek, G. Gebel, and S. Mossa. *Inhomogeneous transport in model hydrated polymer electrolyte supported ultrathin films*. ACS Nano **7**, 6767–73, 2013^{*}.

⁵⁰D. Damasceno Borges, G. Gebel, A. A. Franco, K. Malek, and S. Mossa. *Morphology of Supported Polymer Electrolyte Ultrathin Films: A Numerical Study*. J. Phys. Chem. C **119**, 1201–1216, 2015^{*}.

(topology) of the membrane on transport properties in Nafion; demonstrating the relevance of "model" systems (like ionic surfactant phases), with well-controlled local and long-range order, as facilitated playgrounds for grasping the details of the local structure in Nafion⁵¹; trying to clarify the role played by the soft nature of the hydrophobic confining environments on the properties of absorbed fluids. We note that these issues go beyond the impact of the nature of the interactions with the matrix, and also consider the role played by the flexibility and mobility of the matrix. This is a point which is being increasingly investigated, in colloids science⁵² for instance.

More in details, in Section 2.2 I will describe our work on Nafion thin films formed upon a substrate (or support) with controlled wetting properties. Here two confining environments on water and hydronium ions are present: the substrate, which limits the space available for growth and controls the details of the formation of a low-dimensional system; and the hydrophobic polymer matrix, which delimits the ionic domains available for transport of water and charges. We have given a comprehensive picture of possible morphologies at different water contents and hydrophilicity degree and, most important, have demonstrated highly heterogeneous space-dependent transport properties in different regions of the film. Interestingly, our data allow to speculate about the possibility that this heterogeneity could be the manifestation in a regularized environment of that postulated to exist locally in the (bulk) membrane. I will also give hints about possible future research directions, including the investigation of the mechanical properties of these systems, both in the bulk and in reduced dimension.

The need of simplified systems for investigating the structure/transport interplay in bulk ionomers is the motivation for our work on ionic surfactant phases, which will be detailed in Section 2.3. I will show how it is possible to be extremely precise in the characterization of the static features of the confining matrix and the absorbed fluid, keeping close contact with experimental results. This part will close with some hints about our present work on the transport properties of the absorbed fluid.

In Section 2.4 I will give details about our work on organic solvents mixtures used as electrolytes in Lithium-ion batteries⁵³. Here confinement manifests in a quite uncommon way, in the form of an extremely tight and symmetric coordination shell around lithium, whose chemical composition is determined by extremely long-ranged structural fluctuations. Interestingly, we have discovered that a key point is the mixing of molecules with highly different dipoles: adding to the mixture a component with very low molecular dipole actually increases the total dipole of the solvation sphere around the ion, strongly impacting structure/transport properties. Future investigations include how these static features impact transport of Lithium and the effect of confinement, i.e., the nanostructuring of solvents mixtures at the interface with the electrode or in porous matrices. I will next close with some perspective on the *electrolytes of the future*: ionic liquids.

⁵¹S. Hanot, S. Lyonnard, and S. Mossa. *Water confined in self-assembled ionic surfactant nano-structures*. *Soft Matter* **11**, 2469–2478, 2015★.

⁵²G. L. Hunter, K. V. Edmond, and E. R. Weeks. *Boundary Mobility Controls Glassiness in Confined Colloidal Liquids*. *Phys. Rev. Lett.* **112**, 218302, 2014.

⁵³I. Skarmoutsos, V. Ponnuchamy, V. Vetere, and S. Mossa. *Li+ Solvation in Pure, Binary, and Ternary Mixtures of Organic Carbonate Electrolytes*. *J. Phys. Chem. C* **119**, 4502–4515, 2015★.

1.4.2 Topic B: Heat & sound at the nanoscale

In Chapter 3 I will describe my work on vibrational excitations in hard matter, both in glasses and superlattices^{54–57}. These latter, in particular, are nanostructured materials configurations increasingly adopted in many modern technologies (thermal management in electronic devices or thermoelectric energy conversion) where extremely low thermal exchanges, even below the amorphous limit, are crucial. This need obviously implies an in-depth understanding of heat and sound transport at the nanoscale in the former.

In this case there is no transfer of mass or charge, as in Topic A, but rather of vibrational energy. Interestingly, it turns out that transport phenomena of vibrational excitations are determined by their constrained evolution in an heterogeneous medium. More precisely, in glasses (Section 3.2), transport of sound and heat is controlled by interaction with regions randomly distributed in space and characterized by locally heterogeneous elastic response to mechanical perturbations (some regions are softer, others harder). In superlattices (Section 3.3), in contrast, the relevant heterogeneity is concentrated at the interfaces between layers with different chemical composition. This controls the features of the vibrational excitations, and a wise design of the material, allows to devise (meta)-structures which conduct heat as efficiently as a crystal in one plane, and worse than a glass in the orthogonal direction. I will conclude with some hints on future research directions, including unusual configurations, like systems evolving on curved substrates (e.g., the surface of a sphere), or applications to active matter.

⁵⁴H. Mizuno, S. Mossa, and J.-L. Barrat. *Measuring spatial distribution of the local elastic modulus in glasses*. Phys. Rev. E **87**, 042306, 2013^{*}.

⁵⁵H. Mizuno, S. Mossa, and J.-L. Barrat. *Elastic heterogeneity, vibrational states, and thermal conductivity across an amorphisation transition*. Europhys. Lett. **104**, 56001, 2013^{*}.

⁵⁶H. Mizuno, S. Mossa, and J.-L. Barrat. *Acoustic excitations and elastic heterogeneities in disordered solids*. Proc. Natl. Acad. Sci. U. S. A. **111**, 11949–11954, 2014^{*}.

⁵⁷H. Mizuno, S. Mossa, and J.-L. Barrat. *Beating the amorphous limit in thermal conductivity by superlattices design*. arXiv preprint arXiv:1503.04080, 2015^{*}.

Chapter 2

A. Inhomogeneous structure and transport in electrolytes

Electrolytes play a crucial role in both fuel cells and batteries. In particular, the details of their nano-structuration profoundly impact the transport properties of charges and, therefore, devices performances.

2.1 Fuel cells & batteries

Energy issues. – Energy production and consumption based on combustion of fossil fuels have a severe impact on economy and implies important ecological issues. The development of a "hydrogen economy"⁵⁸ is, therefore, a largely shared dream, as it is based on the use of electrochemical energy production as an alternative energy source. Systems for electrochemical energy storage and conversion include batteries, fuel cells and electrochemical capacitors⁵⁹. The idea is to exploit these devices in an integrated green energy system, where photovoltaic energy is used to produce hydrogen by electrolysis of water. Hydrogen is in turn fed into fuel cells to produce electric energy, which is stored in storage devices like batteries or super-capacitors. Although the energy storage and conversion mechanisms are different, there are strong similarities among these devices. Conceptual or technological advances for any of them one is therefore expected to have significant cross-fertilisation impact on the development of the others.

Computer simulation: why and which one? – Materials found to be effective for use in novel energy devices are *nanostructured*⁶⁰, i. e., they show unusual features combining simultaneously *bulk & surface* properties. Also, they are *multi-scale*, in the sense that their behaviour is non trivial on a multiplicity of mutually connected length and time scales. Characterization and optimisation therefore imply the control of physical processes ranging from the scale of the single atom to that of the entire device. As a consequence, attacking experimentally the above difficulties cannot be just based on macroscopic techniques. Recently these traditional approaches have therefore been increasingly complemented by cutting-edge modern techniques, able to shed light on system properties at the microscopic level. Indeed, advanced spectroscopy and scattering techniques, including

⁵⁸M. Eikerling, A. Kornyshev, and A. Kucernak. *Driving the hydrogen economy*. *Physics World* **20**, 32, 2007.

⁵⁹M. Winter and R. J. Brodd. *What are batteries, fuel cells, and supercapacitors?* *Chem. Rev.* **104**, 4245–4270, 2004.

⁶⁰A. S. Aricò, P. Bruce, B. Scrosati, J.-M. Tarascon, and W. Van Schalkwijk. *Nanostructured materials for advanced energy conversion and storage devices*. *Nat. Mater.* **4**, 366–377, 2005.

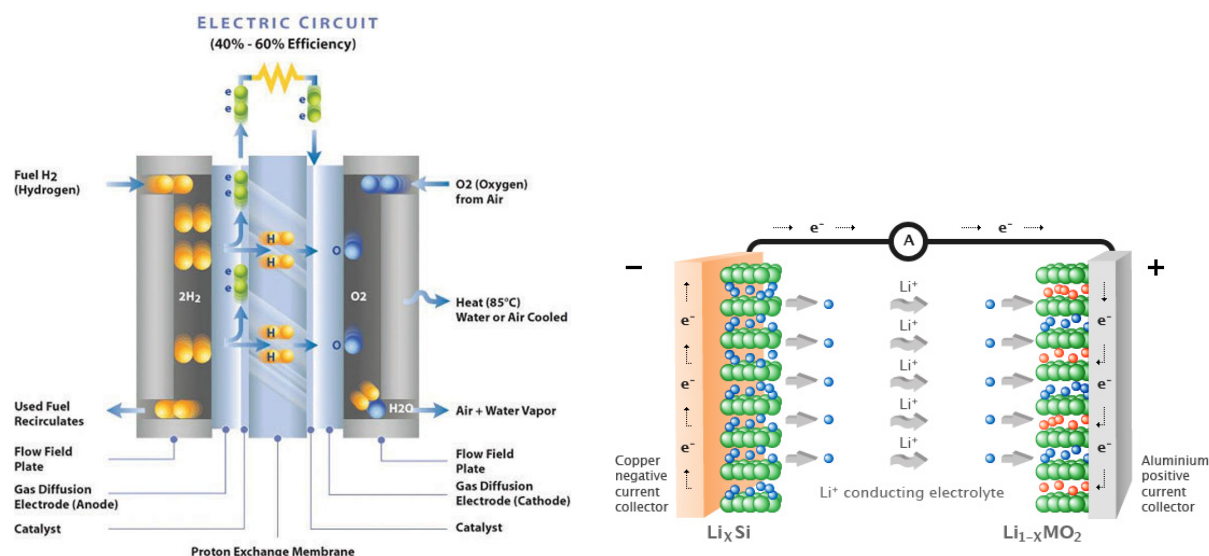


Figure 2.1: *Left*: A polymer electrolyte membrane fuel cell. The functioning principle is briefly described in the text. We focus on the proton-conducting polymer electrolyte membrane, both in the bulk and at the boundaries close to the catalyst layer. Points of scientific interest include both the understanding of details of the microscopic structure of the phase separated domains and the correlated transport of water molecules and protons. *Right*: A Lithium-ion battery. We study the coordination properties of the ion when immersed in heterogeneous mixtures of organic solvents. These have important impact on both ionic transport in the electrolyte and intercalation processes at the electrodes.

Neutrons and X-Rays elastic and inelastic scattering, have allowed to access an extremely large range of length and time scales⁶¹. However, without the help of theory the systems responses to those experimental probes are often difficult to interpret.

Modelling and computer simulations can help to clarify these issues, as they do in all branches of nanotechnology⁶². Available computational techniques range from ab-initio quantum mechanical calculations to phenomenological simulation of the performances of the entire device, going through classical atomistic and mesoscopic molecular dynamics simulations (Monte Carlo techniques also play an important role)⁶³. This approach has led to some improvements, but it is still quite recent and, apparently, has not contributed to impressive advances in the characterization of those materials. We believe that this is mainly due to a chemical-engineering-like approach, which focuses on particular materials of technological interest in view of direct applications. This point of view has a severe drawback: an overwhelming emphasis put on particular chemical structures, with no sufficient attention to universal physical properties. This is, in contrast, the realm of modern statistical mechanics of complex systems.

Our choice is therefore to consider molecular dynamics simulation of simple coarse-grained models. We trade an acceptable degradation of spatial resolution for less mobile or relevant interacting units for a complete molecular description of the most important objects. This allows to

⁶¹G Gebel and O Diat. *Neutron and X-ray Scattering: Suitable Tools for Studying Ionomer Membranes*. *Fuel Cells* **5**, 261–276, 2005.

⁶²M. Lundstrom, P Cummings, and M Alam. “Investigative Tools: Theory, Modeling, and Simulation” in: *Nanotechnology Research Directions for Societal Needs in 2020*. Springer, 2011. 29–69

⁶³J. A. Elliott and S. J. Paddison. *Modelling of morphology and proton transport in PFSA membranes*. *Phys. Chem. Chem. Phys.* **9**, 2602–2618, 2007.

constantly keep the possibility of following the evolution of the most important degrees of freedom and grasping the crucial mechanisms at stake, rather than focusing on chemical details. Emphasis is, therefore, not on the details of the interactions among the systems units but, rather, on universal processes controlled by the generic nature of involved forces (e. g., hydrophilic/hydrophobic, long-/short-range).

Fuel Cells. – Polymer electrolyte fuel cells^{64–68} (PEMFC) (see Fig. 2.1 left) are complex devices constituted by soft and hard materials, which are characterized by heterogeneous nano-structure and transport properties. PEMFCs essentially perform reverse electrolysis of water and are based on the use of modern proton-conducting polymer electrolyte membranes⁵⁸. Hydrogen is the fuel, which is oxidized in the catalyst layer at the anode. The resulting protons and electrons follow separated paths to the cathode. Because the membrane is electrically insulating, electrons are forced to circulate in an external circuit, supplying power. In contrast, protons cross the membrane and recombine with air (oxygen), to produce water⁶⁹. The catalyst layers are the interfacial regions between the membrane and the electrodes, and play a crucial role, controlling the electrochemical behaviour of hydrogen gas at the anode, and oxygen at the cathode.

The membrane must therefore be an insulator against electrons transport, promote proton conductivity also in low hydration and high temperature conditions, and be mechanically stable. The most successful material used in these days is Nafion⁷⁰ which, upon hydration, phase-separates in hydrophobic and hydrophilic domains. The former provide mechanical strength, while the latter result in regions available for transport of water and protons. While the macroscopic structure of Nafion has been probed in depth, some details of the nano-structure still remain controversial^{71–73}. Two main correlated issues must be investigated in-depth and optimized in view of applications⁶⁷: 1) transport of protons^{66,74,75} within an aqueous environment, to be understood at the molecular level, and 2) details of structure and topology of the percolating network formed by the water-filled domains.

Protons transport is a phenomenon ubiquitous in Nature, ranging from advanced synthetic materials to living systems in biology. It takes place via structural and classical diffusion. In struc-

⁶⁴K.-D. Kreuer. *On the Development of Proton Conducting Materials for Technological Applications*. Solid State Ionics **97**, 1–15, 1997.

⁶⁵K.-D. Kreuer. *On the Development of Proton Conducting Polymer Membranes for Hydrogen and Methanol Fuel Cells*. J. Membrane Sci. **185**, 29–39, 2001.

⁶⁶K.-D. Kreuer, S. J. Paddison, E. Spohr, and M. Schuster. *Transport in proton conductors for fuel-cell applications: simulations, elementary reactions, and phenomenology*. Chem. Rev. **104**, 4637–4678, 2004.

⁶⁷M. Eikerling, A. A. Kornyshev, and E. Spohr. “Proton-conducting polymer electrolyte membranes: water and structure in charge” in: *Fuel Cells I*. Springer, 2008. 15–54

⁶⁸A.-C. Dupuis. *Proton Exchange Membranes for Fuel Cells Operated at Medium Temperatures: Materials and Experimental Techniques*. Prog. Mater. Sci. **56**, 289–327, 2011.

⁶⁹M. Eikerling, A. A. Kornyshev, and A. R. Kucernak. *Water in polymer electrolyte fuel cells: Friend or foe?* Physics Today **59**, 38–44, 2006.

⁷⁰K. A. Mauritz and R. B. Moore. *State of understanding of Nafion*. Chem. Rev. **104**, 4535–4586, 2004.

⁷¹T. D. Gierke, G. E. Munn, and F. C. Wilson. *The Morphology in Nafion Perfluorinated Membrane Products, as Determined by Wide- and Small-Angle X-Ray Studies*. J. Polym. Sci., Polym. Phys. Ed. **19**, 1687–1704, 1981.

⁷²L. Rubatat, G. Gebel, and O. Diat. *Fibrillar Structure of Nafion: Matching Fourier and Real Space Studies of Corresponding Films and Solutions*. Macromolecules **37**, 7772–7783, 2004.

⁷³K. Schmidt-Rohr and Q. Chen. *Parallel Cylindrical Water Nanochannels in Nafion Fuel-Cell Membranes*. Nat. Mater. **7**, 75–83, 2007.

⁷⁴S. Paddison. *Proton conduction mechanisms at low degrees of hydration in sulfonic acid-based polymer electrolyte membranes*. Annu. Rev. Mater. Res. **33**, 289–319, 2003.

⁷⁵C. Knight and G. A. Voth. *The curious case of the hydrated proton*. Acc. Chem. Res. **45**, 101–109, 2011.

tural (Grotthuss) diffusion, excess protons diffuse through the hydrogen bonds network of water molecules, via the formation or breaking of covalent bonds. In the classical diffusion process, the proton can move over microscopic distances, together with a number of water molecules (electro-osmotic drag). Due to the classical character of our molecular dynamics simulation methods, the former mechanism is absent in our description.

The micro-structure of the membrane is an other very complex issue. When hydrated, the membrane forms a disordered soft charged confining environment. Details of the local organization and topology of this confining matrix are controversial (see for instance Ref.⁷⁶). They are strongly dependent on the water content and substantially affect both diffusion mechanisms detailed above.

Lithium-ion batteries. – Energy storage is a the crucial energy-related issue of the future. Indeed, the demand for portable power applications is increasing, thus giving considerable drift to the development of novel electrochemical devices, such as electric double-layer capacitors and Lithium-ion (Li^+) batteries. These latter are very common in consumer electronics, such as laptop computers and cell phones, while they are also growing in popularity for automotive applications, to decrease the greenhouse gas emissions in the atmosphere and prevent global warming⁷⁷. In general Lithium-ion batteries can be deployed in a wide spectrum of energy storage applications, ranging from energy-type batteries of a few kilowatts per hour in residential systems with rooftop photovoltaic arrays, to multimegawatt containerized ones, for the provision of grid ancillary services.

All batteries are composed of two electrodes with an intercalated ion-conductive material, the electrolyte⁷⁷. The two electrodes have different chemical potentials, determined by the chemical reactions taking place at each one. When the electrodes are connected through an external device, electrons flow from the more negative to the more positive potential. Ions are therefore transported through the electrolyte, maintaining the charge balance, and electrical energy flows in the external circuit. In secondary (rechargeable) batteries, a larger voltage applied in the opposite direction can cause the battery to recharge.

Li-ion cells mainly employ intercalation materials as positive and negative electrodes and aprotic electrolytes to conduct Li^+ (see Fig. 2.1 right). The chemical nature of the electrodes determines the energy output, while the electrolyte affects the rate of the energy release by controlling mass transport properties within the battery⁷⁸. The interactions between the electrolyte and the electrode materials are also very important, and the formation of electrified interfaces between them often dictates the performance of the device.

An electrolyte must meet a list of minimal requirements in order to be used in such devices. In general it should be a good ionic conductor and electronic insulator, have a wide electrochemical window, exhibit electrochemical, mechanical, and thermal stability, and be environmentally friendly and inert to other cell components such as cell separators, electrode substrates, and cell packaging materials. The interest in clarifying the impact of the properties of solvents, both organic solvents and ionic liquids, on transport of lithium, is therefore obvious. In our work we point in this direction, as we will see below.

⁷⁶K.-D. Kreuer and G. Portale. *A Critical Revision of the Nano-Morphology of Proton Conducting Ionomers and Polyelectrolytes for Fuel Cell Applications*. *Adv. Funct. Mater.* **23**, 5390–5397, 2013.

⁷⁷M. Armand and J.-M. Tarascon. *Building better batteries*. *Nature* **451**, 652–657, 2008.

⁷⁸K. Xu. *Nonaqueous liquid electrolytes for lithium-based rechargeable batteries*. *Chem. Rev.* **104**, 4303–4418, 2004.

2.2 Heterogeneous water transport in Nafion thin-films

Although some details of the phase separation of Nafion in the bulk are still debated, an urgent issue is clarifying how the ionomer organizes in the catalyst layer. We begin by discussing our investigation of structure and transport in Nafion thin-films in contact with a substrate with controlled wetting properties. Interestingly, our data point to a highly inhomogeneous character of transport, which should survive in some form in the bulk. This allows us to introduce our work on ionic surfactant phases, recently recognized as promising model phases for the local structure of the polymeric ionomer.

From the catalyst layer to supported thin-films. – The *catalyst layer*⁷⁹ is the complex interface region between the electrode and the membrane (see Fig. 2.1 left), which forms in an uncontrolled fashion during the fabrication process. Here, carbon supported platinum nanoparticles mix with the ionomer and self-organize into extremely heterogeneous structures. In those regions, Nafion can be found as an ultra-thin film, coating the catalyst and the catalyst support surfaces. Despite significant efforts in the understanding of the bulk Nafion morphology, only a few studies have been devoted to the structure of the hydrated ionomer ultra-thin films formed at the interfaces with platinum and carbon. Indeed, the ionomer is expected to self-organize in different forms, depending on substrate properties such as chemical composition, geometry and, ultimately, wetting behaviour. The features of the film have significant impact on many processes including, among others, the electrochemical double layer structure with the associated charge distribution, proton conductivity, diffusion of reactants and products, degradation kinetics of platinum and carbon support which, in turn, can impact the effective electro-catalytic properties^{80,81}.

Computer simulations that have been used for a better understanding of the catalyst layer structure^{82–86} are based on very detailed modeling of the solid phase in contact with the hydrated ionomer, both at the level of nano-structure and heterogeneity of interactions. In our work we have chosen a different approach, which focuses very little on chemical details but aims at grasping the main general physical features. This strategy has been successfully applied in studies of molecular liquids, like pure water in contact with infinite structured walls⁸⁷, or even simple atomic supercooled liquids^{88,89}. We have therefore considered a mean-field-like interaction ionomer/substrate,

⁷⁹J. Zhang. *PEM Fuel Cell Electrocatalysts and Catalyst Layers: Fundamentals and Applications*. Springer, 2008.

⁸⁰A. A. Franco, ed. *Polymer Electrolyte Fuel Cells: Science, Applications and Challenges Advances in Computer Simulation*. Pan Stanford Publishing Pte. Ltd., Singapore, 2013.

⁸¹K. Malek and A. A. Franco. *Microstructure-Based Modeling of Aging Mechanisms in Catalyst Layers of Polymer Electrolyte Fuel Cells*. *J. Phys. Chem. B* **115**, 8088–8101, 2011.

⁸²K. Malek, M. Eikerling, Q. Wang, T. Navessin, and Z. Liu. *Self-Organization in Catalyst Layers of Polymer Electrolyte Fuel Cells*. *J. Phys. Chem. C* **111**, 13627–13634, 2007.

⁸³K. Malek, T. Mashio, and M. Eikerling. *Microstructure of Catalyst Layers in PEM Fuel Cells Redefined: A Computational Approach*. *Electrocatalysis* **2**, 141–157, 2011.

⁸⁴T. Mashio, K. Malek, M. Eikerling, A. Ohma, H. Kanesaka, and K. Shinohara. *Molecular Dynamics Study of Ionomer and Water Adsorption at Carbon Support Materials*. *J. Phys. Chem. C* **114**, 13739–13745, 2010.

⁸⁵J. Liu, M. Selvan, S. Cui, B. Edwards, D. Keffer, and W. Steele. *Molecular-Level Modeling of the Structure and Wetting of Electrode/Electrolyte Interfaces in Hydrogen Fuel Cells*. *J. Phys. Chem. C* **112**, 1985–1993, 2008.

⁸⁶M. E. Selvan, Q. He, E. M. Calvo-Muñoz, and D. J. Keffer. *Molecular Dynamic Simulations of the Effect on the Hydration of Nafion in the Presence of a Platinum Nanoparticle*. *J. Phys. Chem. C* **116**, 12890–12899, 2012.

⁸⁷N. Giovambattista, P. G. Debenedetti, and P. J. Rossky. *Effect of Surface Polarity on Water Contact Angle and Interfacial Hydration Structure*. *J. Phys. Chem. B* **111**, 9581–9587, 2007.

⁸⁸P. Scheidler, W. Kob, and K. Binder. *Cooperative Motion and Growing Length Scales in Supercooled Confined Liquids*. *Europhys. Lett.* **59**, 701–707, 2002.

⁸⁹P. Scheidler, W. Kob, and K. Binder. *The Relaxation Dynamics of a Supercooled Liquid Confined by Rough Walls*. *J.*

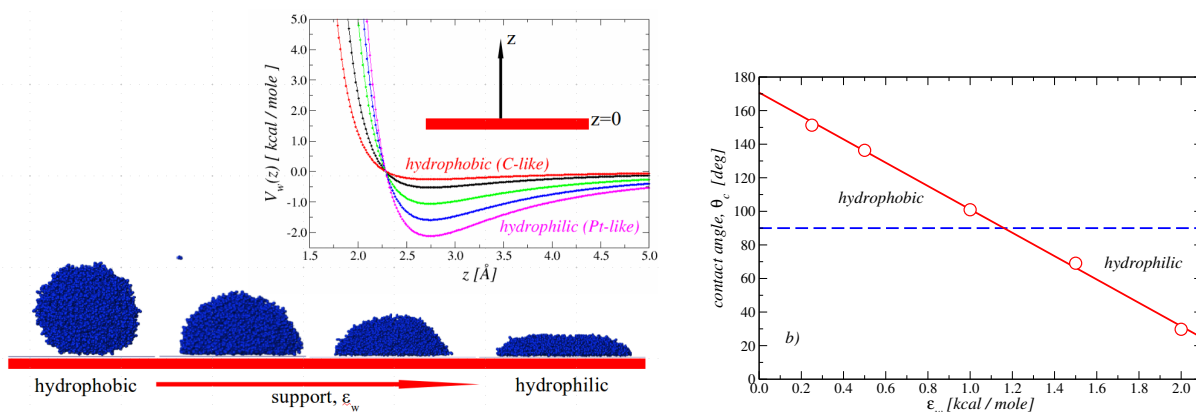


Figure 2.2: *Left*: In the top panel we show $V_w^\alpha(z)$, which only depends on the distance, z , of the unit from the substrate, for values of ϵ_w encompassing hydrophobic to strongly hydrophilic behaviour, from top to bottom. In the bottom panel we show the resulting shapes of droplets of water molecules deposited on substrates with increasing ϵ_w . These data allow to determine the contact angles, θ_c , which are shown in the *Right* Figure (taken from Ref.⁴⁹).

that allows to precisely control the hydrophilic character of the substrate by using a unique tunable control parameter. We have explored self-assembly and thin-film formation of a detailed model for the Nafion ionomer, when placed in contact with unstructured infinite hydrophobic and hydrophilic surfaces (supports), under different hydration conditions^{48–50}. Also, we have focused on transport properties of water molecules, and found evidences of strongly heterogeneous behaviour in different regions of the film.

Modelling the ionomer and the substrate. – Here, we give some information about the interaction potential, providing hints about the modelling style followed. Nafion⁷⁰ is composed by a hydrophobic poly-tetrafluoroethylene backbone with intercalated perfluorinated side chains, which are terminated by a hydrophilic SO_3^- group. An united-atom description was used to represent $CF_{2,3}$ groups in the polymer chain. In contrast, radical sulfonic acids, water molecules and hydronium ions were described with all-atoms resolution. Parameters for the intra-molecular and non-bonded interactions were similar to those of Refs.^{90,91}. Water molecules were described with atomic resolution by the SPC/E model⁹², the model for the hydronium ion was taken from Ref.⁹³.

All system units interact with a smooth unstructured wall (the substrate), placed at $z = 0$ and parallel to the xy -plane, via a 9–3 Lennard Jones potential, $V_w^\alpha(z)$, which only depends on the distance, z , of the unit from the support (see Fig. 2.2 left). The index α identifies complexes (H_2O , H_3O^+ , SO_3^-) with significant dipolar coupling to the (hydrophilic) support ($\alpha = \text{phyl}$), or units corresponding to the hydrophobic sections of the polymer ($\alpha = \text{phob}$) which, in contrast, interact

Phys. Chem. B **108**, 6673–6686, 2004.

⁹⁰A. Venkatnathan, R. Devanathan, and M. Dupuis. *Atomistic Simulations of Hydrated Nafion and Temperature Effects on Hydronium Ion Mobility*. J. Phys. Chem. B **111**, 7234–7244, 2007.

⁹¹T. Masuda, H. Naohara, S. Takakusagi, P. R. Singh, and K. Uosaki. *Formation and Structure of Perfluorosulfonated Ionomer Thin Film on a Graphite Surface*. Chem. Lett. **38**, 884–885, 2009.

⁹²H. J. C. Berendsen, J. R. Grigera, and T. P. Straatsma. *The Missing Term in Effective Pair Potentials*. J. Phys. Chem. **91**, 6269–6271, 1987.

⁹³I. Kusaka, Z.-G. Wang, and J. H. Seinfeld. *Binary Nucleation of Sulfuric Acid-Water: Monte Carlo Simulation*. J. Chem. Phys. **108**, 6829–6848, 1998.

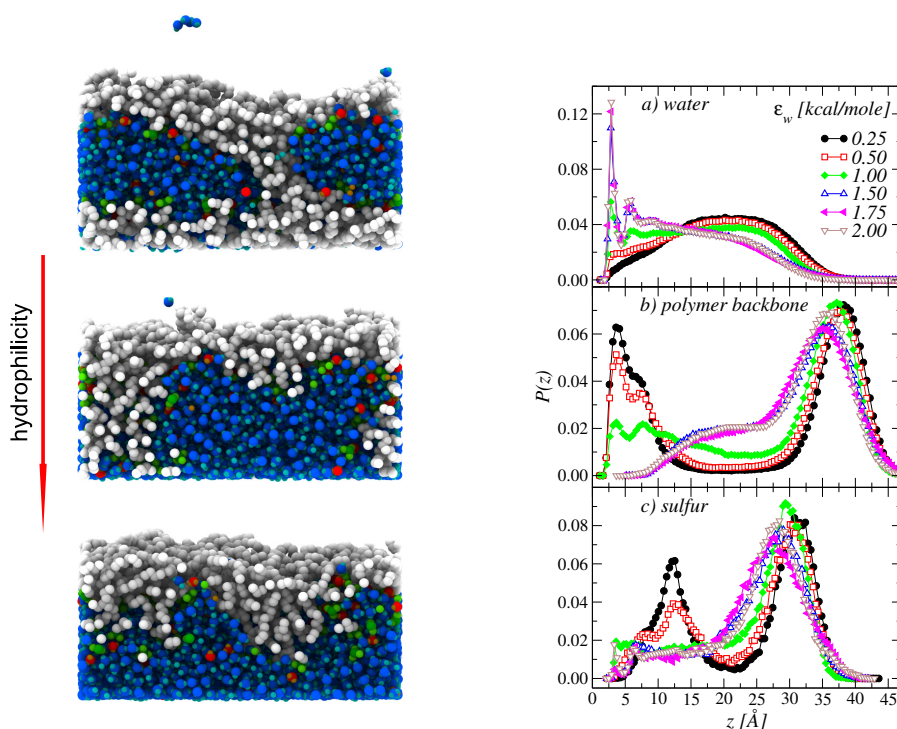


Figure 2.3: *Left*: Snapshots of hydrated Nafion ultra-thin films, at $T = 350$ K and $\lambda = 22$, for an interaction with the support of increasing hydrophilic character ($\epsilon_w = 0.25, 1.0, 2.0$ kcal/mole, from top to bottom). λ is the number of water molecules per sulfonic acid group. We observe the formation of extended water pools (blue) which are separated from the confining polymer matrix (grey) by the charged sulfonic groups interface (green); hydronium complexes are also shown (red). For $\epsilon_w = 2.0$ kcal/mole the ionomer is completely desorbed from the substrate. Note the evaporated water molecules, on the top of the films. *Right*: Mass probability distributions as a function of the distance from the support, z , at the indicated values for ϵ_w . We have considered a) water oxygens, b) polymer backbone units, and c) sulfur atoms. Figures are taken from Ref.⁴⁹.

very mildly. The energy well ϵ_w^{phob} is the same for all units, while $\epsilon_w^{\text{phyl}} = \epsilon_w$ is our control parameter. The typical interaction length scale σ_w^α also is the same in all cases. We calculated for an extended range of values of ϵ_w the values of the contact angle, θ_c , of a droplet of water molecules interacting with the support *via* $V_w^\alpha(z)$ ^{94,95}, and demonstrated that this range encompasses hydrophobic to strongly hydrophilic behaviour (lower to higher ϵ_w , respectively), as shown in Fig. 2.2 right.

Thin-films morphology. – In Fig. 2.3 left we show typical snapshots of the self-organized ionomer ultra-thin film at high hydration, for interactions with the support of increasing hydrophilic character (from top to bottom). We observe the hydrophobic character of the ionomer/air interface⁹⁶ and the formation of extended hydrophilic pools, separated from the confining polymer matrix by an interface decorated with the sulfonate groups. Significant re-organization of the ionomer on

⁹⁴B. Shi and V. K. Dhir. *Molecular Dynamics Simulation of the Contact Angle of Liquids on Solid Surfaces*. J. Chem. Phys. **130**, 034705, 2009.

⁹⁵T Werder, J. H. Walther, R. Jaffe, T Halicioglu, and P Koumoutsakos. *On the Water-Carbon Interaction for Use in Molecular Dynamics Simulations of Graphite and Carbon Nanotubes*. J. Phys. Chem. B **107**, 1345–1352, 2003.

⁹⁶M. Bass, A. Berman, A. Singh, O. Konovalov, and V. Freger. *Surface Structure of Nafion in Vapor and Liquid*. J. Phys. Chem. B **114**, 3784–3790, 2010.

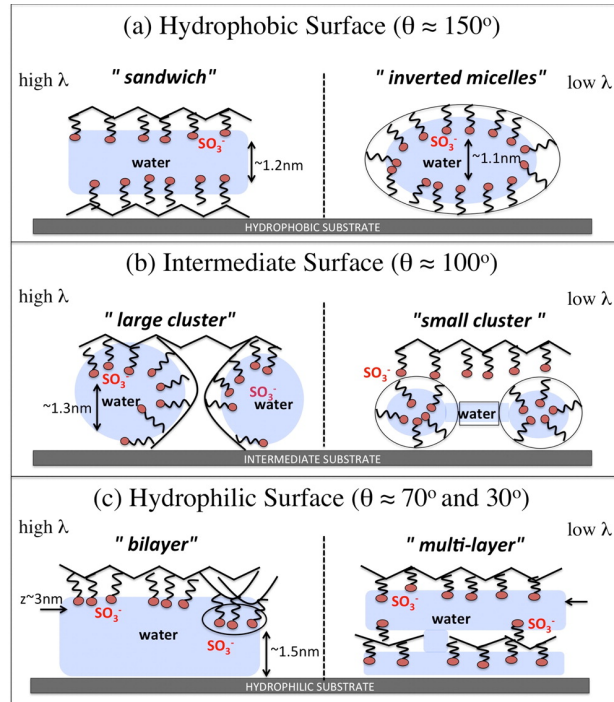


Figure 2.4: Qualitative picture of film morphologies, at different values of θ , ranging from highly hydrophobic (top) to very hydrophilic (bottom) and at different hydration levels λ (high and low hydration on left and right, respectively). Figure is taken from Ref.⁵⁰.

increasing ϵ_w is also visible. In order to quantify these changes, we calculated the mass probability distributions for water, polymer backbone beads and side-chains sulfur atoms, that we plot in Fig. 2.3 right. For the most hydrophobic cases we found a sandwich structure, with a wide water distribution centered at $z \simeq 20$ Å and most part of the polymer in contact with the support and at the open interface with air. Distribution of the sulfonate groups coherently shows two peaks at the ionomer/water interfaces. By increasing ϵ_w , the ionomer abruptly desorbs from the support, inducing a significant re-organization of water domains. Water completely floods the region close to the support, where density layering is observed. A substantial decrease of hydration in regions far from the support is an expected consequence.

With our simplified approach we were able to generate an extremely extended sets of data, in very different conditions⁵⁰. In Fig. 2.4 we summarize our findings for the qualitative dependence of morphology on both the hydration and hydrophilicity level of the substrate. This is to the best of my knowledge, the first comprehensive description of the possible film morphologies that could form at given water content and wetting nature of the substrate. In Ref.⁵⁰ we have also discussed the relevance of our findings on the details of the two interfaces ionomer/support and ionomer/air for fuel cells technology.

Water dynamics is space-dependent. – An important question we could address in our study was how these variable morphologies finally impact the dynamic of the absorbed water. In the inset of Fig. 2.5 left we show the total (self-)diffusion coefficient of the water molecules, in the plane of the substrate and averaged over the entire film (at high λ). The analogous quantity calculated in the (bulk) membrane, far from any boundaries, is also shown. (D of the (pure) water model used

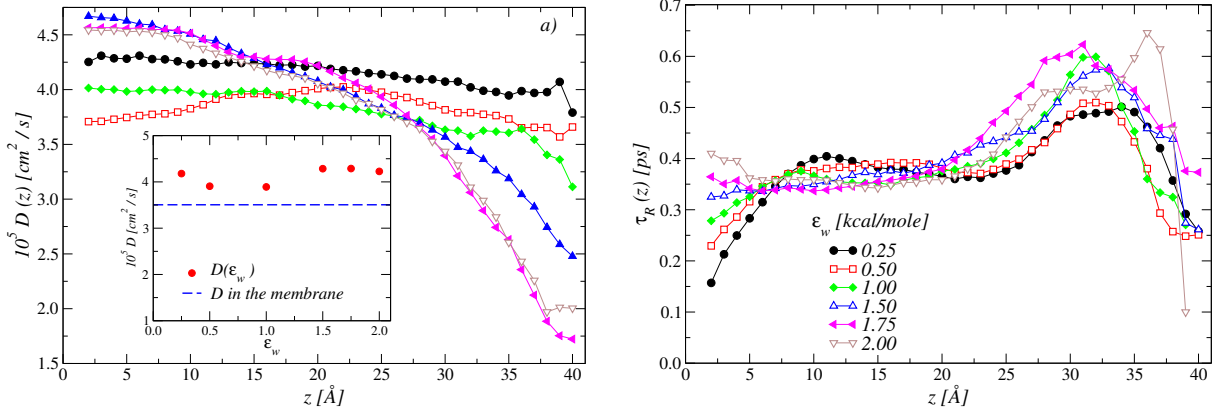


Figure 2.5: *Left*: Water molecules diffusion coefficient at the investigated values of ϵ_w . Inset: Total diffusion coefficient, D , (circles) integrated on the entire film. D is almost constant on the investigated range, but always higher than the value calculated in the membrane (dashed line). Main panel: the space-dependent diffusion coefficient, $D(z)$. The considered values of ϵ_w are indicated in the panel on the right. *Right*: z -dependent rotational relaxation time, $\tau_R(z)$, extracted from an appropriate time-correlation function of the unit vectors normal to the water molecular plane. It is clear a strong correlation with the sulfonate groups mass distribution of Fig. 2.3 right. These Figure are taken from Ref.⁴⁹.

here, in the same conditions of temperature and pressure, is $\simeq 7.9 \times 10^{-5} \text{ cm}^2/\text{s}$.) Interestingly, we observed a diffusion in the film augmented (of about 15%) compared to the membrane, and constant at all values of substrate hydrophilicity degree. Due to the precision of our simulation, we could go much further. From the above structural observations, we predicted an impact of changes in morphology on local mass transport properties of water molecules in different regions within the film. These are, indeed, expected to depend on the interplay between confinement due to the hydrophobic matrix and support, and direct interaction with the sulfonate groups.

To quantify space-dependent transport, we therefore restricted to the xy -plane, sliced the film in overlapping slabs of finite width δz equally spaced by 1 \AA , and considered, together with other time-correlation functions, a generalized form of the mean-squared displacement, $\langle r^2(t, z) \rangle = 1/N \sum_{i=1}^N \langle |\mathbf{r}_i(t) - \mathbf{r}_i(0)|^2 \delta(z_i(0) - z) \rangle$. Here $\langle \rangle$ is the thermodynamic average and $\mathbf{r}_i(t)$ is the xy projection of the three-dimensional position vector of the oxygen atom of water molecule $i = 1, \dots, N$. Only molecules satisfying $z_i(0) = z$ give non-zero contribution to the summation. As a consequence, $\langle r^2(t, z) \rangle$ corresponds to the dynamics of molecules which, at time $t = 0$, were at a distance z away from the support. This clearly gives access to space-dependent information on dynamics. Following this route, we were in the position to define a z -dependent in-plane diffusion coefficient, $D(z)$, via a space-dependent Einstein relation. This strategy has been demonstrated to properly characterize space-dependent translational diffusion in confined geometries^{88,89}.

We plot our data as a function of z in the main panel of Fig. 2.5 left. For the more hydrophobic substrates, $D(z)$ turns out to be quite uniform across the film, and everywhere close to the average total value. This is consistent with a picture where, at high hydration, water is embedded in a crowded confining environment which is anyhow quite homogeneous within the film. In contrast, for higher values of hydrophilicity, we observed dramatic changes, following the accumulation of the ionomer at intermediate and large distances, with the consequent formation of pure water layers at small z . Diffusion clearly becomes strongly heterogeneous, steadily decreasing across the film with a rate which increases with ϵ_w . In the region close to the support, diffusion is enhanced compared to the integrated value, as also reported in the case of simple liquids confined by

smooth boundaries⁸⁸. At intermediate distances, $D(z)$ was close to the integrated values, becoming strongly suppressed at higher distances ($z > 25\text{\AA}$), where interactions with polymer backbones and sulfonate groups are very strong. We checked the validity of these results by extracting a space-dependent structural relaxation time, $\tau(z)$, from a generalized one-particle intermediate scattering function $F_q(t, z)$ (q is the wave-vector).

Even more interesting was the effect of the film nano-structuration on orientational dynamics. In Fig. 2.5 right we show the rotational relaxation time, $\tau_R(z)$, extracted from the space-dependent correlation function of the orientations of the vector normal to the molecular plane of the water molecules (in terms of second order Legendre polynomials). This correlation function is customary used to characterize the orientational dynamics of molecular liquids, and can be measured in light scattering experiments. The effect of the interaction of water molecules dipoles with sulfonate groups is striking, with a non-monotonic modulation of the rotational relaxation time which strictly follows the SO_3^- mass distributions of Fig. 2.3 right. This is a clear evidence that both topology (connectivity) of the confining hydrophobic matrix, *and* direct interaction with the interfaces control dynamics of the absorbed fluid.

Take-home messages. – Our work has been probably the first simulation study aiming at observing simultaneously both the formation of the Nafion thin-film on the substrate and the transport properties of the absorbed fluid, and trying to correlate the two. Moreover, by tuning a single control parameter, the strength of the interaction with the support, we have been able to investigate in a unique framework a variety of environments peculiar of the catalyst layer, ranging from hydrophobic to hydrophilic (representative of carbon and platinum, respectively). We have found that an increase of the hydrophilic character of the support has strong impact on the conformation of the film, which transforms from an irregular lamellar phase (where an extended water pool is sandwiched by ionomer sheets) to a phase-separated configuration, where water floods the interface with the support and polymers accumulate at the top. We have also clarified how all these features vary with the water content, providing clear hints on the morphologies to be expected at given λ by varying the hydrophilicity degree of the substrate.

The intriguing finding that important morphological mutations did not seem to have strong impact on *average* transport features of water molecules, captured our attention. As a consequence, by implying a quite involved analysis of diffusion at different distances from the support, we finally discovered that dynamics for very hydrophilic substrates was highly heterogeneous (space-dependent) across the film. We also showed that the diffusion coefficient is enhanced above the average value in regions close to the support, and strongly suppressed close to the ionomer/air interface, with a rate continuously controlled by ϵ_w . Moreover, very close correlation exists between rotational dynamics and spatial sulfonate groups distribution, highlighting the role played by water molecules located in regions very close to the confining matrix. This is a very important point, that we will address in depth in the future.

Can we help with experiments? – We expect a significant impact of our work on the interpretation of experimental results. Indeed, in our simulations we have access to all available degrees of freedom of the system, at the atomic level. This is in contrast with large part of modern experimental techniques, which measure properties averaged on quite large real-space domains, often providing wave-vectors dependent spectra. Our data can therefore be, in some cases, directly compared with experiments or, most importantly, to be used to rationalize and clarify exceedingly coarse-grained information. Note that, in the case of Nafion thin films, this possibility is even more

beneficial, due to a corpus of available experimental data which is still quite limited.

Experimental techniques which have been employed for the characterization of Nafion thin films include Transmission Electron Microscopy (TEM)⁹⁷. This is able to provide a quite coarse-grained picture of the existing ionic domains, possibly qualitatively comparable with the snapshots of Fig. 2.3 left. More recently, even three-dimensional (tomography) analysis of Nafion layers in fuel cell electrodes have been demonstrated to be now feasible⁹⁸.

Due to the well extended wave-vectors range available in our simulation boxes, a more quantitative comparisons of our data is possible with detailed information about the topology of the ionic domains coming from Neutron reflectivity experiments⁹⁹, or Grazing-Incidence Small-Angle X-ray Scattering (GISAXS)^{97,99,100}. In this case, the mass distributions of the different chemical species shown in Fig. 2.3 right can be used for devising the structural fitting models needed for the interpretation of experimental data. Also, modern Nuclear Magnetic Resonance techniques¹⁰¹, provide information very similar to the rotational observable considered above.

Mechanical properties. – An other interesting direction to explore is the application of our calculations to Atomic Force Microscopy (AFM). In particular, AFM provides very detailed imaging of the structure at the molecular level of the systems of interest here, both in the bulk¹⁰² and in reduced dimensionality¹⁰³. Also, recent advances provide the possibility of a nano-mechanical spectroscopy of soft matter^{104,105}, and simultaneous topographical imaging, elastic constants determinations and compositional mapping are by now possible¹⁰⁶. It would therefore be extremely beneficial to determine directly by simulation the global and local mechanical properties of our polymeric thin-films, and elucidate the role played by the presence of the substrate¹⁰⁷, for instance. Even more intriguing, we could envisage to directly simulate a realistic tip-polymer interaction, in the spirit of Ref.¹⁰⁸. This would allow us to accurately compare elastic moduli calculated directly and those extracted by this approach, or directly correlate local mechanical response to nanoscale

⁹⁷M. A. Modestino, D. K. Paul, S. Dishari, S. A. Petrina, F. I. Allen, M. A. Hickner, K. Karan, R. A. Segalman, and A. Z. Weber. *Self-Assembly and Transport Limitations in Confined Nafion Films*. *Macromolecules* **46**, 867–873, 2013.

⁹⁸M Lopez-Haro, L Guétaz, T Printemps, A Morin, S Escribano, P-H. Jouneau, P Bayle-Guillemaud, F Chandezon, and G Gebel. *Three-dimensional analysis of Nafion layers in fuel cell electrodes*. *Nature Communications* **5**, 2014.

⁹⁹S. Eastman, S. Kim, K. Page, B. W. Rowe, S. Kang, C. L. Soles, and K. G. Yager. *Effect of Confinement on Structure, Water Solubility, and Water Transport in Nafion Thin Films*. *Macromolecules* **45**, 7920–7930, 2012.

¹⁰⁰M. Bass, A. Berman, A. Singh, O. Konovalov, and V. Freger. *Surface-Induced Micelle Orientation in Nafion Films*. *Macromolecules* **44**, 2893–2899, 2011.

¹⁰¹J. Li, J. K. Park, R. B. Moore, and L. A. Madsen. *Linear Coupling of Alignment With Transport in a Polymer Electrolyte Membrane*. *Nat. Mater.* **10**, 507–511, 2011.

¹⁰²T. Awatani, H. Midorikawa, N. Kojima, J. Ye, and C. Marcott. *Morphology of water transport channels and hydrophobic clusters in nafion from high spatial resolution afm-ir spectroscopy and imaging*. *Electrochem. Commun.* **30**, 5–8, 2013.

¹⁰³R. Koestner, Y. Roiter, I. Kozhinova, and S. Minko. *AFM imaging of adsorbed nafion polymer on mica and graphite at molecular level*. *Langmuir* **27**, 10157–10166, 2011.

¹⁰⁴E. T. Herruzo, A. P. Perrino, and R. Garcia. *Fast nanomechanical spectroscopy of soft matter*. *Nature Communications* **5**, 2014.

¹⁰⁵R. Garcia and R. Proksch. *Nanomechanical mapping of soft matter by bimodal force microscopy*. *Eur. Polym. J.* **49**, 1897–1906, 2013.

¹⁰⁶D. Ebeling, B. Eslami, and S. D. J. Solares. *Visualizing the subsurface of soft matter: Simultaneous topographical imaging, depth modulation, and compositional mapping with triple frequency atomic force microscopy*. *ACS Nano* **7**, 10387–10396, 2013.

¹⁰⁷P. C. Chung, E. Glynos, and P. F. Green. *The Elastic Mechanical Response of Supported Thin Polymer Films*. *Langmuir*, 2014.

¹⁰⁸N Onofrio, G. Venturini, and A Strachan. *Molecular dynamic simulation of tip-polymer interaction in tapping-mode atomic force microscopy*. *J. Appl. Phys.* **114**, 094309, 2013.

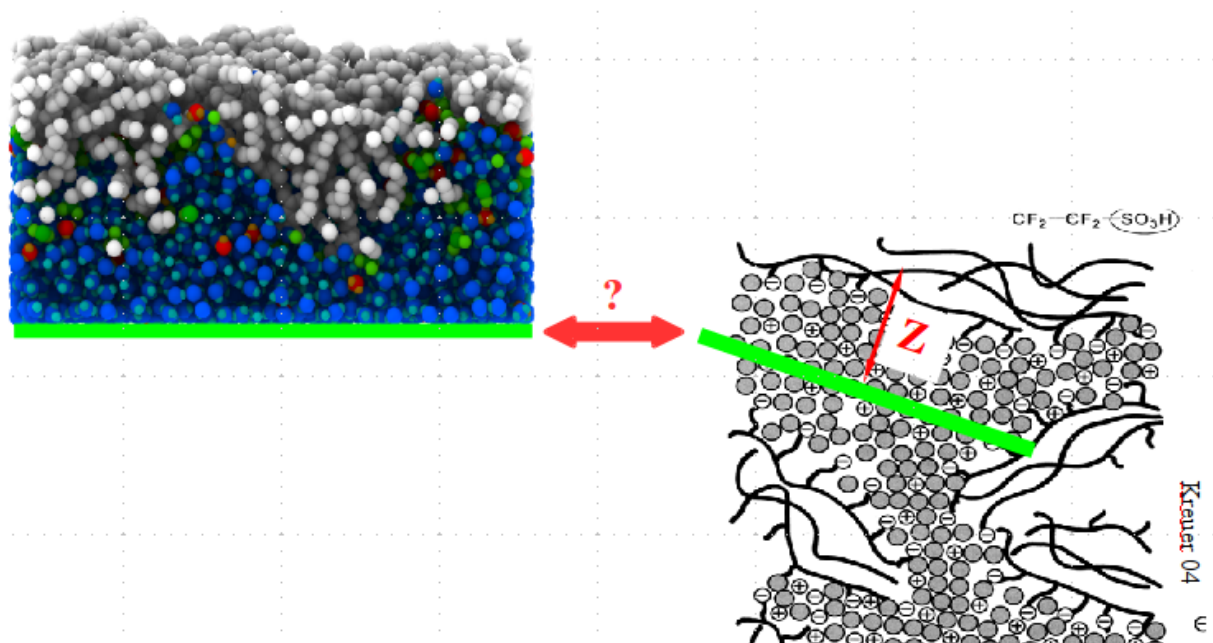


Figure 2.6: From Nafion thin-films to membranes. Highly hydrated ionomer configurations deposited on very hydrophilic substrates (*Left*) could be probably considered as regularized models for the local morphology of ionic domains in the membrane (*Right*), with the substrate substituting the symmetry plane (in green) of the channel available for transport of water and charges.

chemical composition, or transport features.

A suggestive hypothesis. – Our work on thin-films could surprisingly also have implications on our understanding of the interplay transport/nano-structure in (bulk) Nafion membranes. Details of proton and water transport in the ionic domains confined by the Nafion ionomer matrix are still an open issue⁶⁶. Interestingly, recent Quasielastic Neutron Scattering (QENS) spectra¹⁰⁹ have been rationalized in terms of populations of water/hydronium molecules with different (fast/slow) dynamics. It is tempting to speculate about the possibility that those populations could be the manifestation of the inhomogeneous dynamical properties described above. The idea, depicted in Fig. 2.6, is that highly hydrated ionomer configurations deposited on very hydrophilic substrates (as the bottom snapshot of Fig. 2.3 left), could be considered as regularized models for the *local* morphology of ionic domains in the membrane, with the support constituting the symmetry plane of the channel available for transport.

Although this conjecture is tempting, one should be able to detect some form of space-dependent transport heterogeneity directly in the Nafion membrane, which is an additional possibility of future (hard) work. An other option is to make one's life easier and step back to more "comfortable" materials. These should ideally present typical local conformations similar to those of Nafion, with some form of long-range order bringing under better control at least one of the ingredients of the structure/transport interplay issue. This is the main idea in the background of the next Section, where we give some details about our work on ionic surfactant phases.

¹⁰⁹J.-C. Perrin, S. Lyonnard, and F. Volino. *Quasielastic Neutron Scattering Study of Water Dynamics in Hydrated Nafion Membranes*. J. Phys. Chem. C **111**, 3393–3404, 2007.

2.3 Water confined in ionic surfactants nano-structures

Hydrated perfluorooctanesulfonic acids have been recently proposed as valid model phases to clarify the details of the local structural organization in Nafion. We have developed a coarse-grained model for this macromolecule, and investigated in unprecedented details the main features of the confining matrix and of the absorbed fluid, together with the role played by the interfaces.

Ionic surfactants. – Surfactants are molecules that contain hydrophilic and hydrophobic groups¹¹⁰, a peculiar amphiphilic character which is the origin of their outstanding properties and widespread employment for many practical applications¹¹¹. When mixed with water, surfactants self-organize in order to minimize interfacial energies. This self-assembly process is driven by a subtle interplay of attractive and repulsive interactions, leading to the formation of a rich morphology of hydration-dependent structures¹¹⁰. The variable complexity of the observed phase diagrams has been shown to mainly depend on the nature of the hydrophobic tails and the hydrophilic heads¹¹².

In *ionic* surfactants a negative (or positive) charge is located on the hydrophilic head, the total charge of the system being neutralized by the presence of counter-ions. The features of these materials are even more complex than those of non-ionic surfactants, due to the additional long-range coulombic interactions¹¹³. If the solvent used is polar (as water), it acts as a dielectric medium effectively screening the coulombic interactions. The presence of charges influences the molecular interactions and, therefore, surfactant aggregation, generating novel macroscopic properties¹¹¹.

Why do we care? – Our interest in surfactants is mostly due to the observation that they provide well suited model systems for fundamental investigation of the effect of confinement in *soft* hydrophobic environments. In general, transport properties of solvent molecules or solvated ions are highly influenced by confinement at the nano-scale. Size, shape and connectivity of the confining matrix, together with the nature of the charged interfaces and the interplay among hydrophobic, electrostatic and Van der Waals forces, have been shown to significantly alter the fluid properties compared to those of the bulk^{114–118}. Most part of these studies has focused on confinement in hard matrices but, more recently, the interest in soft confinement, where boundaries mobility cannot be

¹¹⁰R. A. Jones. *Soft condensed matter*. IOP Publishing, 2002.

¹¹¹L. L. Schramm, E. N. Stasiuk, and D. G. Marangoni. *Surfactants and their applications*. Annual Reports Section C (Physical Chemistry) **99**, 3–48, 2003.

¹¹²E. Boek, A. Jusufi, H. Löwen, and G. Maitland. *Molecular design of responsive fluids: molecular dynamics studies of viscoelastic surfactant solutions*. J. Phys.: Condens. Matter **14**, 9413, 2002.

¹¹³C. F. Faul and M. Antonietti. *Ionic self-assembly: Facile synthesis of supramolecular materials*. Advanced Materials **15**, 673–683, 2003.

¹¹⁴M. Alcoutlabi and G. B. McKenna. *Effects of confinement on material behaviour at the nanometre size scale*. J. Phys.: Condens. Matter **17**, R461, 2005.

¹¹⁵B. Frick, C. Alba-Simionesco, G. Dosseh, C. Le Quellec, A. Moreno, J. Colmenero, A. Schönhals, R. Zorn, K. Chrissopoulou, S. Anastasiadis, and K. Dalnoki-Veress. *Inelastic neutron scattering for investigating the dynamics of confined glass-forming liquids*. J. Non-Cryst. Solids **351**, 2657–2667, 2005.

¹¹⁶J. C. Rasaiah, S. Garde, and G. Hummer. *Water in Nonpolar Confinement: From Nanotubes to Proteins and Beyond*. Annu. Rev. Phys. Chem. **59**, 713–740, 2008.

¹¹⁷J.-M. Zanotti, K. Lagrené, N. Malikova, P. Judeinstein, K. Panesar, J. Ollivier, S. Rols, M. Mayne-L’Hermite, M. Pinault, and P. Boulanger. *Nanometric confinement: Toward new physical properties and technological developments*. The European Physical Journal Special Topics **213**, 129–148, 2012.

¹¹⁸S. Perkin and J. Klein. *Soft matter under confinement*. Soft Matter **9**, 10438–10441, 2013.

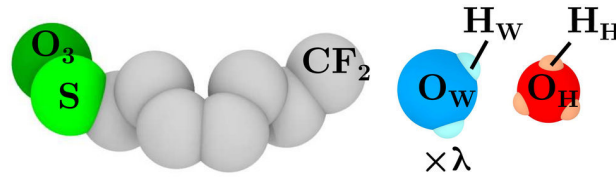


Figure 2.7: Sketch of the geometry of our model for the perfluorooctanesulfonic acid: ionic surfactant (left), water (center), hydronium (right). The geometry of the surfactant molecule is discussed in the main text. The parameter λ indicates the water content, and is defined as the number of water molecules per surfactant. The total positive charge associated to the hydronium complexes neutralizes that (negative) pertaining to the surfactants sulfonic heads. Figure taken from Ref.⁵¹.

neglected, has substantially grown^{52,119}. This is also the case of hydrated Nafion, as we have seen in the previous Section.

PFOSA & Nafion. – The class of *perfluorooctanesulfonic acids* (PFOSA)¹²⁰ surfactants, which feature a highly hydrophobic perfluorinated chain while polarity is provided by the sulfonic acid group, have a particular interest for us. The combination of a perfluorinated backbone and superacid terminal functions favours the formation of a sharp interface between hydrophobic aggregates and the aqueous phase, thus making PFOSA an ideal model system for investigating surfactant self-assembly and solvent properties. More specifically, the quite ordered PFOSA surfactant phases were recently considered as a facilitated playground for clarifying microstructure and transport properties of nanoscopic phase-separated ionomers^{121,122}. In particular, the PFOSA molecule is very similar to the pendant side-chain of Nafion¹²³, which can be extremely useful. Indeed, even the most modern scattering techniques provide averaged spatial information only⁶¹, which does not allow to form a comprehensive consistent picture of both the organization of the materials at the nanoscale and the consequent impact on transport properties. Hydrated sulfonated ionic surfactants have therefore been proposed as model systems for the *local* organization of ionomers, to quantify, among other issues, the effects of well-controlled confining geometries on proton mobility¹²².

Our hybrid description. – We decided to follow this path, and developed a numerical model for ionic surfactants in solution⁵¹, very similar to PFSOA systems. We chose an acceptable degradation of spatial resolution for the surfactants molecules for a complete molecular description of the fluid, keeping the possibility of following the evolution of important degrees of freedom and grasping both the details of the nano-structure of water domains (1-15 Å) and the macroscopic ordering of surfactant aggregates (20-100 Å). This is at variance with the model for Nafion that we used in our study of thin-films, where atomically-resolved structure for the side chains was used⁹⁰.

¹¹⁹L.-M. Wang, F. He, and R. Richert. *Intracellular glass transition and liquid dynamics in soft confinement*. Phys. Rev. Lett. **92**, 095701, 2004.

¹²⁰E. Kissa. *Fluorinated surfactants and repellents*. CRC Press, 2001.

¹²¹S Lyonnard, Q Berrod, B.-A. Brüning, G Gebel, A Guillermo, H Ftouni, J Ollivier, and B Frick. *Perfluorinated surfactants as model charged systems for understanding the effect of confinement on proton transport and water mobility in fuel cell membranes. A study by QENS*. The European Physical Journal Special Topics **189**, 205–216, 2010.

¹²²Q. Berrod, S. Lyonnard, A. Guillermo, J. Ollivier, B. Frick, and G. Gébel. “QENS investigation of proton confined motions in hydrated perfluorinated sulfonic membranes and self-assembled surfactants” in: *EPJ Web of Conferences*. vol. 83 EDP Sciences 2015. 02002

¹²³K.-D. Kreuer. *Ion Conducting Membranes for Fuel Cells and other Electrochemical Devices*. Chem. Mater. **26**, 361–380, 2013.

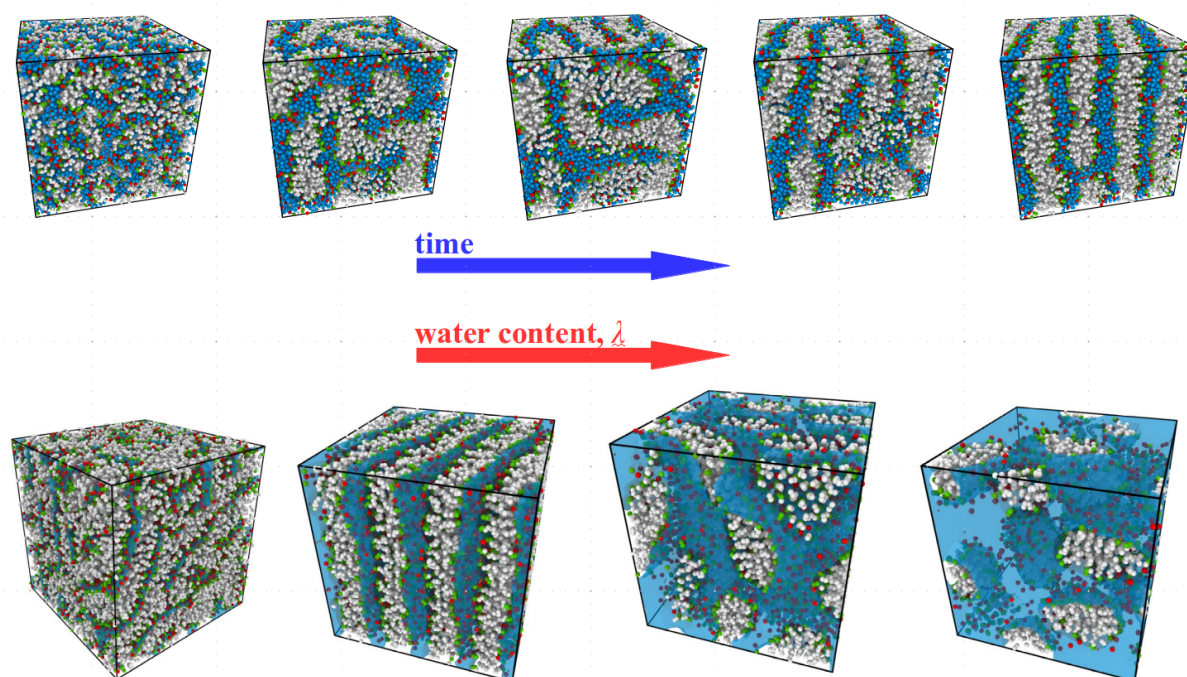


Figure 2.8: *Top*: An example of the time evolution (time window of 4 ns) of the unbiased ordered phase self-assembly, generated by our parametrization starting from a completely disordered system configuration ($\lambda = 4$ in this case). *Bottom*: Typical snapshots of the equilibrated simulation boxes, at hydration levels increasing from left to right ($\lambda = 1, 4, 12, 32$, respectively). The phase behaviour represented by these configurations is discussed in the main text.

We considered a simplified three-components mixture (see Fig. 2.7), formed by the surfactant macro-molecules, the polar solvent (water, W), and the solvated counter-ions (hydronium, H). We chose a united-atoms representation for the surfactant molecule, inspired by the model for the side-chain of Nafion of Ref.¹²⁴. The hydrophobic part of the molecule is represented with a series of 7 Lennard-Jones (LJ) neutral beads, each representing an entire CF_2 group. Similarly, the head group is schematized by two charged LJ beads, one for the sulfur atom S and one for the O_3 group, with a total charge $q = -e$. The physics of the material is controlled by the interplay of: *i*) the energy of the interfaces formed between the amphiphilic aggregates and the fluid phase, and *ii*) the electrostatic interactions among the charged hydrophilic heads and the solvated cations. Developing a good model is tantamount with tuning the relative weights of these two terms, stabilizing the attended phases at different water contents. In order to enhance the formation of well ordered lamellar phases at low hydration, we therefore re-optimized the original values of the parameters controlling the non-bonded interactions. In Fig. 2.8 top we show an example of the very efficient *unbiased* self-assembly generated by our parametrization, starting from a completely disordered system configuration ($\lambda = 4$ water molecules per surfactant). At all hydrations, the initial seed of the final phase formed quite quickly, on time-scales of the order of a few nanoseconds, followed by slow relaxation, to locally optimize mechanical stress.

¹²⁴E. Allahyarov and P. L. Taylor. *Simulation study of the correlation between structure and conductivity in stretched nafion*. J. Phys. Chem. B **113**, 610–617, 2008.

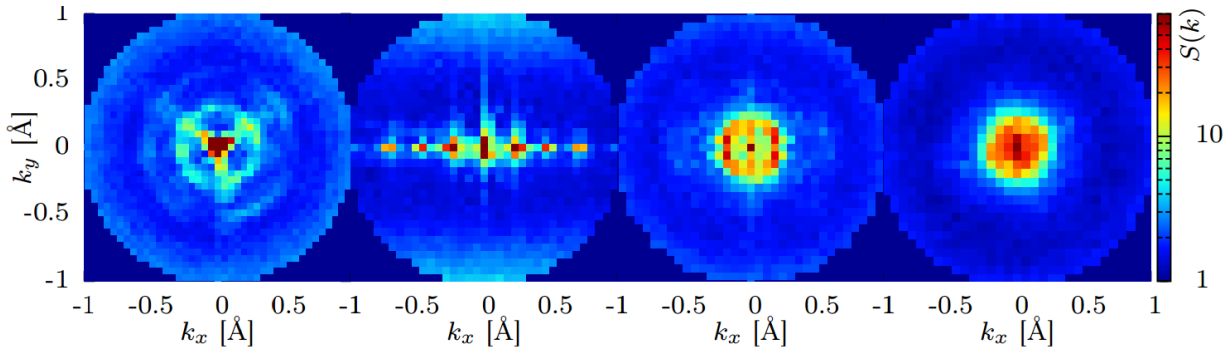


Figure 2.9: Neutrons diffraction patterns calculated from the system units coordinates in different equilibrium phases, at hydration levels increasing from left to right. The intensity is visualized as a color-map in the (k_x, k_y) -plane. From these data we can calculate the Neutrons static structure factors, $S(k)$, by angular averaging. Figure taken from Ref.⁵¹.

The phase diagram. – The phase diagram of our model conforms to that of concentrated amphiphile solutions discussed in many textbooks¹¹⁰. In Fig. 2.8 bottom we show typical snapshots of the system at hydration levels decreasing from right to left. Starting from the highly hydrated systems ($\lambda \geq 16$), we found a micellar solution, with aggregates of different sizes and elongations, concentrating the hydrophobic beads at the center and exposing the sulfonate groups to water. By increasing surfactants concentration ($12 < \lambda < 16$) repulsion between aggregates becomes significant, and micelles start to show an increasingly elongated character. This is due to the fact that, at high density, cylinders pack in space more efficiently than spheres. This process controls the transition for $8 \leq \lambda \leq 12$ to a cylindrical structure with some degree of closed-packed order, although it does not express as a fully developed hexagonal phase. In the intermediate range, $6 \leq \lambda < 8$, cylindrical aggregates merge and start to transform in flat bilayers. Eventually, for $\lambda \leq 4$, surfactants arrange in extremely well-ordered lamellar phases, spanning the entire simulation box, with increasingly thin ionic channels intercalating the lamellae (see discussion below). In the case $\lambda = 0$, notwithstanding the absence of water, the presence of the hydronium complexes is sufficient to drive phase separation with a local disordered lamellar structure.

Altogether, these data demonstrated that our model is able to grasp the overall phase behavior of sulfonated ionic surfactants¹²¹, in a wide range of hydration conditions. In all cases a sharp phase separation was evident, with the charged sulfonic heads decorating the interface between the adsorbed fluid and the hydrophobic sections of the surfactants. Hydroniums were found condensate at the charged interface at the lowest values of λ , while a significant fraction is solvated by water, far from the interfaces at high hydration.

Neutrons diffraction. – The above qualitative description of the phase diagram was completed by characterizing the system organization via the Neutrons scattering static structure factors. We calculated both the diffraction diagrams measured in experiments (color maps in Fig. 2.9) and the angular average, $S(k)$, where k in the wave-vector. For the almost dried system, $\lambda = 0$ (Fig. 2.9 left), we observed strong Bragg peaks on three preferred directions, consistent with the picture of disordered local lamellar arrangements which bend and branch. In the subsequent image ($\lambda = 4$), high intensity spots corresponding to genuine first, second and third-order Bragg peaks, appear at three non-zero positions. These are aligned along a preferential direction, which is characteristic of the lamellar arrangement with long-range order. By increasing hydration, the

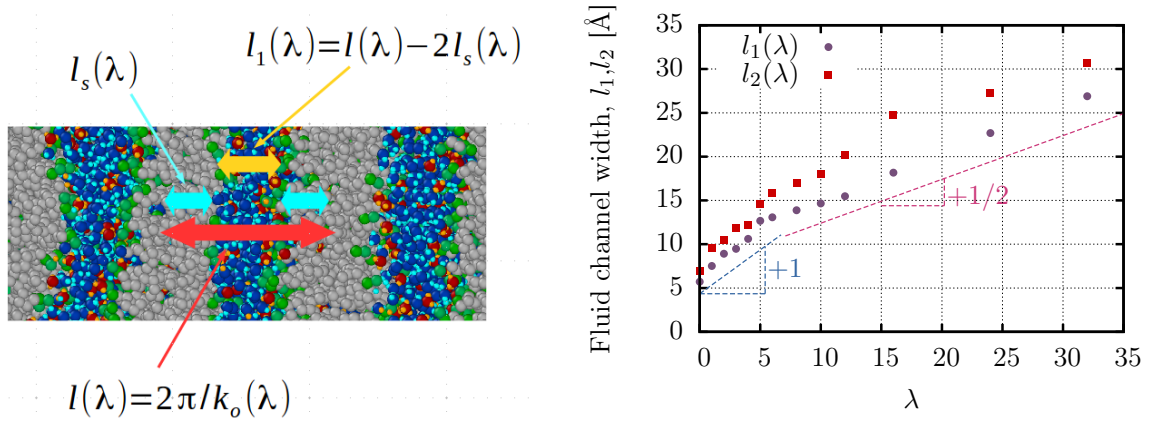


Figure 2.10: *Left*: Graphical scheme for the calculation of $l_1(\lambda)$, detailed in the main text. *Right*: λ -dependence of the size of ionic channels as calculated from the position of the first Bragg peak, l_1 , in the static structure factors and from the direct determination of the aqueous domains extent, l_2 , as discussed in the text. The dashed lines are guides for the eyes, of slope 1 and 0.5 at low and high hydration, respectively. This Figure is taken from Ref.⁵¹.

second and third order peaks fade, indicating a lower degree of order. At the highest hydration, the high-intensity region eventually arranges in a ring-like shape, indicating that no preferred orientational order is present in the system, as expected in the fully developed micellar phase.

The size of the ionic channels. – Interestingly, the *global* spatially-averaged static structure factors $S(k)$ (not shown) provide precise information about *local* geometrical properties of the confining matrices. With our data, we were therefore in the position to quantify the variation of the typical size of the ionic domains available for transport of the absorbed fluid, as a function of the hydration level (see Fig. 2.10 left). Indeed, from the position $k_0(\lambda)$ of the first-order Bragg peak in the $S(k)$, we can extract $l(\lambda) = 2\pi/k_0(\lambda)$, which is commonly associated to the average distance between the centers of mass of the hydrophobic aggregates. From these data we can build $l_1(\lambda) = l(\lambda) - 2l_s(\lambda)$, where l_s is the average end-to-end distance of the surfactants. Helped by Fig. 2.10 left, it is easy to conclude that $l_1(\lambda)$ is an *indirect* measure of the size of the ionic channels. The final data are shown in Fig. 2.10 right, and quantify the swelling behavior of the system. For $\lambda \leq 6$, l_1 increases linearly with λ , with a slope $\simeq 1$. This corresponds to the expected swelling in the lamellar phase (see, for instance, Ref.¹²²), where the distance between surfactant domains increases affinely, following the volume increase of the intercalated fluid. At higher values of λ , a clear cross-over is visible, with l_1 that can be interpolated by a straight line of slope $\simeq 1/2$. Rationalizing this behavior is however difficult, due to the presence of interfaces of increasing curvature and sensible disorder in the distribution of the hydrophobic aggregates.

These data could be further strengthened by a *direct* independent measure of the width of the ionic channels, by computing the distribution of the distances of the fluid molecules (both water and hydronium) to the closest surfactant sulfonated head. From these distributions we estimated the channels sizes, l_2 , as the distance encompassing 99% of the fluid molecules. These data are also shown in Fig. 2.10 right. For $\lambda \leq 6$ we have $l_1 \simeq l_2$, as expected for highly symmetric phases. At higher values of λ , l_2 is always higher than, although of the same order of, l_1 , providing an upper bound to the size of the ionic domains in the presence of disordered curved interfaces.

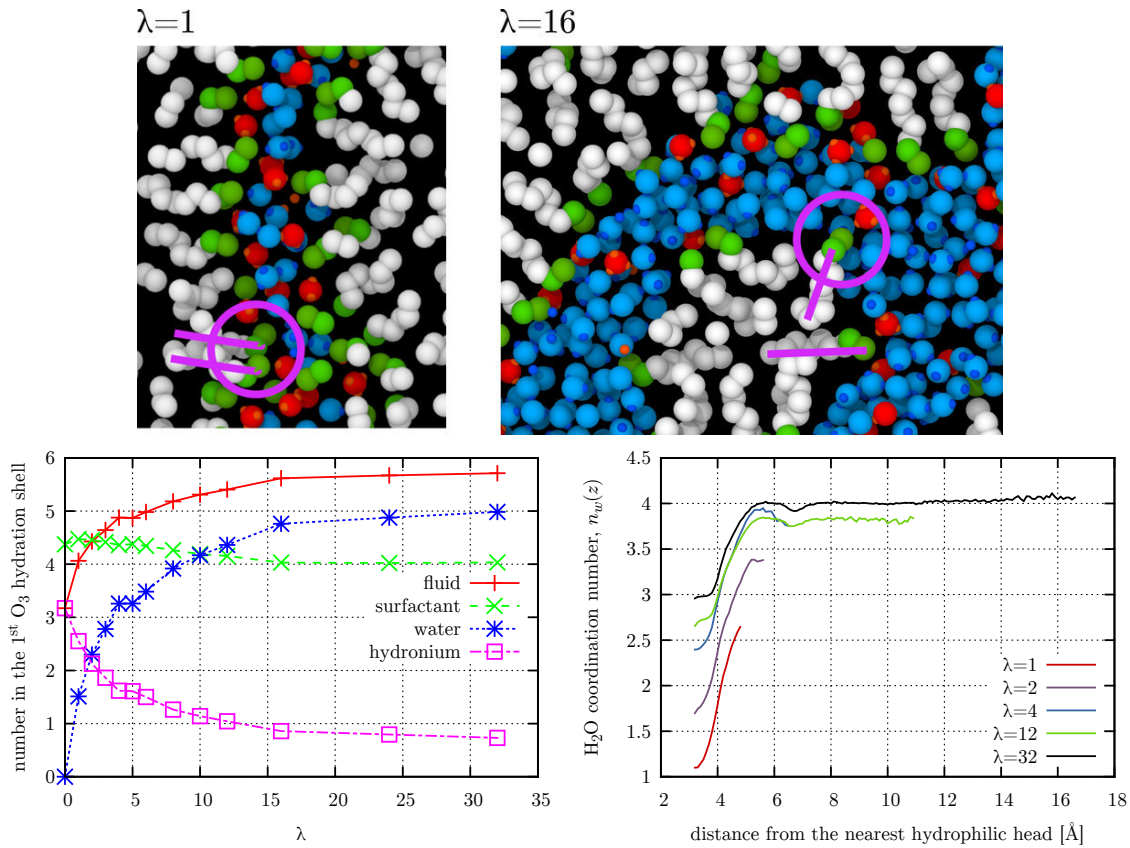


Figure 2.11: *Top*: Details of typical generated interfaces with different curvature radius, together with a schematic representation of the hydration sphere (circles) used for our calculations and the mutual orientations of adjacent surfactants (lines). The snapshot on the left corresponds to $\lambda = 1$ (flat interface), to $\lambda = 16$ that on the right (curved interface). *Bottom*: In the *Left* plot, we show the λ -dependence of the average number of molecules of the indicated species localized into the first coordination shell of the O₃ bead of the surfactant heads. In the *Right* plot, we show the space-dependent water/water coordination number, $n_W(z, \lambda)$, as a function of the distance, z , of the molecule from the closest hydrophilic head, at the indicated values of λ .

Wetting at the interfaces. – Our simulations allowed us to study with unprecedented precision the wetting properties at the interfaces surfactant/water. It is worth to discuss this point in details. In Fig. 2.11 top we show local configurations of the interfaces generated in the (pseudo-)lamellar and micellar phases, respectively. The sketched segments indicate the relative orientations of selected adjacent surfactants, parallel (left) and at a non-zero angle (right). Obviously these conform to the charge distribution geometry at the interfaces, planar in one case and with a finite curvature radius in the other. We can expect the coordination features of both surfactants and fluid molecules, and therefore wetting properties at the interface, to be sensibly different in the two cases.

In Fig. 2.11 bottom-left, we plot the average number of molecules of the different species comprised in the first coordination shell of the surfactant heads, indicated by the circles in the top panel. These data show that, for $\lambda \leq 5$, the first coordination shell of the surfactant heads contains about 4.3 atoms pertaining to surfactant molecules. In the same hydration range, the number of fluid molecules in the shell increases from 3.1 to slightly less than 5. Interestingly, there is no variation of this number between $\lambda = 4$ and 5. More precisely, at $\lambda = 4$ the first shell is saturated

and added water molecules organize far from the interfaces. For $\lambda \geq 5$, we observed that the number of surfactant molecules inside the coordination shell decreases, while it increases for fluid molecules. This is the manifestation of the lamellar-to-cylindrical phase transition. By increasing λ , the system efficiently packs more fluid molecules at the hydrophilic interface, by increasing the tilt angle between adjacent surfactant and, as a consequence, the mutual distance of the sulfonic heads. This curves the exposed interface, giving rise to increasingly well defined cylindrical structures. At $\lambda = 16$, the number of both fluid and surfactant particles in the coordination shell reach limiting values, which show very mild variation at higher degrees of hydration. This is a direct signature of the transition to the micellar phase, where spherical aggregates are dissolved in (bulk) water, with a total surface area of the interfaces almost independent of λ .

The analysis was pushed even further by determining $f_W(\lambda)$, the fraction (over the total number) of water molecules in direct contact with the interface at λ (not shown). In summary, at very low hydration almost all water molecules and hydronium ions are condensed in contact with the nearest hydrophilic head, in very thin ionic layers intercalated between the surfactant planes. For $1 \leq \lambda \leq 4$ we observed an almost linear decrease of f_W , which however still kept a quite high value. Indeed, in that hydration range half of the width of the fluid channel is smaller than or comparable to the radius of the coordination shell, meaning that most part of the added water molecules were placed at the interface. At $\lambda = 5$, where the lamellar order is still present, the fluid channels are no longer spanned by the coordination regions of facing surfactant heads, which are saturated, and additional fluid molecules are therefore placed outside the interfaces. For $\lambda > 5$, the sequence of phase transitions described before occurs, implying the progressive curvature of the interfaces. This effect increases the interfaces area available for fluid adsorption compared to that present in the lamellar phase and controls the reduction of f_W upon hydration, determining a cross-over to a less-than-linear behaviour at high λ .

Space-dependent structure of the absorbed fluid. – The above interface/bulk character of water molecules in different regions of the ionic domains has an important effect on the coordination properties of the absorbed fluid itself. We focused on the water-water average coordination number and its variation at different distances from the interfaces. We first calculated the average coordination number of water molecules, $n_W(\lambda)$ at all considered hydration levels (not shown). At high hydration, we recovered the value of bulk water $n_W \simeq 4$. By decreasing λ , n_W steadily decreases to $n_W \simeq 3$ at $\lambda = 6$, at the boundary with the lamellar phases. Next, due to the increasing extent of affine confinement, the observed decrease was much steeper, and n_W reached a minimum value $\simeq 1.2$ at $\lambda = 1$. At this hydration level, water molecules, hydronium ions and sulfonate groups are intercalated in the ionic channels, organizing in almost mono-planar configurations.

Our simulations allowed us to access even more detailed information, e. g., the space-dependent coordination number of water molecules, in different regions of the ionic channels. In the right panel of Fig. 2.11 bottom, we show the average coordination number of molecules at distance z from the closest sulfonate group, $n_W(z, \lambda)$. These data show that, at all λ 's, $n_w(z, \lambda)$ steadily increases from a highly suppressed value at $z_{min} \simeq 3 \text{ \AA}$ in contact with the interface to a maximum at the λ -dependent z_{max} , at the center of the channels. The overall variation of $n_W(z, \lambda)$ with the distance depends on λ , decreasing from a factor of $\simeq 2.5$ at $\lambda = 1$ to $\simeq 1.3$ for $\lambda = 32$.

The details of the curve corresponding to the highest hydration level are particularly instructive. Indeed, they highlight the presence of three different regions inside the ionic domains, determining the most prominent character of the confined water molecules: *i) bulk-like* at large distances, in the center of the ionic domains and far from any boundaries; *ii) intermediate*, corresponding to

distances where the shallow spatial modulation of n_W is due to the well-known layering of water molecules; and *iii) interface-limited*, where the extent of nano-confinement is so high to completely destroy any resemblance of the hydrated environment with the one in the bulk phase. We expect water molecules in different regions of the ionic channels to be characterized by different dynamical properties and are currently working on this point, as we will see below.

Can we help with experiments? – Interestingly, a nice agreement is found between our data and the experimental results. Neutron and X-rays scattering measurements on PFOSA molecules of size comparable to that of our model were reported recently^{121,122}. The boundaries of the different phases, typical average inter-aggregate correlation distances and overall swelling behaviour originating by the analysis of the two sets of data are similar. Our model is therefore capable of realistically reproducing the PFOSA surfactant solution behaviour. This suggests that it can be used as an *in-silico* partner to the experimental study of a variety of surfactants. For instance, we could easily tune the surfactant length and generate different commercially available materials, as PFHSA (6 carbons) or PFBuSA (4 carbons)¹²⁰. The phase behaviour of these systems being quite universal, we expect limited variations compared to the present case, with the modified length of the surfactants probably controlling the hydration-level location of the different phase boundaries.

Back to Nafion? – An other important outcome of this work is that our model can also be valuably applied to generate and investigate *polymeric* systems, in particular Nafion membranes. More in general, we are now in the position to unify in a single bottom/up computational framework the entire vast class of perfluorinated materials. Indeed, we demonstrated that our re-optimized force-field correctly encodes the phase behaviour and the most important structural features of a PFOSA system. Due to the similarities of the latter with the side chain of Nafion, we can employ this structure as the fundamental building-block to upscale our description to the entire ionomer, by grafting it to a strongly hydrophobic polymer backbone with tuned mechanical properties (*i.e.*, persistence length). This is of course in the same spirit of the original work of Ref.¹²⁴, but with the crucial difference that we can now count on a model with physically-sound behaviour at all length scales, ranging from local lamellar-like structures to long-range organization of ionic and hydrophobic domains. We also note that our approach naturally provides all ingredients for generating a virtually infinite range of composite materials, obtained by doping the ionomer with elongated charged macro-molecules, including ionic liquids^{125,126}.

Sub-diffusion and populations dynamics. – We are currently investigating how the above static features of the confining matrix impact the dynamical properties of the absorbed fluid. Indeed, our model is an efficient tool for elucidating transport of water absorbed in soft charged environments with controlled confining length scales, ranging from almost two-dimensional one-molecular-layer thick arrangements at low water content, to ionic channels several nanometers wide at higher hydration. This should allow us to study in details the dynamical differences between water molecules at the interface, and those outside the hydration layer, which are expected to be increasingly bulk-like. In addition, by varying the water content we should also be able to tune the respective strength

¹²⁵R. Sood, C. Iojoiu, E. Espuche, F. Gouanvé, G. Gebel, H. Mendil-Jakani, S. Lyonnard, and J. Jestin. *Proton conducting ionic liquid doped Nafion membranes: nano-structuration, transport properties and water sorption*. *J. Phys. Chem. C* **116**, 24413–24423, 2012.

¹²⁶F. Lu, X. Gao, S. Xie, N. Sun, and L. Zheng. *Chemical modification of Nafion membranes by protic ionic liquids: the key role of ionomer–cation interactions*. *Soft Matter* **10**, 7819–7825, 2014.

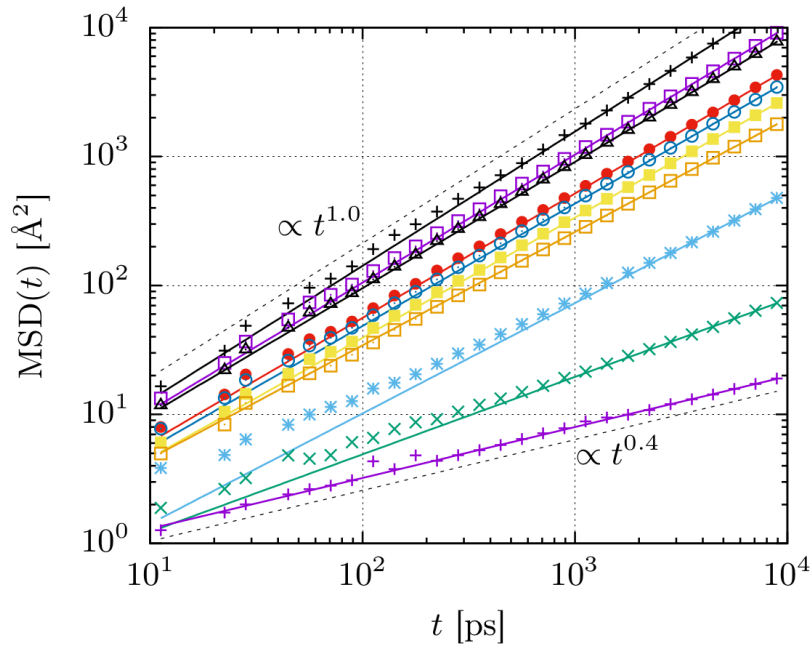


Figure 2.12: Time dependence of the mean-squared displacements of the water molecules at all investigated hydration levels, decreasing from top to bottom. The lines are fits to the data of the form $\langle r^2(t) \rangle \propto t^\alpha$, with $\alpha = 1$ at the highest water content, and $\alpha < 1$ in all other cases, with α decreasing with λ . This is the hallmark of non-Fickian diffusion due to confinement, as discussed in the main text. These data are unpublished.

of these two effects, interpolating between the low hydration condition, where the vast majority of water molecules are accommodated at the interfaces, and the highly hydrated state, where most part of the absorbed fluid is expected to be bulk-like.

We already have some preliminary results, which are very encouraging. First, the mean-squared displacement of the water molecules is found to be linear at long times in the most hydrated case only, while at lower water contents dynamics is *sub-diffusive*, i.e., $\langle r^2(t) \rangle \propto t^\alpha$, with $\alpha = \alpha(\lambda) < 1$ (see Fig. 2.12). The degree of sub-diffusivity is therefore controlled by water content and diffusion is non-Fickian, implying the existence of a length-(time-)scale dependent effective diffusion coefficient, $D_{eff} = \partial_t \langle r^2(t) \rangle / 6 = \alpha \langle r^2(t) \rangle / 6t$. Interestingly, probing D_{eff} at different length scales allows us to reproduce the hydration dependence of the diffusion coefficients extracted from QENS and NMR experiments, which sample the dynamics on short and large length-scales, respectively. Our model therefore seems to provide not only a realistic dynamical behaviour compared to the real system, but also a framework to interpret experimental results, without needing any fitting procedure (beside the determination of α).

Second, we are currently investigating the origin of this average sub-diffusive behaviour and how this impacts the details of the intermediate scattering functions, $F(q, t)$, measured in Neutrons scattering experiments. More in details, we already mentioned that recent QENS data¹⁰⁹ have been rationalized in terms of populations of water/hydronium molecules with different (fast/slow) dynamics. This simple model also seems to work well with our partial spectra, calculated from the signal coming from water molecules only. We can now go much further, and verify the possibility that these two groups could correspond to sub-diffusive water molecules at the interface, and diffusive bulk-like ones outside the hydration layer. Note that this adds space-resolution to our

picture, connecting heterogeneous dynamical behaviour to different regions in the ionic channels, similarly to what we have suggested in the last paragraph of Section 2.2. In addition, based on the analysis of well designed correlation functions which quantify the typical survival times of water molecules at the interface, we also have some evidence that the above partition is dynamical, in the sense that molecules transit between the two groups, with an exchange rate which increases with water content and ultimately fixes the typical (long) time scale measured in experiments. We expect very interesting insight to come from these data.

General take-home message. – The above work possibly deserves an additional remark: our results go beyond the particular (sulfonic) moiety considered. More generally, our model can be seen as a powerful tool for generating efficient self-assembly of soft interfaces with variable degree of curvature. Recent fundamental work^{127–129} has focused on assembly driven by hydrophobic forces, even in the presence of hydrophilic units, as it is the case here. It has been shown that the properties of water molecules at the interface with extended molecular aggregates are certainly controlled by the nature of the interactions between water molecules and the aggregates, but a crucial role is played by the extent of the surface occupied by the aggregates itself. In particular, the associated curvature radius strongly affects the wetting features, or the hydrogen bonding formation. In the limiting case of purely hydrophobic aggregates of large available surface, water molecules at the interface even acquire a gas-like character, with a strongly suppressed interfacial density¹²⁸ and a number of formed hydrogen bonds significantly lower than that in the bulk¹²⁷.

In our surfactants phases the situation is sensibly more complex, with the presence of hydrophilic interactions between surfactant heads and water molecules, and the possibility to form additional hydrogen bonds with both the hydronium complexes condensed at the interfaces and the fully dissociated sulfonated groups. Also, at the lowest hydration degrees, mutual interference between interfaces and extremely tight confinement length scales must be expected. However, our data also point to non-trivial modifications of the character of water molecules, in the presence of interfaces with different degrees of curvature. In particular, the degradation of both average and space-dependent (at different distances from the interfaces) coordination properties are expected to impact structure and life-times associated to the hydrogen bonds network and, in general, transport properties of the adsorbed fluid itself, as we have seen above. In conclusion, we are convinced that this work provides a well-designed general foothold to attack all these issues, which are of paramount importance in modern science, ranging from soft synthetic materials to systems of biological interest^{130,131}.

¹²⁷D. Chandler. *Interfaces and the driving force of hydrophobic assembly*. Nature **437**, 640–647, 2005.

¹²⁸A. P. Willard and D. Chandler. *The molecular structure of the interface between water and a hydrophobic substrate is liquid-vapor like*. arXiv preprint arXiv:1407.4365, 2014.

¹²⁹D. Chandler and P. Varilly. *Lectures on molecular-and nano-scale fluctuations in water*. arXiv preprint arXiv:1101.2235, 2011.

¹³⁰A. R. Bizzarri and S. Cannistraro. *Molecular dynamics of water at the protein-solvent interface*. J. Phys. Chem. B **106**, 6617–6633, 2002.

¹³¹E. Yamamoto, T. Akimoto, M. Yasui, and K. Yasuoka. *Origin of subdiffusion of water molecules on cell membrane surfaces*. Scientific Reports **4**, 2014.

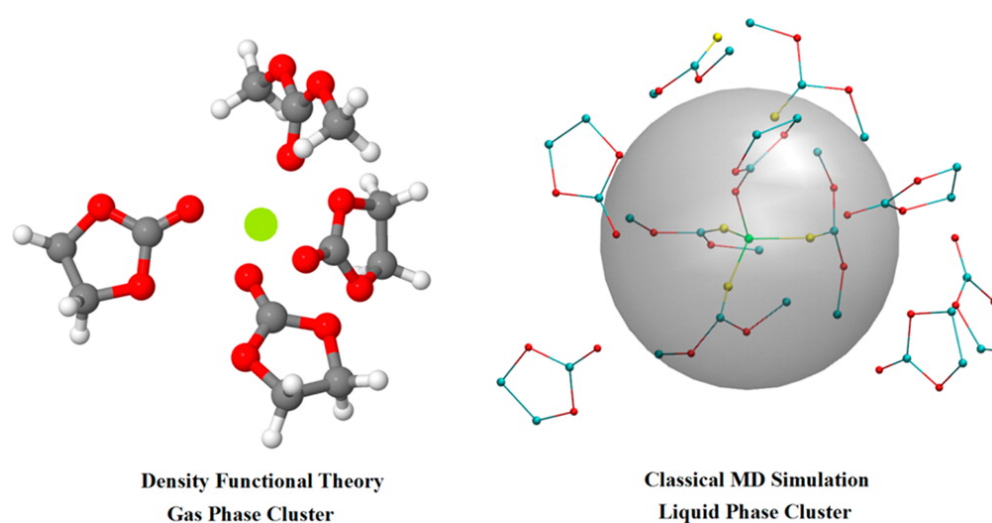


Figure 2.13: Quantum chemical density functional theory (DFT) calculations (Left) and classical Molecular Dynamics simulations (Right) have been employed to investigate the solvation of Lithium cations in pure organic carbonate solvents (ethylene carbonate (EC), propylene carbonate (PC), and dimethyl carbonate (DMC)) and their binary (EC-DMC, 1:1 molar composition) and ternary (EC-PC-DMC, 1:1:3 molar composition) mixtures. Figure is the graphic abstract of Ref.⁵³.

2.4 Electrolytes for Li^+ transport

Non-aqueous electrolytes used in Lithium-ion batteries technology can appear much simpler than the hydrated poly-electrolytes considered in the previous Sections. We have shown that this expectation is not true in the case of mixtures of organic solvents, even at very low Li^+ content.

Organic carbonates-based electrolytes. – The role played by the electrolyte is also crucial in Li^+ ion batteries (see Fig. 2.1 right). As mentioned above, the transport of Li^+ ions inside the electrolyte determines the rate of the energy transfer, which has been stored on the electrodes. By now, the most commonly employed strategy for developing effective electrolytes with optimal properties is to use mixtures of cyclic and non-cyclic organic carbonates¹³². Here, the high dielectric constant of cyclic carbonates is combined with the low viscosity of acyclic carbonates, ensuring good performances under low-temperature conditions. Also, the higher thermal stability of cyclic carbonates guarantees a reasonable operating temperature range for the mixed solvent. According to the present understanding, the transport of Li^+ ions is controlled by a *two-steps* mechanism involving first the solvation of the ions by the solvent molecules, followed by the migration of the solvated ions¹³³. A deeper understanding of the solvation of Li^+ ions is therefore crucial for the rational design of novel electrolytes with improved Li^+ conductivity.

Very recently we have started some work in this direction⁵³, in the aim to clarify the relative stability of possible local arrangements of solvent molecules around lithium, for the cases of pure solvents and binary and ternary mixtures of those. Detailed quantum chemical Density Functional

¹³²G. G. Eshetu, J.-P. Bertrand, A. Lecocq, S. Grugeon, S. Laruelle, M. Armand, and G. Marlair. *Fire behavior of carbonates-based electrolytes used in Li-ion rechargeable batteries with a focus on the role of the LiPF_6 and LiFSI salts*. *J. Power Sources* **269**, 804–811, 2014.

¹³³K. Yuan, H. Bian, Y. Shen, B. Jiang, J. Li, Y. Zhang, H. Chen, and J. Zheng. *Coordination Number of Li^+ in Nonaqueous Electrolyte Solutions Determined by Molecular Rotational Measurements*. *J. Phys. Chem. B* **118**, 3689–3695, 2014.

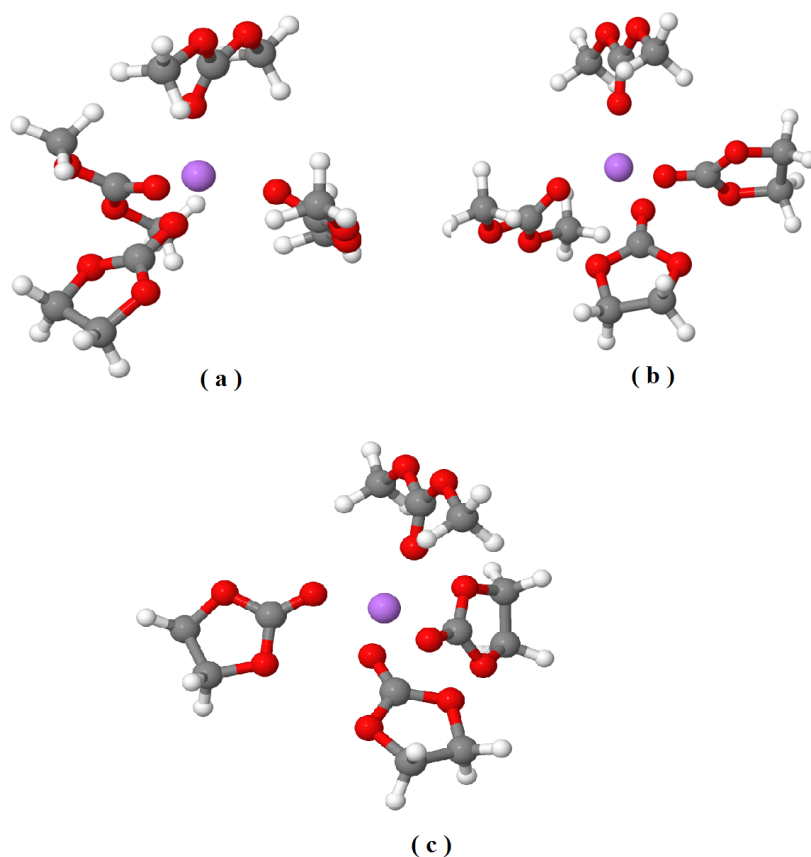


Figure 2.14: Structure of the optimized (a) $\text{Li}^+(\text{EC})(\text{DMC})_3$, (b) $\text{Li}^+(\text{EC})_2(\text{DMC})_2$, and (c) $\text{Li}^+(\text{EC})_3(\text{DMC})$ clusters calculated by DFT. Figure is taken from Ref.⁵³.

Theory (DFT) calculations of isolated clusters were complemented by molecular dynamics simulations of the bulk liquid state (see Fig. 2.13). These have allowed us to clarify the relevance of the most stable isolated structures as templates for the local organization in the bulk. (Interestingly, this methodology recall our work on locally preferred structures in liquids^{16,17}.) We have found that the Li^+ ion is locally confined by chemically heterogeneous, very compact and highly symmetric coordination environments, possibly characterized by extremely long life-times. We are working at present at clarifying the impact of these findings on transport properties, and at understanding the modifications due the presence of an external confining environment.

Li^+ solvation properties. – Despite a tremendous amount of work focusing on the interactions of Li^+ with pure and mixed carbonate-based electrolytes, the solvation structure and dynamics of lithium cations in these solvents is still a subject of debate. Interestingly, even the determination of the coordination number around the lithium ions in pure carbonate-based solvents has not been definitely resolved (see, among many others, Ref.¹³⁴). While the generally accepted picture comprises a *tetrahedral* coordination of the carbonyl oxygen atoms around Li^+ , some experimental

¹³⁴J. W. Smith, R. K. Lam, A. T. Sheardy, O. Shih, A. M. Rizzuto, O. Borodin, S. J. Harris, D. Prendergast, and R. J. Saykally. *X-Ray absorption spectroscopy of LiBF_4 in propylene carbonate: a model lithium ion battery electrolyte*. Phys. Chem. Chem. Phys. **16**, 23568–23575, 2014.

and theoretical studies propose the existence of local structures exhibiting slightly higher coordination numbers. The dependence of this local coordination number on the ion concentration is also somehow controversial, due to the difficulty in designing experimental methods able to provide a *direct* measurement of this quantity.

Isolated clusters stability (DFT). – We therefore started by investigating the solvation properties of Li^+ in pure carbonate-based solvents (ethylene carbonate (EC), propylene carbonate (PC), and dimethyl carbonate (DMC)), and their binary (EC-DMC, 1:1 molar composition) and ternary (EC-PC-DMC, 1:1:3 molar composition) mixtures, using a combination of DFT calculations and classical MD simulations. In particular, we determined the changes in the free energy associated with the transitions between different types of clusters formed by the lithium cation and the solvent molecules, to determine relative stabilities of clusters with different chemical compositions.

These calculations showed that the formation of complexes with four solvent molecules is indeed the most favourable, in all cases (see a few example of most stable clusters for the binary mixture in Fig. 2.14). For mixed clusters containing EC and DMC molecules, the DFT calculations also demonstrated a preferential binding of Li^+ with EC rather than with DMC, as expected due to the significant charge-dipole coupling in the former case. For ternary clusters, however, the situation was sensibly more complex, and although $\text{Li}(\text{EC})_2(\text{DMC})(\text{PC})^+$ was predicted to be the most favorable structure, the free energy changes for the transition paths between several clusters were very small, indicating that many of the considered structures could possibly exist in the bulk phase. This issue was surmounted by MD simulation of the liquid state, as we will see below.

The role of entropy. – In addition, our DFT calculations pointed to the surprising observation that, although energetically the preference of Li^+ to bind with the highly polar PC and EC molecules is clear, the addition of DMC molecules contributes to the decrease of the free energy, by an increase of the associated *entropic* term. Based on this observation, we concluded that the effect of entropy must be taken into account in the most precise way to elucidate the relevance of these structures for the local organization in the bulk, also considering the small free energy differences observed for the transition paths leading from one cluster to the other. This would be possible, in principle, by investigating larger clusters sizes in the DFT calculations, but very hard computationally. We rather decided to more efficiently shift to MD simulations of the liquid state, based on the force fields of Refs.^{135,136}.

Long-range structural heterogeneities. – These revealed the existence of significant compositional inhomogeneities around a lithium cation, extending up to a length scale which is more than five times the size of the first shell radius (see Fig. 2.15). As a result of these fluctuations, the structure around Li^+ in the mixed solvents can be described in terms of a short-range structure (up to $4 \div 5$ for Li^+), where the composition is rich in DMC, and by a longer-range structure where in the case of the binary solvent mixture the composition is rich in EC and in the case of the ternary one in PC (see Fig. 2.15, left and right, respectively). Only at more extended length scales, the local mole fractions of each solvent attain their bulk values. These findings also indicated that the

¹³⁵J.-C. Soetens, C. Millot, and B. Maigret. *Molecular Dynamics Simulation of Li^+ BF_4^- in Ethylene Carbonate, Propylene Carbonate, and Dimethyl Carbonate Solvents*. J. Phys. Chem. A **102**, 1055–1061, 1998.

¹³⁶M. Masia, M. Probst, and R. Rey. *Ethylene carbonate- Li^+ : A theoretical study of structural and vibrational properties in gas and liquid phases*. J. Phys. Chem. B **108**, 2016–2027, 2004.

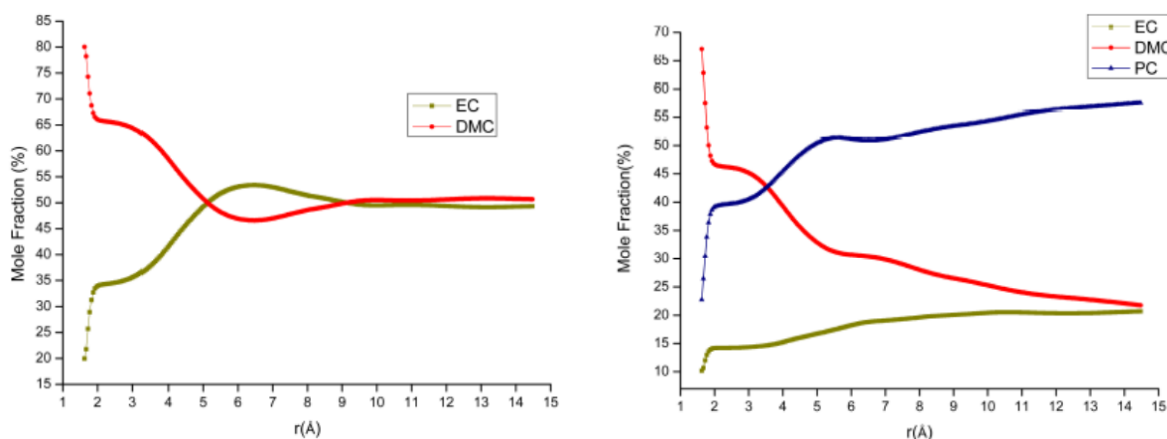


Figure 2.15: Local mole fractions (%) of EC, PC, and DMC as a function of the distance from the lithium cation in the binary (*Left*) and ternary (*Right*) mixtures. Figure is taken from Ref.⁵³.

collective effects arising from the interactions between regions of different composition play a role in stabilizing the (local) structure of the first solvation shell of Li^+ .

Tetrahedral order and the local dipole. – Our data also show that there is a very significant tetrahedral local ordering around Li^+ in all cases, and the addition of co-solvents does not distort this structural order. This effect is evident in Fig. 2.16 left, where we plot the probability distributions of the tetrahedral order parameter. By calculating an entropic term associated with this local tetrahedral order around Li^+ , it was also demonstrated that the clusters having a high fraction of DMC molecules (three and four molecules) exhibit a higher tetrahedral order, which is reflected in the lower values of this entropic term. Therefore, from an entropic point of view the presence of DMC contributes to the stabilization of the local tetrahedral structure around Li^+ .

An other very interesting finding is that inside the first solvation shell of Li^+ in ternary and binary mixtures, which exhibit a high concentration of nonpolar DMC molecules, the *total* dipole of the solvent molecules is higher than in the cases where Li^+ is solvated by the highly polar EC and PC molecules (see Fig. 2.16 right). The observed local tetrahedral packing of the solvent molecules in the first solvation shell of Li^+ causes a cancellation of the individual molecular dipole vectors, which seems to be more important in the cases where molecules of the same type are present. These collective effects are therefore crucial in determining the local permittivity around a Li^+ cation, and the relative binding preferences should be based upon this total dipole moment of the solvation shell and not in terms of the pair ion-dipole interactions, which is traditionally considered as the most important factor determining the preferential solvation in such systems.

What next? – Further work is currently in progress to elucidate the impact of the above complex long-range structuration on transport properties of the solvated Li^+ ion. Indeed, based on interesting preliminary data, it is clear that the formed complex coordination shells are extremely long-lived, on time scales which can be of the order of nanoseconds and depend on the chemical composition. As a consequence, dynamics of the ion by no means can be described as transport of a charge in a background characterized by a uniform dielectric constant. In contrast, we expect it to be determined by both the exchange dynamics of the solvent molecules between the coordination sphere(s) and the bulk, and the diffusion of this sphere as a rigid entity. We are at present trying to

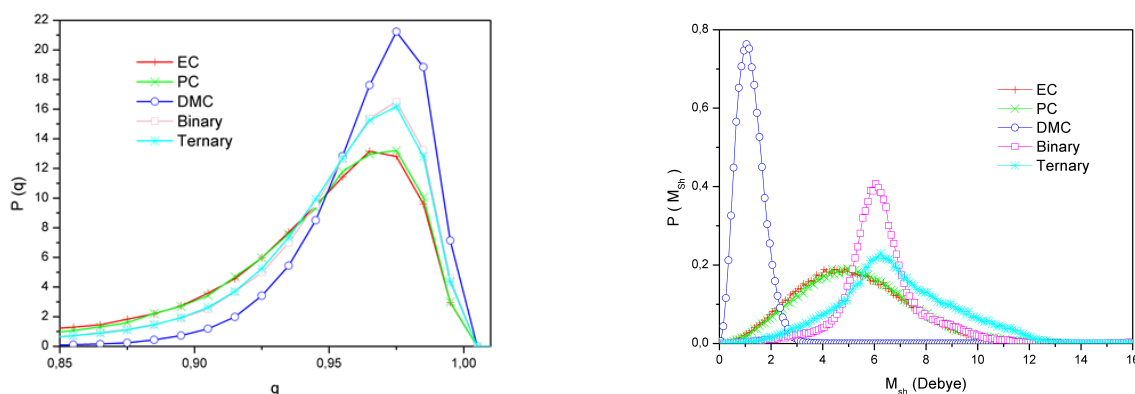


Figure 2.16: *Left*: Normalized distribution of the tetrahedral order parameter around Li^+ in all the investigated solvents. *Right*: Calculated normalized probability density distributions $P(M_{sh})$ of the magnitude of the total dipole inside the solvation shell of Li^+ . Figure is taken from Ref.⁵³.

link in a comprehensive picture the diffusion properties of the "dressed" ion to the typical life-times of the most probable coordination shell structures.

Two additional issues must be considered to elucidate the relevance of the above results for real-life configurations. First, in our work we have considered the limit of infinite dilution, which certainly is a robust reference situation but is clearly inadequate to mimic realistic conditions. Due to the long-range composition fluctuations of Fig. 2.15, one can predict substantial overlap between the coordination environments of nearest-neighbour ions, even in the case of very low concentration. These modifications will, in turn, impact in non-trivial fashion the total dipole distributions around the ions (Fig. 2.16 right), which will turn out to be both deformed and correlated. How these structural changes modify transport of Li^+ at different concentrations is an open interesting matter. Second, focusing on the behaviour of the electrolyte in the vicinity of the interface with a solid phase, even in the presence of an external electric field, is a natural continuation of our work on these materials. Indeed, it would be extremely beneficial to clarify the details of the nanostructuring of the solvent mixtures at the interface, by estimating the resulting electrostatic potential profiles, or the effective radius of the solvated ions (size of the coordination shell) at different concentrations. This could help, for instance, in fixing realistic boundary conditions for much more detailed studies of the intercalation processes at the electrodes.

Moving to ionic liquids. – The work described above tends to strengthen our understanding of interesting new properties which emerge from mixing of a relatively well known class of substances. An other viable strategy to the development of performing electrolytes is to focus on promising classes of new materials, including ionic liquids^{137,138} (ILs). ILs mix bulky and asymmetric organic cations to smaller anions, providing virtually infinite possibilities for design of electrolytes with optimized features. Transport properties of the Li^+ ion when Li^+ salt is added to ILs, however, can suffer from a critical issue that we briefly discuss here.

A large number of investigated ILs show a peculiar feature in the static structure factor, an

¹³⁷C. A. Angell, Y. Ansari, and Z. Zhao. *Ionic Liquids: Past, present and future*. Faraday Discuss. **154**, 9–27, 2012.

¹³⁸A. Lewandowski and A. Świdorska-Mocek. *Ionic liquids as electrolytes for Li-ion batteries? An overview of electrochemical studies*. J. Power Sources **194**, 601–609, 2009.

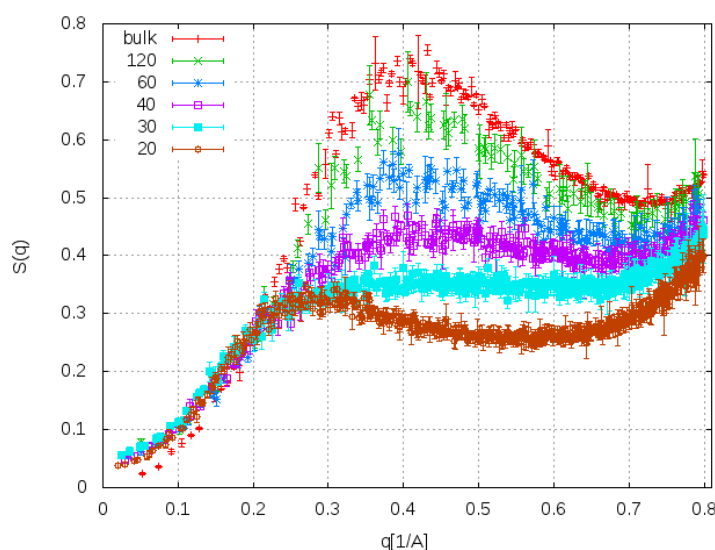


Figure 2.17: Neutrons scattering static structure factor, $S_N(q)$, for the ionic liquid model of Ref.¹⁴⁰, calculated both in the bulk and in confinement. The slab widths, L_C , considered, and the considered wave-vectors, q , lie in the plane of the slab. The extent of confinement indeed controls the intensity of the peak corresponding to long-range order correlations. These data are unpublished.

additional peak at wave vectors in the range $q \simeq 0.2 \div 0.4 \text{ \AA}^{-1}$ ¹³⁹, whose intensity seems to strongly depend on the size of the cation. The nature of this long-range structural correlation is still debated. Unfortunately, similarly to the case of the mixed organic solvents detailed above, these long-range structural correlations strongly impact the local environment of the ion and certainly degrade transport and conductivity features. Our work in this direction focuses on the possibility of controlling (destroying) this structural feature by confinement at the nanoscale, which should frustrate the extension of this hidden order at large distances.

We already have some promising preliminary data. We have considered the coarse-grained model for $[\text{C}_7\text{mim}][\text{PF}_6]$ of Ref.¹⁴⁰, without Li^+ salt and confined in a slab geometry of width L_C . The static structure factors, $S(q)$, calculated by averaging over wave-vectors lying in the plane of the slab are shown in Fig. 2.17, at the indicated values of L_C (in \AA). The case of the bulk is also shown, which features a well developed maximum at $q_0 \simeq 0.4 \text{ \AA}^{-1}$. These data seem to confirm that it is indeed possible to destroy the correlation probed in the plane of the slab by confinement in the orthogonal direction.

Interestingly, these results could allow us to shed light on the origin of this unusual correlation. Our idea is that a careful analysis of the partial components, $S_{\alpha\beta}(q)$, should help in substantially restricting the subset of degrees of freedom possibly responsible for the correlation. We expect that the most probable candidates will be those showing the most evident variation with L_C of a (positive) peak centred at q_0 , with the other irrelevant components showing no evident variations at the same value of wave vector. Of course, the final goal is to understand how the modifications of Fig. 2.17 impact the dynamical properties of the ionic liquid itself or those of the Li^+ cation, when present.

¹³⁹A. Triolo, O. Russina, H.-J. Bleif, and E. Di Cola. *Nanoscale segregation in room temperature ionic liquids*. *J. Phys. Chem. B* **111**, 4641–4644, 2007.

¹⁴⁰B. L. Bhargava, R. Devane, M. L. Klein, and S. Balasubramanian. *Nanoscale organization in room temperature ionic liquids: a coarse grained molecular dynamics simulation study*. *Soft Matter* **3**, 1395–1400, 2007.

Chapter 3

B. Heat and sound in glasses and nanostructured materials

In the previous Chapter we have dealt with soft matter systems showing strong heterogeneities, in the nature of the confining environments or behaviour of structural and dynamical properties. Here we focus on solid state matter, both crystals and glasses, which do not flow and support shear stress. In these cases we investigate vibrational excitations, whose interaction with mechanically heterogeneous environments or with interfaces boundaries between sub-systems of different chemical composition controls the transport properties of both sound and heat.

3.1 Thermal properties at the nanoscale

What makes the difference when sound or heat propagate in a crystal or in a glass is a crucial but still open issue in the physics of materials. Indeed, one hundred years ago, Debye rationalized the perfectly ordered crystal case in terms of phonons. In contrast, years of efforts have failed to provide a convincing comprehensive picture for vibrations in disordered solids. This is a true difficulty, also considering that technology by now provides the techniques to control materials structure at the nanoscale, and some innovative applications try to degrade sound and thermal transport of nano-structured materials beyond the "glassy" limit^{141,142}. These needs clearly imply the most complete understanding of how this glassy limit behaves.

In thermoelectricity applications¹⁴³, for instance, one needs to optimize (maximize) the figure of merit, Z , defined as $ZT = (k_{ele}/k_{lat}) S^2 T$. Here, k_{ele} and k_{lat} are the electrical and thermal conductivity, respectively, S is the Seebeck coefficient, and T the temperature. Unfortunately it is far from obvious how one could simultaneously maximize k_{ele} while minimizing k_{lat} . A first step toward possible solutions is to first try to control k_{lat} in absence of any electronic degrees of freedom. This is what we have tried to do with our work, which is described here.

At variance with the cases described above, where mass and charge transport were ubiquitous, in this Chapter we focus on vibrational degrees of freedom. Interestingly, we will see that, also in

¹⁴¹C. Chiritescu, D. G. Cahill, N. Nguyen, D. Johnson, A. Bodapati, P. Keblinski, and P. Zschack. *Ultralow Thermal Conductivity in Disordered, Layered WSe₂ Crystals*. *Science* **315**, 351–353, 2007.

¹⁴²G. Pernot, M Stoffel, I Savic, F Pezzoli, P Chen, G. Savelli, A Jacquot, J Schumann, U Denker, I Mönch, et al. *Precise control of thermal conductivity at the nanoscale through individual phonon-scattering barriers*. *Nat. Mater.* **9**, 491–495, 2010.

¹⁴³J.-F. Li, W.-S. Liu, L.-D. Zhao, and M. Zhou. *High-performance nanostructured thermoelectric materials*. *NPG Asia Materials* **2**, 152–158, 2010.

this case, the main processes observed are due to some peculiar form of confinement, when the heat carriers (phonon-like excitations) interact with heterogeneous environments, which profoundly impact their properties. We have considered two cases.

First, in glasses, sound-like excitations undergo Rayleigh scattering due to complex elastic constants distributions at the nanoscale⁵⁴. At these lengths, the mechanical response of the system does not conform to the attended macroscopic limit. As a consequence, we have demonstrated that in amorphous systems, due to the existence of mechanical heterogeneities^{55,56}, the mean free path of phonons (and therefore k_{lat}) is at the minimum value, corresponding to propagation on length scales of the order of atomic nearest-neighbours distances.

Second, in nanostructured materials, e.g., superlattices, where crystals of heterogeneous chemical compositions are intercalated with a periodic repetition pattern in one preferential direction, heterogeneities are concentrated at the interfaces and decouple the vibrational properties in different sub-lattices. Surprisingly, we have demonstrated that it is possible to design systems which conduct heat as crystals in a plane, and worse than the corresponding glass in the direction of the repetition pattern⁵⁷.

3.2 Glasses and elastic heterogeneities

Glasses feature inhomogeneous mechanical response at the nano-scale, i.e., some regions are sensibly softer than others. These *elastic heterogeneities* interfere with the vibrational excitations supported by the material which, differently to the case of the perfect crystal, cannot be completely described in terms of phonons. We have addressed this issue by MD simulation of a toy model, interpolating from the perfect crystal case, through increasingly defective phases, to fully developed glasses. By calculating different observables, we have demonstrated a direct correlation between vibrational features and the heterogeneous mechanical response at the nano-scale.

The problem: crystals & glasses. – Disordered solids, including glasses, disordered crystals, or even crystals with complex unit cells, have unusual vibrational and thermal properties compared to those of simple crystals, which are well understood by the Debye model. The density of states, $g(\omega)$, shows an excess over the Debye prediction $g(\omega) \sim \omega^2$, the Boson peak, in a frequency range $\omega \sim$ THz. The excess in $g(\omega)$ is mirrored by an excess in the specific heat $C(T)$ over the prediction $C \sim T^3$. The T -dependence of the thermal conductivity $\kappa(T)$ is also very different from that of crystals, with a characteristic plateau value for $T \sim 10$ K.

A possible rationalization of the above issues is based on the existence of *elastic heterogeneities*¹⁴⁴, which can originate from structural disorder, as in structural glasses¹⁴⁵, or disordered inter-particle potentials, even in lattice structures such as disordered colloidal crystals¹⁴⁶. In the theory of Refs.^{147,148}, this amounts to consider spatial fluctuations of the shear modulus. Extended sim-

¹⁴⁴E. Duval and A. Mermet. *Inelastic x-ray scattering from nonpropagating vibrational modes in glasses*. Phys. Rev. B **58**, 8159–8162, 1998.

¹⁴⁵U. Buchenau, N. Nücker, and A. J. Dianoux. *Neutron Scattering Study of the Low-Frequency Vibrations in Vitreous Silica*. Phys. Rev. Lett. **53**, 2316, 1984.

¹⁴⁶D. Kaya, N. L. Green, C. E. Maloney, and M. F. Islam. *Normal Modes and Density of States of Disordered Colloidal Solids*. Science **329**, 656–658, 2010.

¹⁴⁷A. Marruzzo, W. Schirmacher, A. Fratallocchi, and G. Ruocco. *Heterogeneous shear elasticity of glasses: the origin of the boson peak*. Scientific Reports **3**, 2013.

¹⁴⁸W. Schirmacher, G. Ruocco, and T. Scopigno. *Acoustic attenuation in glasses and its relation with the boson peak*. Phys. Rev. Lett. **98**, 025501, 2007.

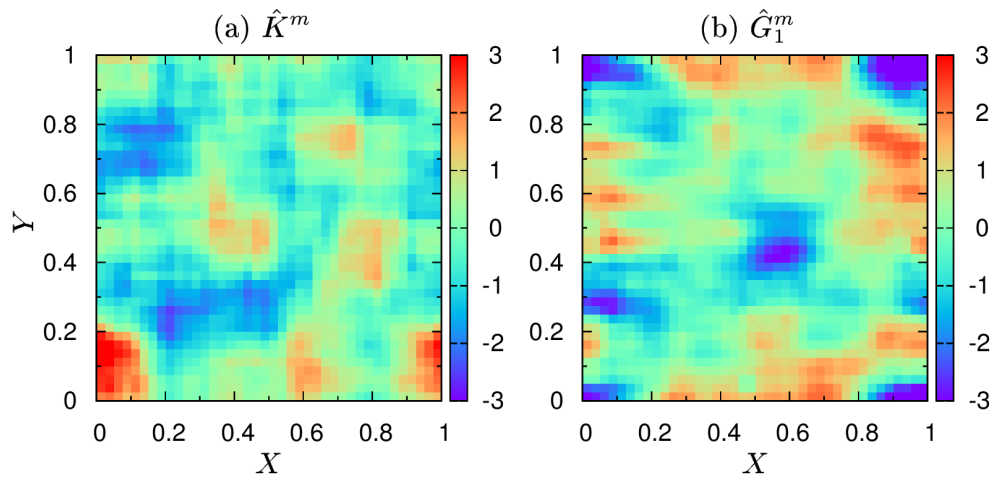


Figure 3.1: Colour maps representations of a xy -slab (centred at $z = L/2$, with L the simulation box size) taken from the spatial distributions of the bulk modulus \hat{K}^m (left) and low shear modulus \hat{G}_1^m (right) for a LJ glass. (Note that \hat{G}_1^m is indicated as G_p^m in what follows.) The values of the local moduli are normalized by their averages and standard deviations. The heterogeneous mechanical response randomly distributed in space is evident, especially in the case of the shear modulus. Figure is taken from Ref.⁵⁴.

ulation work^{149,150}, including our Ref.⁵⁴, clearly demonstrated their existence in disordered solids. This is at variance with simple crystals, characterized by a fully affine response and homogeneous moduli distributions¹⁵¹. More specifically, in the large length scale limit, macroscopic moduli are observed. In contrast, as the length-scale is reduced, moduli heterogeneities are detected, at a typical length scale $\xi \simeq 10 - 15\sigma$ ¹⁵⁰, where σ is the typical atomic diameter. In Fig. 3.1 we show, as color maps, the heterogeneous spatial distribution for the bulk (left) and a shear (right) modulus, in the case of a LJ glass⁵⁴. Breakdown of continuum mechanics¹⁵² and Debye approximation^{153,154} have been demonstrated at the same *mesoscopic* length-scale ξ , where they are still valid for crystals. Remarkably, the wave frequency corresponding to the wavelength $\Lambda \sim \xi$ is very close to Ω^{BP} ¹⁵⁵.

In order to attack these issues, in Refs.^{55,56} we have considered a numerical model featuring an amorphisation transition¹⁵⁶. We showed how to systematically deform the local moduli distributions, evaluated by coarse-graining the system in small domains of linear length-scale w . We characterized the degree of elastic heterogeneity in terms of standard deviation of those distribu-

¹⁴⁹K. Yoshimoto, T. S. Jain, K. V. Workum, P. F. Nealey, and J. J. de Pablo. *Mechanical Heterogeneities in Model Polymer Glasses at Small Length Scales*. Phys. Rev. Lett. **93**, 175501, 2004.

¹⁵⁰M. Tsamados, A. Tanguy, C. Goldenberg, and J.-L. Barrat. *Local elasticity map and plasticity in a model Lennard-Jones glass*. Phys. Rev. E **80**, 026112, 2009.

¹⁵¹H. Wagner, D. Bedorf, S. Küchemann, M. Schwabe, B. Zhang, W. Arnold, and K. Samwer. *Local elastic properties of a metallic glass*. Nature Mater. **10**, 439, 2011.

¹⁵²J. P. Wittmer, A. Tanguy, J.-L. Barrat, and L. Lewis. *Vibrations of amorphous, nanometric structures: When does continuum theory apply?* Europhys. Lett. **57**, 423, 2002.

¹⁵³G. Monaco and V. M. Giordano. *Breakdown of the Debye approximation for the acoustic modes with nanometric wavelengths in glasses*. Proc. Natl. Acad. Sci. U. S. A. **106**, 3659, 2009.

¹⁵⁴G. Monaco and S. Mossa. *Anomalous properties of the acoustic excitations in glasses on the mesoscopic length scale*. Proc. Natl. Acad. Sci. U. S. A. **106**, 16907, 2009^{*}.

¹⁵⁵F. Leonforte, R. Boissière, A. Tanguy, J. P. Wittmer, and J.-L. Barrat. *Continuum limit of amorphous elastic bodies. III. Three-dimensional systems*. Phys. Rev. B **72**, 224206, 2005.

¹⁵⁶L. Bocquet, J.-P. Hansen, T. Biben, and P. Madden. *Amorphization of a substitutional binary alloy: a computer "experiment"*. J. Phys.: Condens. Matter **4**, 2375, 1992.

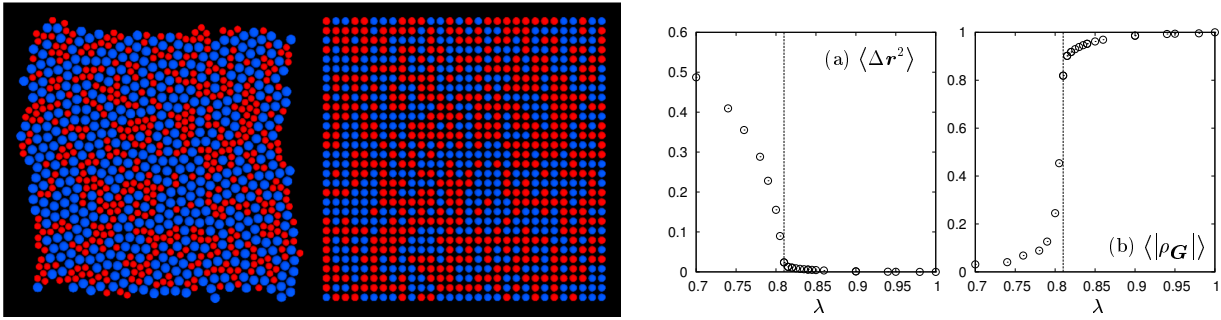


Figure 3.2: *Left*: 2-dimensional representation of the simulated model. Starting from a perfect crystal (right) formed by a binary mixture of initially identical particles ($\lambda = 1$), the size of red particles is gradually decreased, while the radius of blue ones is increased. This is a well-defined method for introducing in the system a controlled increasing amount of structural defects. At a particular value of the ratio of the radii, λ^* , the system undergoes a transition to an amorphous phase (left). *Right*: λ -dependence of the order parameters $\langle \Delta r^2 \rangle$ (a) and $\langle |\rho_{\mathbf{G}}| \rangle$ (b), across the amorphisation transition. Here \mathbf{G} is the smallest reciprocal lattice vector. The system undergoes a transition from a disordered crystal to a fully amorphous state at $\lambda = \lambda^* \simeq 0.81$, indicated by the vertical lines. This Figure is taken from Ref.⁵⁵.

tions, and studied the effect on normal modes (eigenvalues of the Hessian matrix) and thermal conductivity⁵⁵. We also investigated the relation between elastic heterogeneities and acoustic excitations⁵⁶, unifying in a single framework ordered and disordered solid states and considering quantities directly probed by experiments.

Our pick-lock: the amorphisation transition. – We studied by Molecular Dynamics at constant temperature and number density a 50 : 50 mixture, composed by N atoms with different diameters, σ_1 and σ_2 , and same mass, $m = 1$ (see Fig. 3.2 left). Particles interact via a soft-sphere potential, $v_{\alpha\beta} = \epsilon(\sigma_{\alpha\beta}/r)^{12}$, with $\sigma_{\alpha\beta} = (\sigma_\alpha + \sigma_\beta)/2$ and $\alpha, \beta \in 1, 2$. The potential is cut off and shifted at $r = 2.5\sigma_{\alpha\beta}$. Starting from a perfect face-centered cubic crystal, defects were added in the form of size disorder, by simultaneously decreasing σ_1 below the initial value $\sigma_1 = 1$ and increasing σ_2 , keeping a constant $\sigma_{\text{eff}} \equiv 1$ ¹⁵⁶, where $\sigma_{\text{eff}}^3 = \sum_{\alpha, \beta=1,2} \sigma_{\alpha\beta}^3/4$ is an "effective" diameter¹⁵⁷. The ratio $\lambda = \sigma_1/\sigma_2 \leq 1$, quantifies the size disorder and is the control parameter. $\lambda = 1$ corresponds to the perfect crystal case, while for $\lambda = 0.7$ a completely developed amorphous structure is observed (see Fig. 3.2 left). An amorphisation transition occurs at $\lambda = \lambda^* \simeq 0.81$ ^{55,156}, as indicated by the jumps in Fig. 3.2 right.

The elastic heterogeneities. – The heterogeneous, scale-dependent distributions of local elastic moduli can be determined by using several methods^{54,149,150}. Here, the system was divided into 20^3 cubic domains with a linear size $w = 2a = 3.16$, and the elastic moduli were obtained from equilibrium fluctuation formulae. For each subvolume, one local bulk modulus and five local shear moduli are defined, corresponding to the response to isotropic bulk compression and volume-conserving shear deformations, respectively. Of the five shear moduli, two correspond to "pure" shear deformations, and the remaining three are related to "simple" shear deformations. In the following, the local bulk, pure shear, and simple shear moduli are denoted by K^m , G_p^m , and G_s^m , respectively (m indicates a local quantity). Each modulus $C^m = K^m, G_p^m, G_s^m$ is the sum of four

¹⁵⁷B. Bernu, J. P. Hansen, Y. Hiwatari, and G. Pastore. *Soft-sphere model for the glass transition in binary alloys: Pair structure and self-diffusion*. Phys. Rev. A **36**, 4891, 1987.

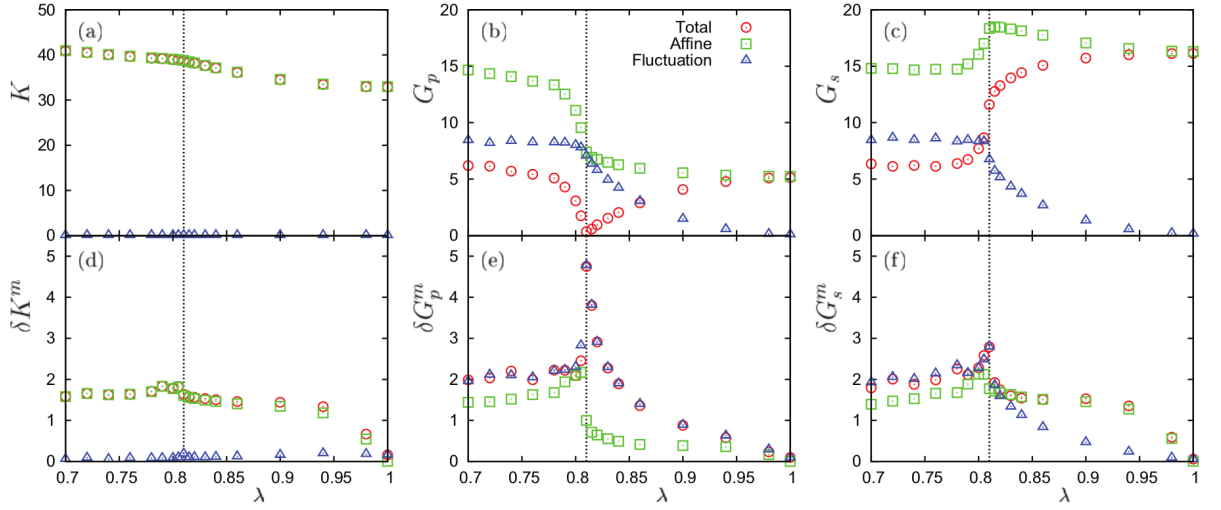


Figure 3.3: The macroscopic values of the moduli (a) K , (b) G_p , and (c) G_s , and the corresponding standard deviations, (d) δK^m , (e) δG_p^m , and (f) δG_s^m , versus the disorder parameter λ . Circles, squares, and triangles represent the values of total modulus $C^{(m)}$, affine contribution $C_A^{(m)}$, and fluctuation term $C_F^{(m)}$, respectively. The vertical lines indicate the transition point, $\lambda = \lambda^* \simeq 0.81$. Figure is taken from Ref.⁵⁵.

contributions, the Born term C_B^m , the kinetic contribution C_K^m , the pressure correction term C_C^m , and the fluctuation term $-C_F^m$. The sum of the first three terms (dubbed as "affine" in Fig. 3.3, C_A^m), corresponds to the response of a system which deforms affinely at all scales. The fluctuation term $-C_F^m$ is a negative correction that accounts for the non affinity of the deformation at small scales, and in disordered systems becomes comparable in magnitude to C_A^m .

The probability distribution functions, $P(C^m)$, which turned out to be closely gaussian, were next obtained by sampling the different cubic subvolumes. Note that $P(G_p^m)$ and $P(G_s^m)$ are different in cubic crystals, while they coincide in isotropic glasses. The average values, C , which corresponds to the macroscopic modulus, and standard deviation, δC^m are reported in Fig. 3.3. In the initial crystalline state $\lambda = 1$, $K > G_s > G_p$, while $K > G_p \simeq G_s$ for the isotropic amorphous states $\lambda \leq 0.78$. For a system with inverse power interactions, the bulk modulus K is determined by the affine contribution only. On the other hand, the fluctuations components become progressively larger with decreasing λ . Remarkably, around the transition λ^* , G_{pF} reaches the affine G_{pA} , so that the total G_p vanishes, $G_p \simeq 0$. Therefore, the transition can be described as an elastic instability associated with the shear modulus G_p . Below the transition ($\lambda < \lambda^*$), the material becomes rapidly isotropic, as it is manifested by the convergence $G_p \simeq G_s$.

Across the amorphisation transition, the elastic heterogeneity, characterized by the standard deviation of the moduli, undergoes important changes, starting from a perfectly uniform distribution at $\lambda = 1$. As λ decreases from 1 to 0.9, δK^m and δG_s^m increase monotonically, mainly in relation to an increase in δK_A^m and δG_{sA}^m , respectively. In the same range, δG_p^m is already dominated by the heterogeneity in the fluctuation term δG_{pF}^m . As λ approaches λ^* , this heterogeneity increases rapidly, and the spatial distribution of G_p^m becomes extremely heterogeneous with a nearly zero average value, $G_p \simeq 0$ and a large standard deviation, $\delta G_p^m \simeq 5$. Below the transition point λ^* , δG_p^m and δG_s^m immediately converge to a very similar value, $\delta G_{p,s}^m \simeq 2$. In the following, these changes in elastic properties will be correlated with the evolution of the vibrational and thermal properties.

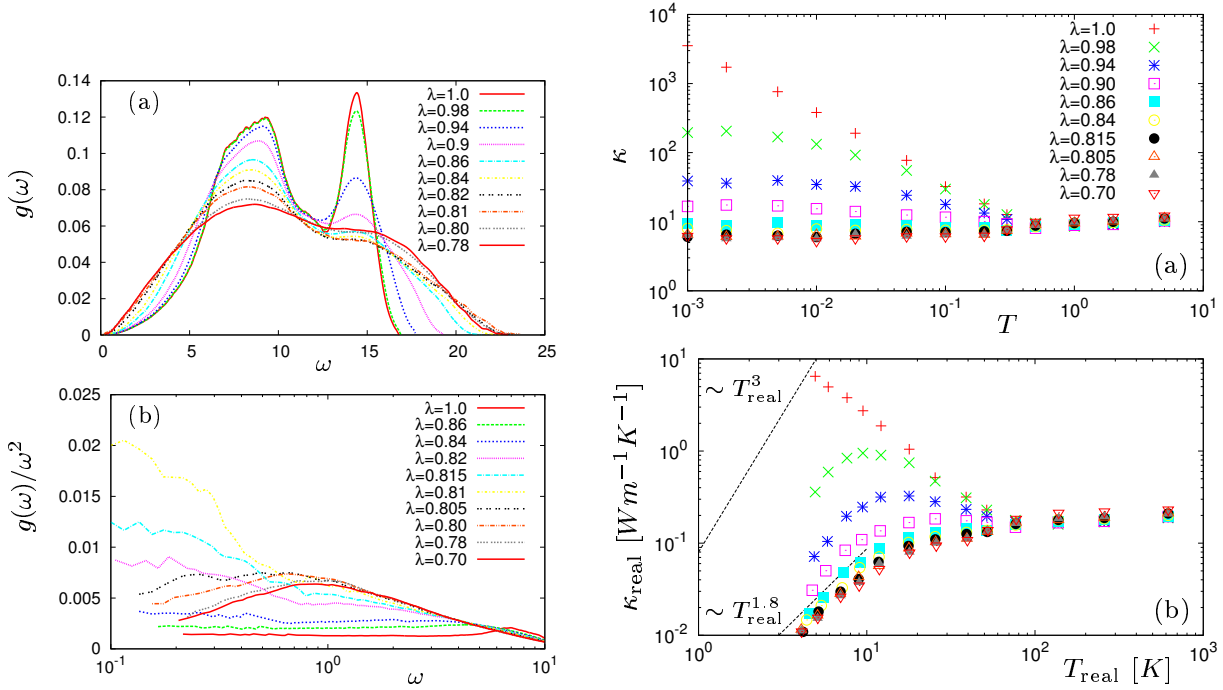


Figure 3.4: Left: (a) Density of states $g(\omega)$ and (b) reduced density of states $g(\omega)/\omega^2$, at the indicated values of λ . Right: Temperature dependence of the thermal conductivity, κ , at all values of $\lambda = 1$. (a) The values obtained from the MD simulation and (b) the same values with the quantum correction discussed in the main text. In (b), T_{real} and κ_{real} are measured in units of K and $W m^{-1} K^{-1}$, respectively. Figures are taken from Ref.⁵⁵.

The normal modes. – Interestingly, we were able to precisely correlate the data of Fig. 3.3 to the behaviour of the normal modes, in the entire range of λ . We performed a normal modes analysis and the resulting vibrational densities of states (VDOS), $g(\omega)$, are shown in Fig. 3.4 left. In the crystalline state $\lambda = 1$, a transverse branch in the range $\omega \in [7 : 9.5]$ and a longitudinal branch around $\omega = 14.5$ can be clearly identified in the VDOS. As λ decreases, these contributions from well identified phonon branches tend to lose their identity. In particular, the peak associated with the longitudinal branch is already suppressed at $\lambda = 0.9$, which is correlated with the appearance of significant heterogeneities of the bulk modulus K^m and of the shear modulus G_s^m . These heterogeneities induce a broadening of the high- ω modes, which leads to the reduction of the intensity of the longitudinal peak. The heterogeneity in low shear modulus G_p^m , on the other hand, is well correlated with the behaviour of the VDOS in the low- ω region, as it is evident by considering the reduced density of state $g(\omega)/\omega^2$ (panel b) of Fig. 3.4 left.

At $1 \geq \lambda \geq 0.84$, $g(\omega)/\omega^2$ coincides with the Debye prediction indicating that low- ω excitations are not affected by the modulus heterogeneities. An excess of modes in $g(\omega)/\omega^2$ over the Debye model starts to appear around $\lambda = 0.82$. This excess is particularly pronounced at very low frequencies, and increases with the spatial heterogeneity of G_p^m as λ approaches λ^* . Below the transition λ^* , the excess of modes drops immediately, accompanying a rapid decrease in the heterogeneity of G_p^m . At $\lambda \leq 0.8$, a typical Boson peak, with an amplitude comparable to what is typically observed in soft sphere or Lennard-Jones¹⁵³ glasses, is formed around $\omega = \omega_{\text{BP}} \simeq 1$. Note that the excess of modes in the disordered crystals close to λ^* is observed at much lower frequencies, presumably down to zero frequency at the transition point, in relation to the vanishing of G_p at the transition.

Altogether, the position and amplitude of the peak appear to be controlled by the shear modulus average value and heterogeneity, in the disordered crystal as well as in the amorphous state. The discussion of the participation ratios, p_k , where k is the eigenmode number, calculated in terms of polarization vectors, \mathbf{e}_k^j , and eigenfrequencies, ω_k , gave results which confirmed the above correlations.

The thermal conductivity. – Most important, heat transport can be also correlated to the elastic heterogeneity. The thermal conductivity κ was also obtained simulations, using the Green-Kubo formulation, in terms of the time correlation function of the heat current vector.¹⁵⁸ In Fig. 3.4 right (top panel) we show the temperature dependence of κ at the indicated values of λ . In the crystalline state $\lambda = 1$, κ decreases with increasing T , due to the increase of anharmonicity. As λ decreases, the disorder scatters heat carriers and reduces κ steeply. The reduction of κ saturates around $\lambda = 0.86$, i.e., before a significant excess of modes is observed in the VDOS. For $\lambda \leq 0.86$, κ is insensitive to T , which means that disorder dominates anharmonic effects.

This behaviour can be rationalized by using the simple formula: $\kappa = (1/3)Cv\ell$ ¹⁵⁸, where C is the heat capacity per unit volume, v and ℓ are the "average" velocity and mean free path of the heat carriers, respectively. C and v are taken as constants, and the attenuation rate $\sim 1/\ell$, a function of T and λ , is decomposed into two components, anharmonic $1/\ell_{\text{anh}}$ and disorder $1/\ell_{\text{dis}}$, which respectively depend on T and λ : $1/\ell(T, \lambda) = 1/\ell_{\text{anh}}(T) + 1/\ell_{\text{dis}}(\lambda)$ ¹⁵⁹. $1/\ell_{\text{dis}}$ is expected to be increased by the modulus heterogeneities. In the perfect crystal ($\lambda = 1$), $1/\ell_{\text{anh}} \gg 1/\ell_{\text{dis}}$, leading to $\ell \simeq \ell_{\text{anh}}$. In this case, the anharmonic effect reduces ℓ with increasing T and causes the reduction of κ . As λ decreases, $1/\ell_{\text{dis}}$ becomes large, and $1/\ell_{\text{anh}} \ll 1/\ell_{\text{dis}}$ at $\lambda \leq 0.86$. Comparing with the results reported in Fig. 3.3, it appears that the increase of $1/\ell_{\text{dis}}$ is mainly correlated to the heterogeneities of K^m and G_s^m .

At $\lambda = 0.86$, we measured $\ell = 3\kappa/Cv \sim 1[\sigma]$, the order of particle diameter, i.e., ℓ and κ reach a "minimum" value, insensitive to temperature. As a consequence, in such a strong scattering state with an extremely short ℓ , heat carriers are no longer propagating phonons, but non-propagating or quasi-stationary excitations, sometimes called diffusons¹⁶⁰. At this stage, even if further disorder makes local moduli more heterogeneous, κ does not decrease any more. This point motivated our work on super-lattices, as we will see below.

In the low temperature regime, the calculations presented above are based on a classical approach, where the specific heat C is independent of T . In a real system, however, $C \sim T^3$, due to quantum effects. In order to asses qualitatively the quantum effects, a simple quantum correction was applied¹⁵⁸. The correction maps "classical" values of T_{MD} and κ_{MD} , obtained from MD simulations, onto "real" values of T_{real} and κ_{real} . The latter can be determined as $\kappa_{\text{real}} = (C_{\text{real}}/C_{\text{MD}})\kappa_{\text{MD}}$, taking into account the real T -dependence of the specific heat, C_{real} which we can calculate from the density of state. We plot our data in Fig. 3.4 right (bottom panel). By using the appropriate units, the values of the crystalline state $\lambda = 1$ are comparable with experimental values for solid argon¹⁶¹. For $\lambda \leq 0.90$, the T dependence becomes similar to the one observed in amorphous materials, with a power-law like increase $\kappa_{\text{real}} \sim T^{1.8}$ at low temperatures ($T < 10$ K),

¹⁵⁸A. J. McGaughey and M. Kaviani. *Phonon transport in molecular dynamics simulations: Formulation and thermal conductivity prediction*. Advances in Heat Transfer **39**, 169–255, 2006.

¹⁵⁹C. Masciovecchio, G. Baldi, S. Caponi, L. Comez, S. D. Fonzo, D. Fioretto, A. Fontana, A. Gessini, S. C. Santucci, F. Sette, G. Viliani, P. Vilmercati, and G. Ruocco. *Evidence for a Crossover in the Frequency Dependence of the Acoustic Attenuation in Vitreous Silica*. Phys. Rev. Lett. **97**, 035501, 2006.

¹⁶⁰P. B. Allen and J. L. Feldman. *Thermal conductivity of disordered harmonic solids*. Phys. Rev. B **48**, 12581, 1993.

¹⁶¹D. K. Christen and G. L. Pollack. *Thermal conductivity of solid argon*. Phys. Rev. B **12**, 3380, 1975.

followed by a plateau. Note that κ displays this glass-like behaviour already in the disordered crystalline states, with $0.90 \geq \lambda \geq \lambda^* \simeq 0.81$.

The acoustic excitations. – In perfect crystals, acoustic plane waves and exact normal vibrational modes coincide. In glasses, in contrast, the situation is sensibly more complicated. In the macroscopic limit ($q \simeq 10^{-2} \text{ nm}^{-1}$) they support sound waves as the corresponding crystalline materials do. On further increasing q , however, the effect of the structural disorder must at one point appear, in a wave-vector range that is accessible to Inelastic X-Rays scattering (IXS) experiments¹⁵³ and molecular dynamics simulations¹⁵⁴. These studies typically probe the dynamic structure factor, $S(q, \omega)$, and clearly indicate the existence in glasses of excitations that appear in those spectra as broad peaks, whose position as a function of q is characterized by a sinusoidal-like dispersion curve. Thus, these excitations strongly recall the acoustic modes in crystalline systems, up to roughly one half of the pseudo-Brillouin zone. For this reason, they are often dubbed as acoustic-like. However, as their broadening clearly indicates, they are far from being crystal-like modes and correspond in fact to a complex pattern of atomic motions. Our model offers us a very nice opportunity: to observe directly exact normal modes in crystals metamorphosing to acoustic-like modes in glasses⁵⁶.

The dynamic structure factors. – We have therefore determined from our trajectories the dynamic structure factors, $S_{L,T}(\mathbf{q}, \omega)$, with L, T referring to longitudinal and transverse component, respectively^{154,162}. In crystals, sound propagation depends on the direction of the wave-vector, \mathbf{q} , at variance with the isotropic amorphous phases where only its modulus is relevant. We have focused in particular on the (110)-direction, which features three branches: the longitudinal and two transverse, T_1 and T_2 at high and low frequency, respectively. It is consensual that transverse modes play the most important role in determining anomalies in vibrational properties¹⁶². More specifically, we have shown above that the transverse branch with the lowest elastic modulus is the one which correlates most to the low-frequency vibrational states. In what follows we therefore focus on the T_2 excitations. In Fig. 3.5 left we plot $S_T(\mathbf{q}, \omega)$, at the indicated values of λ and q . For $\lambda = 0.84$ and 0.81 , where the two transverse sound velocities are well separated, two Brillouin peaks corresponding to the T_1 and T_2 excitations are found. In contrast, a single Brillouin peak is visible in the amorphous phase at $\lambda = 0.7$, where $c_{T_1} \simeq c_{T_2}$.

Sound velocity & broadening. – Propagation frequency, $\Omega(\mathbf{q})$, and line broadening, $\Gamma(\mathbf{q})$, of the sound excitations can be extracted from these data, by fitting the spectral region around the Brillouin peaks to a damped harmonic oscillator model^{154,162}. In Fig. 3.5 right we show the sound velocity, $c_{T_2} = \Omega_{T_2}(\mathbf{q})/q$, and broadening, Γ_{T_2} , at the indicated values of λ . For the sake of clarity, we consider first the isotropic amorphous case, $\lambda = 0.7$. As expected, for vanishing Ω , c_{T_2} corresponds to the macroscopic value (horizontal dashed line), calculated from the value of G_p at the same λ . Next, $c_{T_2}(\Omega)$ decreases (*softening*), reaches a minimum, and eventually undergoes positive dispersion at higher frequencies. In the same region where c_{T_2} shows a minimum, a crossover from $\sim \Omega^2$ at high frequency to a Rayleigh-like $\sim \Omega^\alpha$ with α close to 4 at intermediate frequency is evident for Γ_{T_2} around $\Omega \simeq 1$, which corresponds to Ω^{BP} in this case. Both these features are consistent with previous findings for the Lennard-Jones glass^{147,154}. As λ increases, the sound velocity at a given frequency first decreases, goes through a *minimum* at $\lambda^* \simeq 0.81$, and

¹⁶²H. Shintani and H. Tanaka. *Universal link between the boson peak and transverse phonons in glass*. Nature Mater. 7, 870, 2008.

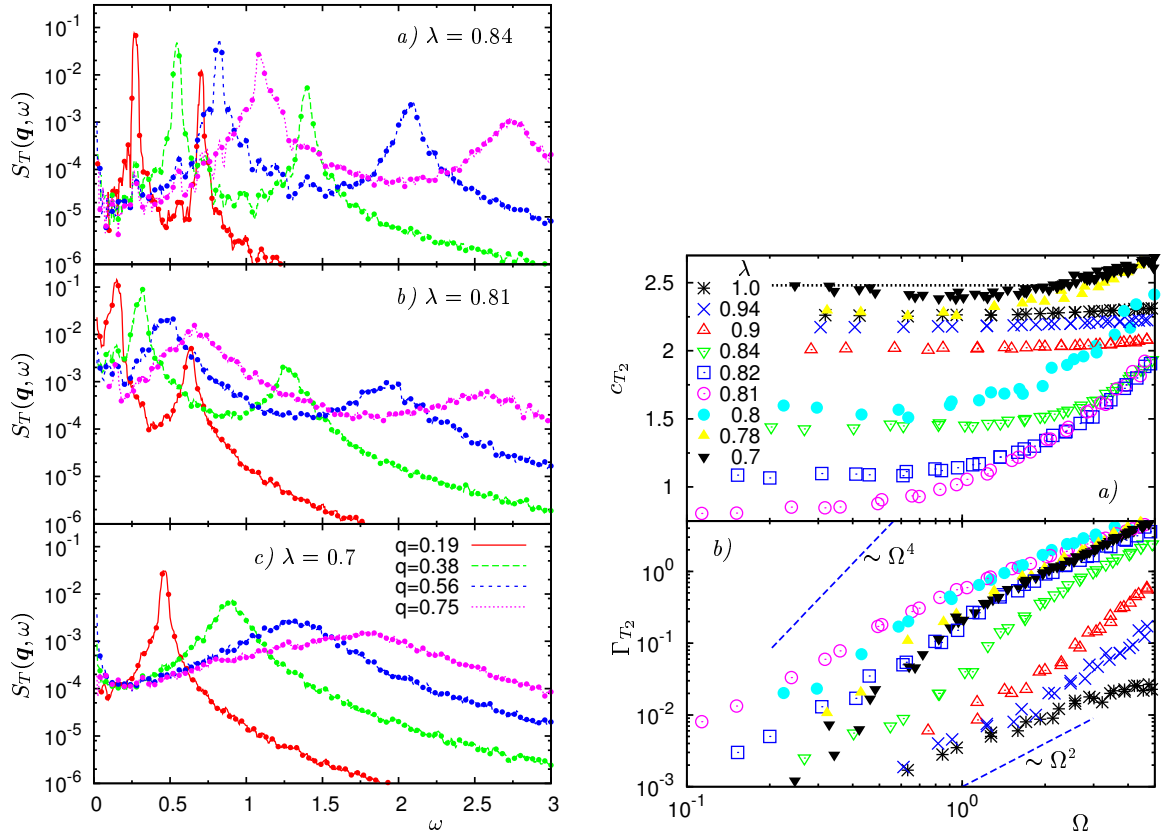


Figure 3.5: *Left*: Transverse dynamic structure factors, $S_T(\mathbf{q}, \omega)$, at the indicated values of the wave vector \mathbf{q} in the (110)-direction. Three values of λ are shown, in a defective crystal state a), at the amorphisation transition b), and in the fully developed glassy phase c). Two Brillouin peaks, corresponding to the T_1 and T_2 branches, are visible for $\lambda = 0.84$ and 0.81 . In the glassy phase ($\lambda = 0.7$) only one degenerate excitation survives. *Right*: Spectroscopic parameters calculated from the dynamical structure factors. a) Transverse phase velocity $c_{T_2}(\Omega) = \Omega_{T_2}(q)/q$, and b) broadening, $\Gamma_{T_2}(\Omega)$, for the T_2 excitations and at the indicated values of λ . These data have been obtained by fitting the calculated $S_T(\mathbf{q}, \omega)$ to the damped harmonic oscillator line shape. The horizontal dashed line in a) corresponds to the macroscopic limit of the sound velocity at $\lambda = 0.7$. The dashed lines, $\propto \Omega^2$ and $\propto \Omega^4$, in b) are also guides for the eye, to emphasize the extremely complex frequency-dependence of Γ_{T_2} at different values of λ . Figures are taken from Ref.⁵⁶.

eventually increases steadily. Interestingly, c_{T_2} seems to mirror at all frequencies the non-monotonic behaviour of the macroscopic sound velocity, calculated from the G_p data of Fig. 3.3.

Sound broadening follows a quite different pattern. As λ increases from 0.7, Γ_{T_2} is enhanced and reaches a *maximum* at λ^* . Next, it is strongly suppressed for $\lambda > \lambda^*$, converging to a very low value at $\lambda = 1$, of anharmonic origin (damping). We remark that in this case, the ratio between the maximum and minimum values reached, covers almost two decades at $\Omega \simeq 1$. We will see below that this finding can be rationalized in terms of a strong correlation with the magnitude of the elastic heterogeneity associated with the appropriate modulus.

Putting everything together. – The Ioffe-Regel (IR) frequency, $\Omega_{T_2}^{\text{IR}}$, at all values of λ can also be determined, by considering an alternative representation (not shown) of the data of Fig. 3.5 right. At the IR frequency, the ratio $\pi\Gamma_{T_2}(\Omega_{T_2}^{\text{IR}})/\Omega_{T_2}^{\text{IR}} = 1$, *i. e.*, the decay time of the excitations

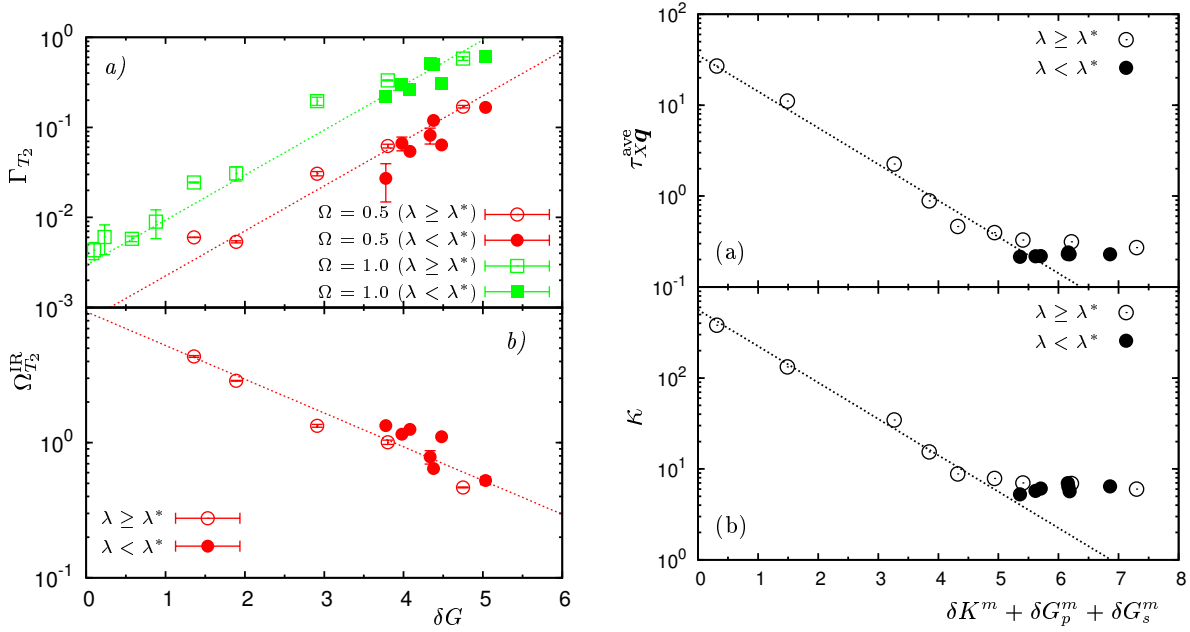


Figure 3.6: *Left*: Direct correlations of vibrational and thermal properties with elastic heterogeneities. Here we show the dependence on the extent of the elastic heterogeneities for broadening, Γ_{T_2} a), and Ioffe-Regel frequency, $\Omega_{T_2}^{\text{IR}}$ b). Data are plotted versus the standard deviation δG of the distribution of the relevant local elastic modulus. $\delta G \simeq \delta G_p$ for $\lambda \geq \lambda^*$ (open symbols), $\delta G \simeq \delta G_p + \delta G_s$ for $\lambda < \lambda^*$, in the amorphous phases (closed symbols). In a) we plot values of Γ_{T_2} corresponding to two different fixed frequencies, $\Omega \simeq 0.5$ and $\Omega \simeq 1$. Dashed lines are guides for the eye. Figure is taken from Ref.⁵⁶. *Right*: (a) The lifetime τ_{Xq}^{ave} of the acoustic wave, averaged over the frequency range, $5 < \omega_{Xq} < 25$, and (b) the thermal conductivity κ . The data are plotted as functions of the extent of the elastic heterogeneities, $\delta K^m + \delta G_s^m + \delta G_p^m$. The dashed lines are guides for the eye. Note that in the highly disordered states with large values of $\delta K^m + \delta G_s^m + \delta G_p^m$, the thermal conductivity κ reaches the minimum allowed value, where the lifetime τ_{Xq}^{ave} corresponds to the Einstein period, $\tau_{Xq}^{\text{ave}} \sim \mathcal{O}(10^{-1})$, and the mean-free-path of acoustic waves is of the order of the particles diameters. These data are unpublished.

equals half of the corresponding vibrational period. $\Omega_{T_2}^{\text{IR}}$ provides an upper bound for the validity of acoustic-like descriptions of the vibrational excitations. Interestingly, the total variation of $\Omega_{T_2}^{\text{IR}}$ on approaching λ^* from above is very large (an order of magnitude), and $\Omega_{T_2}^{\text{IR}}$ apparently is (anti-)correlated with the elastic heterogeneities. Above λ^* , we noticed that the sound broadening also has a quite large overall variation and seems to follow the evolution of the elastic heterogeneities.

We made quantitative these correlations in Fig. 3.6 left, which is the most relevant result of our work. We plot Γ_{T_2} on both sides of the transition, at the low frequencies $\Omega \simeq 0.5$ and 1, and as a function of the extent of the elastic heterogeneities at the corresponding λ . While in the non-degenerate cases $\lambda > \lambda^*$ (open symbols), the appropriate data to consider are $\delta G \simeq \delta G_p$, in the amorphous cases (filled symbols), where the transverse moduli are degenerate, we assume additivity of the disorder sources and use $\delta G \simeq \delta G_p + \delta G_s$. Remarkably, the data follow an exponential behaviour $\Gamma_{T_2} \propto \exp(\delta G/g_\Gamma)$ for both frequencies. Similarly, we find $\Omega_{T_2}^{\text{IR}} \propto \exp(-\delta G/g_{\text{IR}})$, for both lattice and amorphous cases. Note that no adjustable parameters are involved in these plots.

This conclusion is confirmed by the data shown in Fig. 3.6 right. We considered the high-frequency part of the spectrum, with $5 < \omega_{Xq} < 25$, and calculated the normal modes lifetimes τ_{Xq}^{ave} averaged over the same frequency range. These data are plotted as a function of the extent

of the elastic heterogeneities, $\delta K^m + \delta G_s^m + \delta G_p^m$ (top). Clearly, as the extent of the elastic heterogeneities grows, τ_{Xq}^{ave} decreases monotonically, eventually reaching the minimum possible value, corresponding to the Einstein period.

The λ -dependence of κ , at temperature $T = 10^{-2}$, gives consistent results. Our data support the conclusion that elastic heterogeneities, especially those associated to the higher moduli δK^m and δG_s^m , sensibly reduce (by increasing disorder) both the lifetimes of high-frequency sound waves and thermal conductivity. This is evident from the representation of our data shown in the right panel of Fig. 3.6, where we plot κ versus the elastic heterogeneity. This curve seems to follow an exponential relation, $\kappa \sim \exp[-(\delta K^m + \delta G_s^m + \delta G_p^m)/g_\kappa]$, very similar to that for τ_{Xq}^{ave} , with a compatible value of the parameter $g_\kappa \simeq g_{\tau h} \simeq 0.4$. We can conservatively assert that these data are the first strong evidence of a *direct* correlation of quantities related to the intrinsic nature of acoustic-like excitations in ordered/defective/amorphous phases with local mechanical properties at the nano-scale, *i. e.*, heterogeneity of the elastic moduli.

As a final remark, we emphasize that moduli distributions, normal modes, thermal conductivity are almost insensitive to disorder once the amorphisation threshold has been reached. In contrast, we observed important quantitative changes in the disordered crystalline states $\lambda^* < \lambda < 1$. This suggests that introducing disorder into crystals may be a valuable strategy to control material properties, rather than attempting to control the amorphous state. In fact, synthetic nanostructuring in crystals is considered to be most promising way for controlling thermal conductivity. This observation motivated our work on superlattices, that will be discussed in the next Section.

3.3 Nanostructuring: superlattices

Is it possible to design crystalline systems which conduct heat worse than the corresponding amorphous phases? Based on the results discussed in the previous Section this should be very hard: the mean-free-path of the heat carriers is at the minimum allowed value in the glass. Here we describe in details an interesting possibility: to completely block transport of heat by controlling interfaces in superlattices.

Beating the amorphous limit? – Materials with low thermal conductivity, κ , are employed in many modern technologies, such as thermal management in electronic devices or thermoelectric energy conversion^{163,164}. In general, low values of κ are observed in disordered solids¹⁶⁵, including topologically disordered systems and crystalline solids with size or mass disorder (disordered alloys)^{160,166,167}, as we have seen in the previous Section. The value in the glass is generally considered as a lower bound for κ for materials with homogeneous chemical composition^{166,167}. A crucial issue¹⁶⁵ is whether thermal conductivity can be lowered below the glass limit through nanoscale phononic design^{164,168}. This possibility would allow to devise (meta-)materials which are excellent thermal insulators while preserving good electronic properties, as needed in many applications.

Superlattices. – The most popular design to reach this goal is that of a lamellar superlattice^{169–171}, often composed of two chemically different intercalated layers, e.g., Si-Ge¹⁶⁹ or GaAs-AlAs^{170,171} (see also Fig. 3.7). In a superlattice, the thermal conductivity tensor is anisotropic, with the cross-plane component, κ_{CP} , usually lower than the in-plane value, κ_{IP} ¹⁷². In recent experiments^{141,142,173}, ultra-low values of κ_{CP} , suggested to be smaller than the amorphous limit, were measured. Although these works have demonstrated very low values of k in superlattice systems, these have not been systematically compared to the values assumed in the glasses with *exactly* the same chemical composition. Also, a general framework to rationalize in a coherent single picture all these observations is still lacking.

¹⁶³R. Venkatasubramanian, E. Siivola, T. Colpitts, and B. O'Quinn. *Thin-film thermoelectric devices with high room-temperature figures of merit*. Nature **413**, 597, 2001.

¹⁶⁴M. Maldovan. *Sound and heat revolutions in phononics*. Nature **503**, 209–217, 2013.

¹⁶⁵K. E. Goodson. *Ordering Up the Minimum Thermal Conductivity of Solids*. Science **315**, 342–343, 2007.

¹⁶⁶D. G. Cahill and R. O. Pohl. *Lattice Vibrations and Heat Transport in Crystals and Glasses*. Annu. Rev. Phys. Chem. **39**, 93–121, 1988.

¹⁶⁷D. G. Cahill, S. K. Watson, and R. O. Pohl. *Lower limit to the thermal conductivity of disordered crystals*. Phys. Rev. B **46**, 6131, 1992.

¹⁶⁸P. E. Hopkins, C. M. Reinke, M. F. Su, R. H. Olsson, E. A. Shaner, Z. C. Leseman, J. R. Serrano, L. M. Phinney, and I. El-Kady. *Reduction in the Thermal Conductivity of Single Crystalline Silicon by Phononic Crystal Patterning*. Nano Lett. **11**, 107–112, 2011.

¹⁶⁹S.-M. Lee, D. G. Cahill, and R. Venkatasubramanian. *Thermal conductivity of Si-Ge superlattices*. Appl. Phys. Lett. **70**, 2957–2959, 1997.

¹⁷⁰W. S. Capinski, H. J. Maris, T. Ruf, M. Cardona, K. Ploog, and D. S. Katzer. *Thermal-conductivity measurements of GaAs/AlAs superlattices using a picosecond optical pump-and-probe technique*. Phys. Rev. B **59**, 8105–8113, 1999.

¹⁷¹B. C. Daly and H. J. Maris. *Calculation of the thermal conductivity of superlattices by molecular dynamics simulation*. Physica B: Condensed Matter **316 - 317**, Proceedings of the 10th International Conference on Phonon Scattering in Condensed Matter, 247–249, 2002.

¹⁷²B. Yang, W. L. Liu, J. L. Liu, K. L. Wang, and G. Chen. *Measurements of anisotropic thermoelectric properties in superlattices*. Appl. Phys. Lett. **81**, 3588–3590, 2002.

¹⁷³R. M. Costescu, D. G. Cahill, F. H. Fabreguette, Z. A. Sechrist, and S. M. George. *Ultra-Low Thermal Conductivity in W/Al₂O₃ Nanolaminates*. Science **303**, 989–990, 2004.

numerical simulations¹⁷⁵ and recent experiments¹⁷⁶.

For $W > \ell$, the *incoherent* phonon transport is independent in the different layers, and phonons can be effectively treated as particles. In this case, the Boltzmann transport equation applies¹⁷⁷, and the particle-like phonons are scattered within the layers (internal resistance) and at the interfaces (interfacial resistance)¹⁷⁸. Both κ_{CP} and κ_{IP} (the in-plane thermal conductivity) increase with W , due to the decrease of the interfacial resistance density^{177,179}. When $W < \ell$, phonon transport is *coherent*^{175,176,180}, and the wave nature of phonons cannot be neglected. In this regime, κ_{CP} decreases with increasing W , in contrast with the incoherent case. At the crossover length, $W \sim \ell$, between the incoherent coherent regimes, κ_{CP} assumes a minimum value when plotted against W .

Details of the structure of the interface between layers are also known to significantly affect phonon transport. It has been reported that interfacial roughness¹⁸¹ or mixing¹⁸² reduce both κ_{CP} and κ_{IP} , and can even suppress the coherent nature of phonons, with $\kappa_{\text{CP(IP)}}$ increasing monotonously at any W . Both interface topology¹⁸³ and stiffness of interfacial bondings, which can be controlled by applying pressure¹⁸⁴ or tuning chemical bonding¹⁸⁵, have significant effects on the heat transport features.

S1. Crystalline layers with different masses. – In our work, thermal conductivities have been estimated by a Green-Kubo formulation. The number density and the temperature are fixed at $\hat{\rho} = 1.015$ (the corresponding crystal lattice constant is $a = 1.58$) and $T = 10^{-2}$, respectively. Vibrational states were also characterized by using a standard normal-modes analysis.

In Fig. 3.8 we show the thermal conductivities, κ_{CP} and κ_{IP} (symbols), as functions of the replication period, W , for the indicated layers mass ratios. The values of the diffuse limits $\kappa_{\text{CP}}^{\infty}$ and $\kappa_{\text{IP}}^{\infty}$, as well as those of the glass and the disordered alloy constituted by the same species are also shown as lines. In the studied W -range, $W = 2$ to 40 (monolayers), the in-plane value κ_{IP} shows a very weak dependence on W , as was observed for superlattices with perfect interfaces¹⁸¹. The

¹⁷⁵Y. Chen, D. Li, J. R. Lukes, Z. Ni, and M. Chen. *Minimum superlattice thermal conductivity from molecular dynamics*. Phys. Rev. B **72**, 174302, 2005.

¹⁷⁶J. Ravichandran, A. K. Yadav, R. Cheaito, P. B. Rossen, A. Soukiasian, S. J. Suresha, J. C. Duda, B. M. Foley, C.-H. Lee, Y. Zhu, A. W. Lichtenberger, J. E. Moore, D. A. Muller, D. G. Schlom, P. E. Hopkins, A. Majumdar, R. Ramesh, and M. A. Zurbuchen. *Crossover from incoherent to coherent phonon scattering in epitaxial oxide superlattices*. Nature Mater. **13**, 168–172, 2014.

¹⁷⁷G. Chen. *Thermal conductivity and ballistic-phonon transport in the cross-plane direction of superlattices*. Phys. Rev. B **57**, 14958–14973, 1998.

¹⁷⁸E. Lampin, Q.-H. Nguyen, P. A. Francioso, and F. Cleri. *Thermal boundary resistance at silicon-silica interfaces by molecular dynamics simulations*. Appl. Phys. Lett. **100**, 131906, –, 2012.

¹⁷⁹G. Chen and M. Neagu. *Thermal conductivity and heat transfer in superlattices*. Appl. Phys. Lett. **71**, 2761–2763, 1997.

¹⁸⁰N. Yang, G. Zhang, and B. Li. *Ultralow Thermal Conductivity of Isotope-Doped Silicon Nanowires*. Nano Lett. **8**, 276–280, 2008.

¹⁸¹B. C. Daly, H. J. Maris, Y. Tanaka, and S. Tamura. *Molecular dynamics calculation of the In-plane thermal conductivity of GaAs/AlAs superlattices*. Phys. Rev. B **67**, 033308, 2003.

¹⁸²S. C. Huberman, J. M. Larkin, A. J. H. McGaughey, and C. H. Amon. *Disruption of superlattice phonons by interfacial mixing*. Phys. Rev. B **88**, 155311, 2013.

¹⁸³K. Termentzidis, S. Merabia, P. Chantrenne, and P. Koblinski. *Cross-plane thermal conductivity of superlattices with rough interfaces using equilibrium and non-equilibrium molecular dynamics*. International Journal of Heat and Mass Transfer **54**, 2014–2020, 2011.

¹⁸⁴M. Shen, W. J. Evans, D. Cahill, and P. Koblinski. *Bonding and pressure-tunable interfacial thermal conductance*. Phys. Rev. B **84**, 195432, 2011.

¹⁸⁵M. D. Losego, M. E. Grady, N. R. Sottos, D. G. Cahill, and P. V. Braun. *Effects of chemical bonding on heat transport across interfaces*. Nature Mater. **11**, 502–506, 2012.

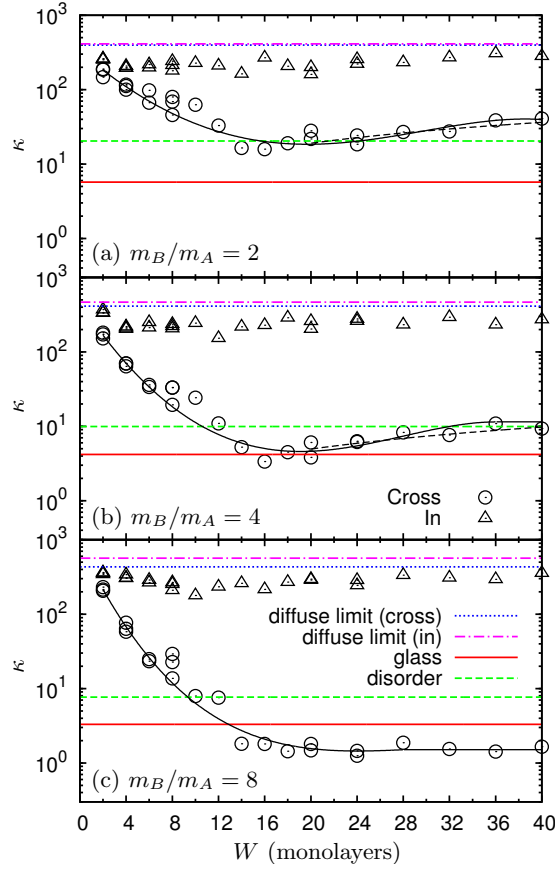


Figure 3.8: Thermal conductivity in superlattice *S1*, composed of two intercalated crystalline layers with different masses. The cross-plane, κ_{CP} , and in-plane, κ_{IP} , components of thermal conductivity are plotted as a function of the repetition period W . The ratio m_B/m_A of the masses in layers *A* and *B* is 2 in panel (a), 4 in (b), and 8 in (c). The values $\kappa_{\text{CP}}^\infty$ and $\kappa_{\text{IP}}^\infty$ of the diffuse limits ($W \rightarrow \infty$), as well as those in the glass and the disordered alloy with the same constituent species are indicated by the horizontal lines. In panels (a) and (b) we also show (dashed black lines), the prediction for κ_{CP} in the incoherent regime, $W > 20$, with the values of R and ℓ_k included in the Table. The solid curve interpolating the κ_{CP} data points in the entire W -range is a guide for eye. For some values of W , multiple data points are shown, calculated by using different system sizes and excluding the presence of finite system size issues.

value of κ_{IP} is close to, although lower than, $\kappa_{\text{IP}}^\infty$, indicating that slight in-plane phonon scattering at the interface is still active. More interestingly, as W increases, the cross-plane value κ_{CP} decreases steeply, reaches a minimum value at $W^* \simeq 20$, and next increases mildly at larger W . This W -dependence is consistent with previous predictions^{176,180,186}, and corresponds to the crossover at W^* from coherent to incoherent phonon transport. Note that for $m_B/m_A = 8$ (Fig. 3.8(c)), we do not observe a clear thermal conductivity minimum. More precisely, even at the largest value $W = 40$, κ_{CP} is still orders of magnitude lower than $\kappa_{\text{CP}}^\infty$, indicating that the interfacial resistance R results in a strong reduction of κ_{CP} in the present range of W . Equivalently, the Kapitza length ℓ_k is significantly larger than the maximum period $W = 40$.

¹⁸⁶T. Kawamura, Y. Kangawa, and K. Kakimoto. *An investigation of thermal conductivity of nitride-semiconductor nanostructures by molecular dynamics simulation*. *Journal of Crystal Growth* **298**, Thirteenth International Conference on Metal Organic Vapor Phase Epitaxy (ICMOVPE XIII), 251–253, 2007.

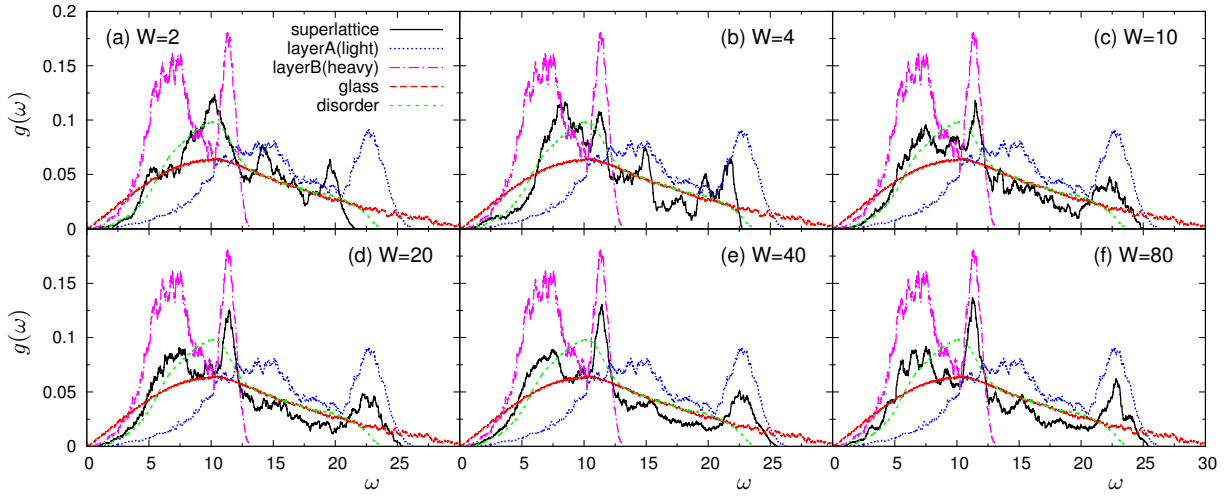


Figure 3.9: Vibrational density of states in superlattice $S1$. Vibrational density of states data for a mass ratio $m_B/m_A = 4$, with $m_A = 0.4$ and $m_B = 1.6$. In panels (a)-(f) we show the data corresponding to the repetitions period values $W = 2, 4, 10, 20, 40, 80$. For sake of comparison, we also plot $g_{A(B)}(\omega)$ for the homogeneous bulk crystal composed by light (heavy) $m_{A(B)}$ masses only, together with the data for the glass and the disordered alloy formed by the same constituent species.

The data shown in Fig. 3.8 demonstrate that κ_{CP} can be indeed lowered below the disordered alloy limit for $m_B/m_A = 2$, and even below the glass limit for higher mass heterogeneities, $m_B/m_A = 4$ and 8 . These results are consistent with experimental work¹⁷³, and demonstrate that the interface formed between dissimilar materials effectively reduces κ_{CP} . It is also worth noting that the thermal conductivity tensor is strongly anisotropic, with $\kappa_{CP} \ll \kappa_{IP}$.

The vibrational modes of the structure, i.e., the superlattice phonons, are key to understand the above behaviour of thermal conductivity. In Fig. 3.9 we show the vibrational density of states, $g(\omega)$, for $m_B/m_A = 4$ and $W = 2$ to 80 . $g_A(\omega)$ and $g_B(\omega)$ of the bulk crystals of type A and B , as well as the VDOS of the glass and the disordered alloy are also plotted, for comparison. At small $W = 2$, $g(\omega)$ of the superlattice roughly follows that of the disordered alloy, implying that the vibrational states in the two layers are strongly mixed. In this situation, phonons are able to propagate in both the cross- and in-plane directions. On the other hand, as W increases, $g(\omega)$ generates features increasingly similar to those identifying $g_A(\omega)$ and $g_B(\omega)$, separately. In particular, in the low- ω region $g(\omega)$ follows $g_B(\omega)$ (the heavy crystal B), whereas $g_A(\omega)$ (the light crystal A) controls $g(\omega)$ in the high- ω region. This result indicates that different parts of the vibrational spectrum are active in the two layers, with high(low)- ω modes preferentially excited in the light (heavy) layer A (B). In this situation, phonon propagation is largely obstructed in the cross-plane direction, leading to the observed large reduction of κ_{CP} . We remark that phonons propagate in the in-plane direction without any constraint, as witnessed by the large value of κ_{IP} close to κ_{IP}^∞ . This implies that phonons, whose propagation is blocked in the cross-plane direction, are actually specularly reflected at the interface and confined in the in-plane direction.

The separation of the vibrational states found in the $g(\omega)$ becomes more clear when considering the vibrational amplitudes associated with the eigenstates k . In Fig. 3.10 we show the vibrational amplitudes, E_A^k and E_B^k in the two layers A and B for each mode k , together with the binned average value (solid line). Based on the relations $E_A^k + E_B^k = 1$ and $0 \leq E_A^k, E_B^k \leq 1$ we can define a relative degree of excitation of particles in the two layers, based on the threshold value 0.5 : large

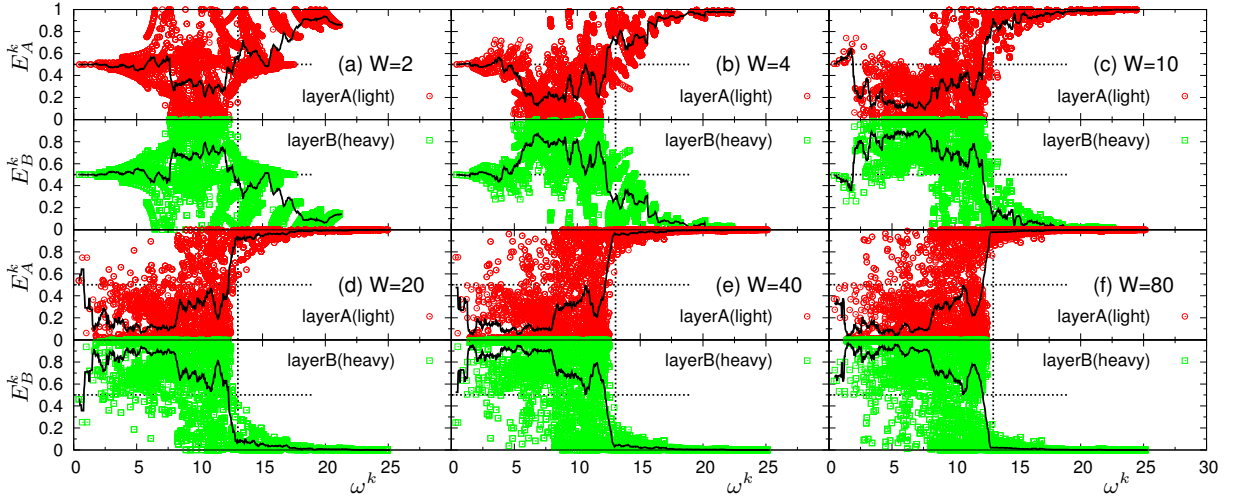


Figure 3.10: Amplitudes of normal modes in superlattice $S1$. Vibrational amplitudes of eigenvectors, E_A^k and E_B^k , in layers A and B for all normal modes k , plotted as a function of the corresponding eigenfrequencies ω^k . E_A^k and E_B^k are defined in the text. The mass ratio of the two layers is $m_B/m_A = 4$. The solid line represents the average values $\langle E_A^k \rangle$ and $\langle E_B^k \rangle$ calculated in bins of the form $\omega^k \pm \delta\omega^k/2$, with $\delta\omega^k = 0.5$. The horizontal dashed lines represent the threshold value $E_A^k = E_B^k = 0.5$, the vertical lines indicate $\omega = \omega_B^{\max} \simeq 13$, corresponding to the high frequency edge of $g_B(\omega)$. For additional details, see also the caption of Fig. 3.9.

excitations correspond to $E_{A,B}^k \geq 0.5$, $E_{A,B}^k < 0.5$ otherwise. If $E_A^k = E_B^k = 0.5$, particle vibrations in both layers are very similar and correlated.

At small $W = 2, 4$ we found, particularly in the low- ω region, a large fraction of vibrational states with $E_A^k \simeq E_B^k \simeq 0.5$. As W increases, in the high frequency region $\omega > \omega_B^{\max}$, where $\omega_B^{\max} \simeq 13$ is the high-frequency boundary in $g_B(\omega)$, only particles in the (light) layer vibrate ($E_A^k \simeq 1$), whereas those in the heavy layer B are almost immobile, as indicated by $E_B^k \simeq 0$. In this ω -region, phonon propagation in the cross-plane direction is therefore almost completely suppressed. In contrast, for $\omega < \omega_B^{\max}$, only particles pertaining to the (heavy) layer B show large vibrational amplitudes ($E_B^k > 0.5$), while vibrations in layer A tend to be small ($E_A^k < 0.5$). More in details, for $W \geq 20$, we see that the averaged amplitudes are much larger in the B layer ($\langle E_B^k \rangle > 0.8$) than in the A layer ($\langle E_A^k \rangle < 0.2$) in the $2 < \omega < 7.5$ range. Contrary to the case of $\omega > \omega_B^{\max}$, however, a significant number of modes is excited in both layers A and B , even with $E_A^k \simeq E_B^k \simeq 0.5$. We therefore conclude that, for $\omega < \omega_B^{\max}$, some phonons still propagate in the cross-plane direction, contributing to κ_{CP} .

We believe that the picture of a vibrational separation provides a simple and accurate framework to rationalize the behaviour of thermal conductivity in superlattices. In particular, it provides a complete characterization of the minimum in the W -dependence of κ_{CP} . Indeed, in the range $W = 2 \div 20$ identifying the coherent regime, the vibrational separation obstructs phonon propagation in the cross-plane direction, leading to the large reduction of κ_{CP} . In contrast, in-plane phonon propagation is very mildly affected by the vibrational separation and, therefore, κ_{IP} keeps high values. Also, by considering $\langle E_A^k \rangle$ and $\langle E_B^k \rangle$ (solid lines in Fig. 3.10), we conclude that the separation saturates to its maximum level at $W \sim 20$. Upon further increase $W > 20$, although averaged values show no significant changes, we recognize an increasing fraction of modes with $E_A^k > 0.5$ and $E_B^k < 0.5$ for $\omega < \omega_B^{\max}$ (panels (e) $W = 40$ and (f) $W = 80$ in Fig. 3.10). This

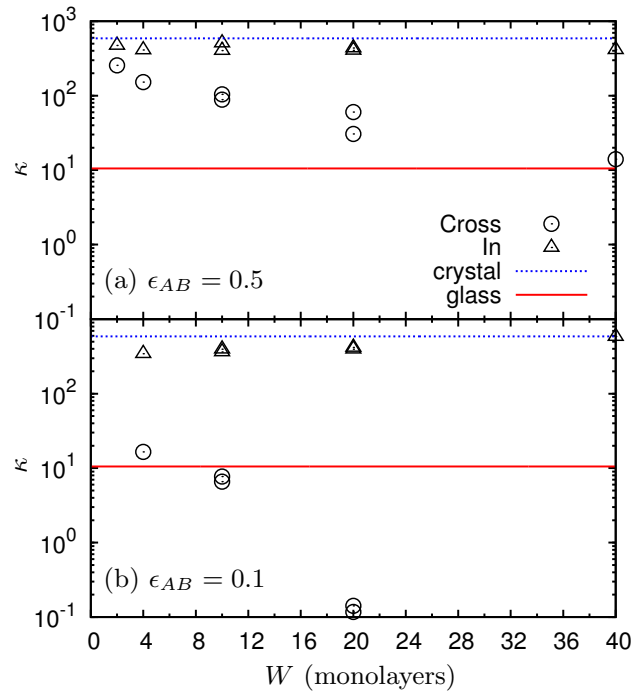


Figure 3.11: Thermal conductivity in superlattice S3 composed of identical crystalline layers with weakened interface. Thermal conductivities κ_{CP} and κ_{IP} are plotted as functions of W . The interface interaction ϵ_{AB} is 0.5 in (a) and 0.1 in (b). We also show the thermal conductivities of the corresponding one-component homogeneous bulk crystal and glass by the horizontal lines.

observation indicates that the separation tendency for modes with $E_A^k < 0.5$ and $E_B^k > 0.5$ becomes weaker, i. e., the correlation of vibrational features in the two layers increases, which corresponds exactly to the incoherent transport picture. Although transport becomes completely incoherent for values of W of the order of the Kapitza length (note that $\ell_z \simeq 1600$ for $m_B/m_A = 4$), this feature appears as soon as the vibrational separation is saturated, at the crossover point $W \sim 20$. Thus, the saturation point of the vibrational separation identifies the minimum value of κ_{CP} , which can be indeed below the glass limit.

S3. Crystalline layers separated by weakly interacting interfaces. – In Fig. 3.11 we show the W -dependence of κ_{CP} and κ_{IP} for the case where the energy scale associated to particles interactions across the interfaces are lowered compared to those intra-layers, with $\epsilon_{AB} = 0.5$ and 0.1 in the two panels. In the figure, we also plot as lines the data for the corresponding one-component crystal and glass. The in-plane value κ_{IP} is almost independent of W , and is very close to the value pertaining to the crystal. In contrast, κ_{CP} decreases monotonically by increasing W , and especially in the weaker case $\epsilon_{AB} = 0.1$, the observed reduction of κ_{CP} is dramatic. At $W = 10$, κ_{CP} equals the value obtained for the glassy sample, and it is almost two orders of magnitude lower than this value at $W = 20$. This extremely low κ_{CP} is consistent with previous experimental work¹⁴¹.

The behaviour of κ_{CP} could be further elucidated by inspection of the main features of the vibrational spectrum. In Fig. 3.12 we plot the $g(\omega)$ of superlattice S3, together with the vibrational amplitudes E_A^k and E_B^k . The $g(\omega)$ shows transverse and longitudinal phonon branches for all cases, similar to the homogeneous bulk crystal. Interestingly, as W increases $g(\omega)$ significantly deforms, following the appearance of an increasing fraction of modes at increasing higher frequencies. This

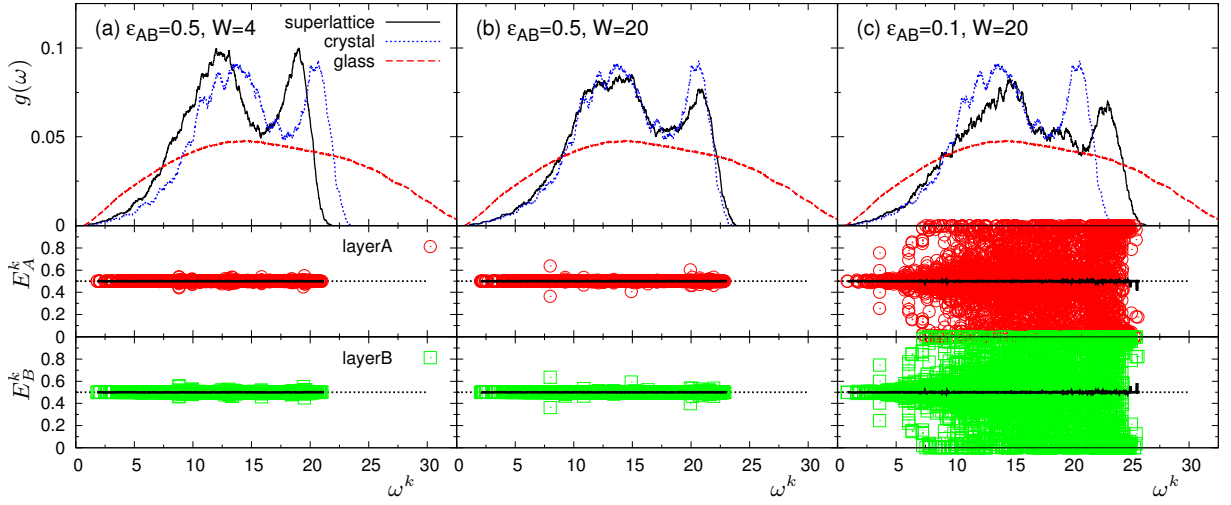


Figure 3.12: Vibrational density of states and vibrational amplitudes in superlattice *S3*. We report data corresponding to the indicated values of the interfacial interaction energy ϵ_{AB} and the repetition period W : (a) $\epsilon_{AB} = 0.5$, $W = 4$, (b) $\epsilon_{AB} = 0.5$, $W = 20$, and (c) $\epsilon_{AB} = 0.1$, $W = 20$. In panels at the top, we show the VDOS $g(\omega)$, together those of the corresponding one-component homogeneous crystal and glass with unmodified interactions. In panels at the bottom we show the vibrational amplitudes, E_A^k and E_B^k , in layers *A* and *B*, plotted as a function of the eigenfrequencies ω^k . The solid line represents the average values $\langle E_A^k \rangle$ and $\langle E_B^k \rangle$, calculated in bins of the form $\omega^k \pm \delta\omega^k/2$, with $\delta\omega^k = 0.5$. The horizontal dashed lines indicate $E_A^k = E_B^k = 0.5$.

behaviour is certainly correlated to the observation we made for $W = 20$, that the distance between monolayers far from the interfaces becomes significantly smaller than $a/2$. The consequent larger mass density makes higher the frequency of phonon modes of given wavelength, leading to the shift of $g(\omega)$ toward higher frequencies. Note that this global shift has as a consequence a mild increase of κ_{IP} with W , as it is clear from Fig. 3.11(b).

We now turn the attention to the vibrational amplitudes, E_A^k and E_B^k (Fig. 3.12, bottom panels). In the cases with $\epsilon_{AB} = 0.5$ and $W = 4$ and 20 , the particles in the two layers show completely equivalent and correlated vibrations for the vast majority of the modes, as indicated by $E_A^k \equiv E_B^k \equiv 0.5$. This result implies that phonons indeed propagate across the weakened interfaces in the cross-plane direction, but they are also partially reflected at the interface, causing the observed reduction of κ_{CP} . The situation changes drastically in the case $\epsilon_{AB} = 0.1$ and $W = 20$, where ultra-low values of κ_{CP} can be reached. Except for the low- ω modes, E_A^k and E_B^k are symmetrically randomly distributed around the average values $\langle E_{A(B)}^k \rangle = 0.5$, indicating that particles in *A* and *B* vibrate independently, in an uncorrelated manner. As a consequence, a very large fraction of vibrational modes do not cross at all the interfaces, but rather undergo a perfect specular reflection. In this situation, heat is not transferred between two adjacent layers, leading to extremely low values of κ_{CP} , while keeping a high κ_{IP} . We conclude by noticing that although specular reflection was also observed in the system *S1*, the physical mechanism behind this phenomenon is different in the two cases: vibrational separation causes reflection in the former, whereas weakened interactions across the interface with the consequent augmented spacing between the layers completely block cross-plane phonon propagation in the latter.

The take-home messages. – We can now summarize our results. We have provided numerically a clear demonstration of very low thermal conductivities in superlattices, below the glassy limit of the corresponding amorphous structures. Blocking phonon propagation in ordered structures via interfaces design is the key principle. We have identified two possible strategies to achieve this goal: imposing a large mass heterogeneity in the intercalated layers (as in system *S1*) or degrading inter-layers interactions compared to those intra-layers (as in *S3*). We found that in both cases phonons are specularly reflected at the interface and confined in the in-plane direction. This reduces the cross-plane thermal conductivity κ_{CP} below the corresponding glass limit, while keeping the in-plane contribution κ_{IP} close to the pure crystalline value.

More specifically, in the case of masses mismatch, propagation of phonons with frequencies $\omega > \omega_B^{\max}$ is almost completely suppressed (blocked), whereas a fraction of low-frequency phonons ($\omega < \omega_B^{\max}$) are still able to propagate across the interfaces, contributing to κ_{CP} (Fig. 3.10(d)). Also, the minimum in thermal conductivity as a function of the repetition period W corresponds to a maximum in the vibrational separation between the layers of type *A* and *B*. These therefore act as true filters in complementary regions of the vibrational spectrum, suppressing almost completely phonons transport in the direction of the nano-structuration pattern.

In contrast, attenuated interactions across the interfaces are able to block phonons at almost all frequencies (see Fig. 3.12(c)), which results into extremely low values of κ_{CP} , even orders of magnitude lower than the corresponding glass limit (Fig. 3.11(b)). In this sense, directly modifying the interfaces seems to be the most effective strategy to obtain very low heat transfer. Note that this is a practically feasible route, since attenuated interfaces can be designed by exploiting materials with weak van der Waals forces among adjacent crystalline planes, as demonstrated in the case of WSe_2 sheets in Ref.¹⁴¹. Interfaces stiffness modification by controlling pressure^{184,187} or chemical bonding¹⁸⁵ are additional possible routes to directly tune the strength of interfaces.

In addition, as we have understood from our analysis of vibrational amplitudes (Figs. 3.10 and 3.12), it is much more problematic to significantly block low- ω (long wavelength, λ) phonons propagation, than those with high- ω (short λ). This situation is similar to what has been observed in bulk glasses, where the long- λ acoustic waves are not scattered by the disorder and can propagate over long distances by carrying heat. Therefore, blocking or efficiently scattering the long- λ phonons is also a key factor to achieve very low thermal conductivities, as was pointed out in Ref.¹⁸⁸.

What next? Elastic response of glasses on curved surfaces. – We are now ready to apply the above insight to different interesting systems. Recent inspiring experimental⁵² and simulation¹⁸⁹ works have focused on the slow dynamics of finite-size liquids made of colloids/particles and confined to move on the surface of a sphere. These appear as very interesting model systems, where the extent of the structural relaxation can be controlled by tuning the curvature of the embedding space. We have the intention to move below the glass temperature, and investigate the effect of this geometrical feature on the mechanical properties of systems arrested in the glass phase, clarifying the effect of a constant positive curvature on the two-dimensional elastic

¹⁸⁷W.-P. Hsieh, A. S. Lyons, E. Pop, P. Keblinski, and D. G. Cahill. *Pressure tuning of the thermal conductance of weak interfaces*. Phys. Rev. B **84**, 184107, 2011.

¹⁸⁸M. N. Luckyanova, J. Garg, K. Esfarjani, A. Jandl, M. T. Bulsara, A. J. Schmidt, A. J. Minnich, S. Chen, M. S. Dresselhaus, Z. Ren, E. A. Fitzgerald, and G. Chen. *Coherent Phonon Heat Conduction in Superlattices*. Science **338**, 936–939, 2012.

¹⁸⁹J.-P. Vest, G. Tarjus, and P. Viot. *Dynamics of a monodisperse Lennard-Jones system on a sphere*. Mol. Phys. **112**, 1330–1335, 2014.

response. Above we have detailed our work on elastic heterogeneities in flat spaces. We are now in the position to clarify by computer simulation the role played by the non-affine displacement field following the application of mechanical strain, and investigate the possibility to control the degree of mechanical heterogeneity by tuning the curvature radius of the embedding surface. The modifications undergone by the normal modes excited in the system will also be elucidated. Note that the nature of vibrational excitations and their transport properties (which are correlated to heat transfer) in complex nano-geometries is a hot topic in modern materials science¹⁹⁰.

In addition, Ref.⁵² suggests that the dynamics of the confined fluid is also modified by the existence of (exogenous) boundary mobility. It is tempting to ask what could be the effect on the above mechanical features of the presence of endogenous stimuli, like in active matter. Vicsek-like active swarms moving on a sphere¹⁹¹ seems to constitute a nice playground to attack these issues.

I must conclude at some point. This is it.

¹⁹⁰Ø. Wilhelmsen, T. T. Trinh, S. Kjelstrup, T. S. van Erp, and D. Bedeaux. *Heat and Mass Transfer across Interfaces in Complex Nanogeometries*. Phys. Rev. Lett. **114**, 065901, 2015.

¹⁹¹R. Sknepnek and S. Henkes. *Active swarms on a sphere*. arXiv preprint arXiv:1407.8516, 2014.

